ELECTRON EMISSION

All electron tubes* depend for their operation on the flow of electrons within the tube, either through high vacuum or an ionized gas. The electrons are emitted from a cathode surface as a result of one of four processes that are distinguished on the basis of the mechanism by which the electrons are enabled to leave the surface. These processes are elevated temperature (thermionic or primary emission); bombardment by other particles, generally electrons (secondary emission); the action of a high electric field (field emission); or the incidence of photons (photoemission).

Thermionic Emission

Thermionic emission occurs when the electrons in the cathode material have enough thermal energy to overcome the forces at the surface and escape.

The thermal emission of electrons from metals obeys the Richardson–Dushman equation

$$J_0 = AT^2 \exp(-11600\phi_0/T)$$

where J_0 is emission density in amperes/cm², A is a constant [amperes/cm²(°K)²], ϕ_0 is the work function (electron-volts), and T is temperature in degrees Kelvin. A and ϕ_0 are characteristic of the specific material.

The current density given by this equation is usually referred to as the saturation emission current density. Typical constants are given in Table 1 for several commonly used cathode materials.

The maximum current of which a cathode is capable at the operating temperature is known as the saturation current and is normally taken as the value at which the current first fails to increase as the three-halves power of the voltage causing the current to flow. Thoriated-tungsten filaments for continuous-wave operation are usually assigned an available emission of approximately half the saturation value. Oxide-coated emitters do not have a well-defined saturation point and are designed empirically. The available emission from the cathode must be at least equal to the sum of the peak currents drawn by all the electrodes.

Figure 1 gives a plot of saturation current as a

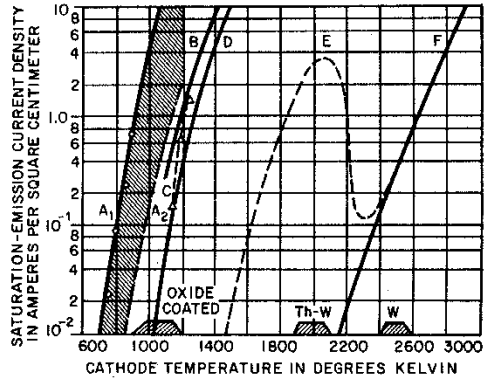

Fig. 1—Emission current density vs. cathode temperature for several types of thermionic emitters. The shaded blocks at the bottom of the figure show the normal operating range for three of the cathodes. Curves are given for (A) *The oxide-coated cathode.* Curve A_1 gives the saturation emission current density under pulsed conditions. Curve A_2 gives the direct-current saturation emission density. The position of this curve may vary substantially with environmental conditions. Direct-current densities much in excess of 0.5 amp/cm² lead to relatively short cathode life. (B) *The pressed nickel cathode.* Curve B shows the direct-current saturation emission current density obtained from a pressed nickel cathode. (C) *The impregnated nickel cathode.* Curve C shows the saturation emission current obtained from the impregnated nickel cathode. The measurements were taken with 40-microsecond pulses and a repetition rate of 60 pulses per second. (D) *Pressed and impregnated tungsten cathodes.* Curve D shows the saturation emission density obtained from pressed and impregnated tungsten cathodes based on $A = 2.5$ amps/cm² (°K)² and $\phi_0 = 1.67$ electron-volts. (E) *The thoriated-tungsten cathode.* Curve E shows the measured saturation emission current density of an uncarburized thoriated-tungsten filament. (F) *Tungsten filaments.* Curve F shows the saturation emission current density of a tungsten filament based on $A = 70$ amps/cm² (°K)² and $\phi_0 = 4.5$ electron-volts. *J. W. Gewartowski and H. A. Watson, "Principles of Electron Tubes," 1965: p. 42. Courtesy of D. Van Nostrand Company, Inc.*

* J. W. Gewartowski and H. A. Watson, "Principles of Electron Tubes," Van Nostrand, Princeton, New Jersey; 1965. J. Millman and S. Seely, "Electronics," 1st ed., McGraw-Hill Book Company, New York; 1941. K. R. Spangenberg, "Vacuum Tubes," 1st ed., McGraw-Hill Book Company, New York; 1948. A. H. W. Beck, "Thermionic Valves, Their Theory and Design," Cambridge University Press, London, England; 1953. "Standards on Electron Tubes: Definitions of Terms, 1950," Institute of Radio Engineers, New York.

TABLE 1—COMMONLY USED CATHODE MATERIALS.

Type	A	ϕ_0	Efficiency (milliamperes/watt)	Specific Emission (amp/cm²)	Emissivity (watts/cm²)	Operating Temperature (°K)	Resistance Ratio (hot/cold)
Bright tungsten (W)	70	4.50	5–10	0.25–0.7	70–84	2500–2600	14/1
Thoriated tungsten (Th–W)	4	2.65	40–100	0.5–3.0	26–28	1950–2000	10/1
Tantalum (Ta)	37	4.12	10–20	0.5–1.2	48–60	2380–2480	6/1
Oxide coated (Ba–Ca–Sr)	*	1.0–1.3	50–150	0.5–2.5	3–5	1000–1150	2.5 to 5.5/1
Impregnated	2.4	1.65		1.8–5.4	2.6–3.8	1300–1400	

* The Richardson-Dushman equation does not apply to a composite surface of this type.

function of temperature for several types of emitters in common use.

Thoriated-tungsten and oxide-coated emitters should be operated close to specified temperature. A customary allowable heating-voltage deviation is ±5 percent. Bright-tungsten emitters may be operated at the minimum temperature that will supply required emission as determined by power-output and distortion measurements. Life of a bright-tungsten emitter is lengthened by lowering the operating temperature. Figure 2 shows a typical relationship between filament voltage and temperature, life, and emission.

Mechanical stresses in filaments due to the magnetic field of the heating current are proportional to I_f^2. Current flow through a cold filament should be limited to 150 percent of the normal operating value for large tubes, and 250 percent for medium types. Excessive starting current may easily warp or break a filament.

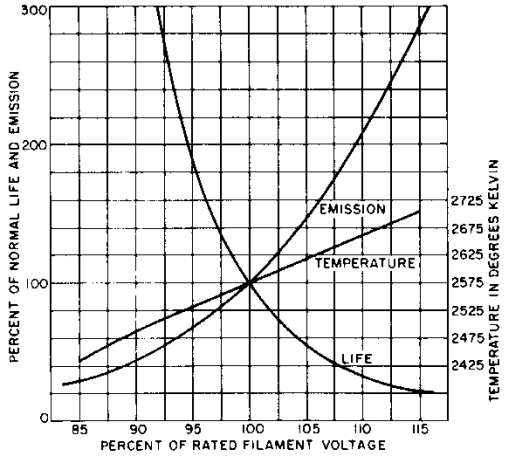

Fig. 2—Effect of change in filament voltage on the temperature, life, and emission of a bright-tungsten filament (based on 2575-degree-Kelvin normal temperature).

Secondary Emission

When the surface of a solid is bombarded by charged particles having appreciable velocity, electrons are emitted from the solid. This is the process of secondary emission,* the most important case being when the bombarding particles are also electrons. One then differentiates between incident and emitted electrons by the terms primary and secondary, respectively. The latter term commonly describes all electrons collected from a secondary emitter; these electrons comprise three groups: (A) true secondaries, (B) inelastically reflected primaries, and (C) elastically reflected primaries. True secondaries are considered to be those of the solid which have been excited above the energy level required for escape across the surface barrier. The three groups are separable to a degree on the basis of energy as indicated in the energy distribution curve of Fig. 3. True secondaries constitute the bulk of emitted electrons at moderate primary energies and have a mode energy of at most a few electron-volts. Their distribution is almost independent of primary energy. Electrons in the relatively flat interval within a, b constitute a mixture of true secondaries and inelastically reflected primaries. It has become customary to arbitrarily designate those emitted electrons having energies less than 50 electron-volts as true secondaries.

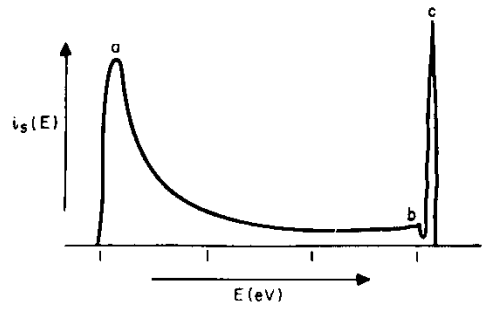

Fig. 3—Total energy distribution of secondary electrons.

Total secondary yield δ, defined as the ratio of secondary to primary electron current, is independent of primary current but strongly dependent on primary energy as indicated in Fig. 4. The shape of the yield curve follows from generating and escape mechanisms; the former leading to an initial rise in yield with primary energy, and the latter causing an eventual reduction owing to increased penetration of primaries and a greater mean depth of escape of secondaries. Significant points of the yield curve are first and second crossover at which yield becomes unity, the maximum yield δ_m, and the primary energy eV_m at which the maximum occurs. For most insulators, first crossover occurs between 15 and 25 eV primary energy. Insulators generally exhibit higher yields than conductors, a property attributed to the absence of conduction electrons which tend to reduce the mean energy and the escape probability of secondaries through collision losses within the solid. The yield of insulators decreases noticeably as temperature is increased, owing to increasing electron–phonon interaction.

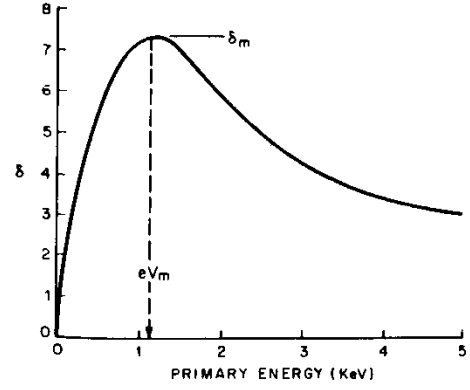

Fig. 4—Secondary-emission yield curve.

Secondary yield increases with angle of primary incidence, the effect being most pronounced at high primary energies. Yield is also a function of surface structure and may be minimized by employing physical trapping such as provided by a porous surface. Lowest yields are obtained for porous carbon deposits and highest yields for single crystal insulators having low electron affinity. Secondary yield may also be influenced by internal electric fields which tend to assist or retard the escape of secondaries. If such fields are strongly dependent on charge transport within the bombarded material, yield may become dependent on primary current which can in turn give rise to anomalous time-dependent effects. Barring such effects, it appears that the interaction time for the secondary-emission process is of the order of 10^{-12} second.

When the rate of bombardment by primary electrons becomes very low, as in single-electron counting, the statistical nature of the secondary-emission process becomes evident. The probability of obtaining 0, 1, 2, ···, n secondaries per incident primary is given by the Poisson distribution.

Commonly used secondary-emission materials are silver-magnesium or copper-beryllium alloy processed to provide a high-yield partly conductive surface film. Typically such surfaces exhibit yields of 2.5 to 4 at 100 eV primary energy.

Secondary emission is employed advantageously in the operation of many electron devices, such as camera tubes, storage tubes, and image intensifiers. A most important application lies in secondary-electron multiplication, which provides a means for amplifying very weak electron currents as in photomultiplier tubes. A conventional electron multiplier consists of a number of secondary-emitting dynodes operated at progressively higher potentials and terminated by an electron-collecting electrode. Electrons incident on the first dynode are multiplied, the resultant secondaries are accelerated to the second dynode where the process is repeated, and so on throughout the multiplier structure.

If the dynodes exhibit uniform yield characteristics, the overall amplification G obtained from a multiplier having n dynodes is

$$G = g^n$$

where g is the gain per dynode. The actual gain g may be slightly less than the secondary yield δ because of multiplier geometry. In the absence of appreciable space-charge effects, maximum gain is realized when the available potential is uniformly distributed across the dynode chain. An empirical relation for g may be obtained by approximating

the initial portion of the yield curve, that is

$$g \cong \delta \cong A \Delta V^m$$

ΔV = interdynode potential (primary energy), and A and m are empirical constants. Using this approximation, one obtains

$$g_{opt} = \epsilon^m$$

$$n_{opt} = A^{1/m}(V/\epsilon)$$

(ϵ = base of natural logarithms), where g_{opt} and n_{opt} are the optimum values of gain/dynode and number of dynodes, respectively, for maximizing overall amplification, given a total potential V available for distribution across the dynodes. The number of dynodes n is taken as the closest integer to the calculated value. In some cases, deviation from a uniform potential distribution and optimum gain conditions is advantageous, for example to reduce space-charge effects and improve time-delay and time-dispersion properties. Increasing the energy of electrons incident on the first dynode improves signal-to-noise ratio and single-electron-counting capability.

In addition to the conventional discrete dynode multiplier, a number of novel arrangements have been devised including crossed-field strip multipliers and tubular multipliers which commonly employ a continuous semiconductive dynode surface for potential distribution and multiplication. Tubular multipliers, when formed into a parallel array of small-diameter elements, may be employed for electron image intensification. Another form of multiplier commonly used for this purpose is the transmission secondary-emission multiplier, wherein secondaries exit from the side opposite primary incidence. The structure normally takes the form of a thin-film or porous supported layer, having the side of primary incidence made electrically conductive.

Field Emission

If an electric field of sufficient magnitude is offered to the surface of a metal, the potential barrier at the surface will be lowered, allowing the escape of electrons, and field emission* will result. The current has been found to vary with the applied field in accordance with

$$J = CE^2 \exp(-D/E) \text{ amperes/centimeter}^2$$

where J is the current density, E the electric field at the surface, and C and D are approximately constant coefficients with D determined mainly by the work function. Field emission must be taken into account in the design of very-high-voltage tubes and apparatus, and is a factor in the operation of cold-cathode gas tubes. Although development is being carried on, there has been little use made yet of field emission in high-vacuum tubes.

Photoemission

If photons with sufficient energy impinge on a photocathode, electrons are emitted.* Such electrons are known as photoelectrons. For an input flux of fixed relative spectral distribution, the number of photoelectrons is proportional to the intensity of the input flux while the energy of the photoelectrons is independent of this intensity. The maximum energy of emitted electrons expressed in volts V depends on the wavelength λ and temperature. At absolute zero, according to Einstein's law

$$e(V+\phi) = hc/\lambda$$

where e = electron charge = 1.6×10^{-19} coulomb, ϕ = work function in volts, h = Planck's constant = 6.6×10^{-34} joule-second, c = velocity of light = 3×10^{8} meters/second, and λ = wavelength in meters.

If a threshold wavelength λ_0 is defined by

$$e\phi = hc/\lambda_0$$

V is seen to be zero (except for thermal velocities) at the wavelength λ_0; for $\lambda > \lambda_0$, there is no photoelectric emission at absolute zero. At temperatures above absolute zero there is always a finite probability of some photoemission at all wavelengths due to the thermalization of the electron distribution.

Photocathode Response to Monochromatic Radiation: The output current dI_λ in amperes, generated by a photocathode subjected to a monochromatic input flux dW_λ in watts, is given by

$$dI_\lambda = s_\lambda \, dW_\lambda$$

where s_λ is the monochromatic radiant sensitivity (or responsivity) of the photocathode in amperes/watt defined by this equation. Similarly, the number of electrons/second dn_λ generated by an input flux dN_λ in photons/second is given by

$$dn_\lambda = q_\lambda \, dN_\lambda$$

where q_λ is the monochromatic quantum efficiency of the photocathode in electrons/photon defined by this equation.

The monochromatic radiant sensitivity s_λ is related to the monochromatic quantum efficiency q_λ by

$$s_\lambda = e\lambda q_\lambda/hc = 8.08\times10^5 \lambda q_\lambda.$$

Typical values of the monochromatic radiant sensitivity s_λ and corresponding monochromatic quantum efficiency q_λ as a function of wavelength λ are shown in Fig. 5 for some commonly used photocathodes, designated by their JEDEC registered "S numbers." Table 2 gives typical peak sensitivities for the various surfaces, while Table 3 indicates the general composition and other properties of the common surfaces.

Photocathode Response to Spectrally Distributed Sources: The total photocurrent I in amperes emitted by a photocathode subjected to a spectrally distributed input flux is given by

$$I = w_{\lambda\,max} s_{\lambda\,max} \int_0^\infty w_\lambda \sigma_\lambda \, d\lambda$$

$$= W_{\lambda_1\lambda_2} s_{\lambda\,max} \left(\int_0^\infty w_\lambda \sigma_\lambda \, d\lambda \Big/ \int_{\lambda_1}^{\lambda_2} w_\lambda \, d\lambda \right)$$

TABLE 2—TYPICAL PEAK PHOTOCATHODE SENSITIVITIES.

S Number	Radiant Sensitivity: $s_{\lambda\,max}$ (amp watt^{-1})	Radiant Sensitivity: λ_{max} (nanometers)	Quantum Efficiency: $q_{\lambda\,max}$ (electron photon^{-1})	Quantum Efficiency: λ_{max} (nanometers)
S1	0.0025	800*	0.004	770*
S3	0.0019	420	0.0058	400
S4	0.042	420	0.13	380
S5	0.052	330	0.21	320
S8	0.0024	360	0.0082	350
S9	0.023	490	0.056	480
S10	0.021	440	0.061	420
S11	0.048	450	0.14	400
S13	0.048	450	0.20	<200
S17	0.083	500	0.26	350
S20	0.066	420	0.20	400
S21	0.024	460	0.07	370

* Neglecting short wavelength peak

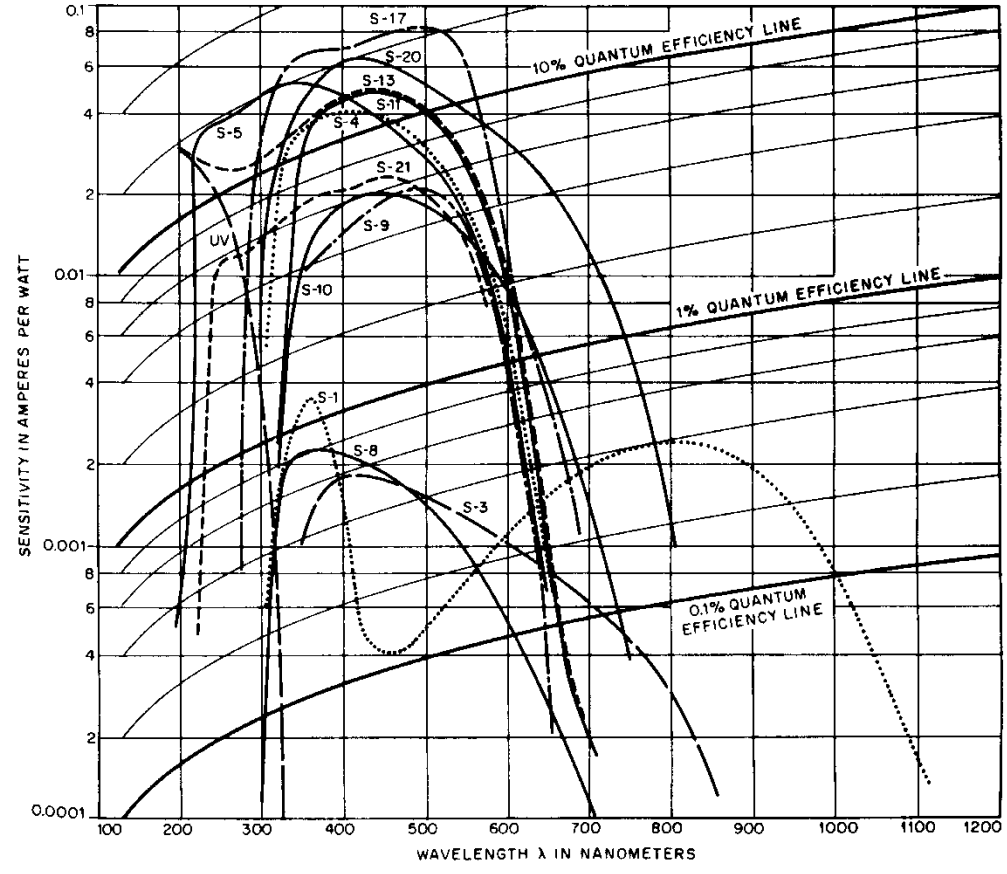

Fig. 5—Typical absolute spectral response characteristics of photoemissive devices.

TABLE 3—CHARACTERISTICS OF STANDARD PHOTOSURFACES.

S Number[1]	Principal Photocathode Components[2]	Entrance Window Material	Photocathode Supporting Substrate[3]	Typical Luminous Sensitivity[4] (μa/lumen)	Typical Photocathode Dark Current[5] at 25°C (amp/cm²)
S1	Ag–O–Cs	Visible-light-transmitting glass[6]	Entrance window or opaque material[7]	25	10^{-11}–10^{-13}
S3	Ag–O–Rb	Visible-light-transmitting glass[6]	Opaque material[7]	6.5	10^{-12}
S4	Cs–Sb	Visible-light-transmitting glass[6]	Opaque material[7]	40	10^{-14}
S5	Cs–Sb	Ultraviolet-transmitting glass	Opaque material[7]	40	10^{-14}
S8	Cs–Bi	Visible-light-transmitting glass[6]	Opaque material[7]	3	10^{-14}–10^{-15}
S9	Cs–Sb	Visible-light-transmitting glass[6]	Entrance window	30	10^{-14}
S10	Ag–Bi–O–Cs	Visible-light-transmitting glass[6]	Entrance window	40	10^{-13}–10^{-14}
S11	Cs–Sb	Visible-light-transmitting glass[6]	Entrance window	60	10^{-14}–10^{-15}
S13	Cs–Sb	Fused silica	Entrance window	60	10^{-14}–10^{-15}
S17	Cs–Sb	Visible-light-transmitting glass[6]	Opaque reflecting material[7]	125	10^{-14}–10^{-15}
S19	Cs–Sb	Fused silica	Opaque material[7]	40	10^{-14}
S20	Sb–K–Na–Cs	Visible-light-transmitting glass[6]	Entrance window	150	10^{-15}–10^{-16}
S21	Cs–Sb	Ultraviolet-transmitting glass	Entrance window	30	10^{-14}
UV[8]	Cs–Te	Sapphire	Opaque material[7]	0	—

Notes:

1. The S number is the designation of the spectral response characteristic of the device and includes the transmission of the device window material.
2. Principal components of the photocathode are listed without regard to order of processing or relative proportions.
3. When the supporting substrate is the entrance window, an intermediate semitransparent electrically conductive layer may be used.
4. Corresponding to the specific absolute response curves shown in Fig. 5 using a 2854°K color-temperature tungsten-lamp test source.
5. Specific dark current excludes direct-current leakage.
6. Lime glass and Kovar sealing borosilicate glass are commonly used for visible-light-transmitting glass.
7. The opaque material used as the supporting substrate for photocathodes in which the input radiation is incident on the same side as the emitted photoelectrons is usually metallic in nature.
8. An S number designation has not yet been assigned to this experimental "solar blind" photoemissive surface.

where $w_{\lambda\,max}$ = peak input flux spectral density (watt/m), $s_{\lambda\,max}$ = peak monochromatic radiant sensitivity of the photocathode (amp/watt), w_λ = relative spectral distribution of the input flux, σ_λ = relative spectral distribution of the radiant sensitivity of the photocathode, λ = wavelength, and $W_{\lambda_1\lambda_2}$ = flux in watts within the wavelength interval $\lambda_1 \leq \lambda \leq \lambda_2$.

Typical values of the dimensionless "spectral matching factor" ratio

$$\int_0^\infty w_\lambda \sigma_\lambda \, d\lambda \Big/ \int_{\lambda_1}^{\lambda_2} w_\lambda \, d\lambda$$

appearing in the above relationship and describing the comparative spectral match between various photocathode and input-flux spectral distributions are shown in Table 4 evaluated for $\lambda_1 = 0$ and $\lambda_2 = 1.2\mu = 1.2\times10^{-6}$ meter.

If the input flux is measured in lumens L instead of watts, the resultant ratio I/L of emitted current I to flux input is designated as the photocathode luminous sensitivity S, and is given by

$$S = I/L = s_{\lambda\,max} \int_0^\infty w_\lambda \sigma_\lambda \, d\lambda \Big/ 680 \int_0^\infty w_\lambda E_\lambda \, d\lambda$$

where 680 = luminous equivalent of 555 Å radiation (lumens/watt), E_λ = relative photopic human eye response, normalized to unity maximum, and

$$\int_0^\infty w_\lambda \sigma_\lambda \, d\lambda \Big/ \int_0^\infty w_\lambda E_\lambda \, d\lambda$$

is a dimensionless ratio that can be computed from the spectral-matching-factor data in Table 4 for various photocathode and input-flux spectral distributions by dividing the spectral-matching-factor data for

$$\int_0^\infty w_\lambda \sigma_\lambda \, d\lambda \Big/ \int_{\lambda_1}^{\lambda_2} w_\lambda \, d\lambda$$

by the spectral-matching-factor data for

$$\int_0^\infty w_\lambda E_\lambda \, d\lambda \Big/ \int_{\lambda_1}^{\lambda_2} w_\lambda \, d\lambda.$$

In the special case where the input spectral distribution w_λ, designated as $w_\lambda(2854)$, corresponds to a standard 2854°K color-temperature tungsten lamp, the luminous sensitivity S, designated as $S(2854)$, and often used as a specification on photocathode sensitivity, is given by

$$S(2854) = s_{\lambda\,max} \times \int_0^\infty w_\lambda(2854)\sigma_\lambda \, d\lambda \Big/ 680 \int_0^\infty w_\lambda(2854) E_\lambda \, d\lambda.$$

This equation relates the peak cathode monochromatic radiant sensitivity $s_{\lambda\,max}$ (also commonly used to specify cathode sensitivity) to the standard luminous sensitivity $S(2854)$. Since the wavelength at which the cathode quantum efficiency has its peak value does not correspond, in general, to the wavelength at which the radiant sensitivity has its peak value (Fig. 5 and Table 2) no general relationship exists between the peak radiant sensitivity $s_{\lambda\,max}$ and the peak quantum efficiency $q_{\lambda\,max}$.

Photocathode Response with Optical Filter: The ratio of (A) the emitted photocurrent, I(filter), with a filter inserted between a given flux source and the photocathode to (B) the current without

TABLE 4—SPECTRAL MATCHING FACTORS.

			$\int_0^\infty w_\lambda\sigma_\lambda\,d\lambda \Big/ \int_0^{1.2\mu} w_\lambda\,d\lambda$ and $\int_0^\infty w_\lambda E_\lambda\,d\lambda \Big/ \int_{\lambda_1}^{\lambda_2} w_\lambda\,d\lambda$			
			Photocathode Type			
Source	λ_1	λ_2	S1	S11	S20	Photopic Eye
2854°K lamp	0	1200	0.52	0.060	0.112	0.071
5000°K blackbody	0	1200	0.53	0.26	0.34	0.140
Mean solar flux	0	1200	0.54	0.32	0.36	0.197
P1 phosphor	0	∞	0.28	0.28	0.69	0.768
P4 phosphor	0	∞	0.31	0.67	0.73	0.402
P11 phosphor	0	∞	0.22	0.91	0.88	0.201
P20 phosphor	0	∞	0.39	0.42	0.58	0.707
NaI(Th)	0	∞	0.53	0.88	0.90	0.046

Note: λ_1 and λ_2 are in nanometers.

TABLE 5—TYPICAL FILTER FACTORS.

Filter				Filter Factor $\int_0^\infty t_\lambda w_\lambda \sigma_\lambda \, d\lambda \Big/ \int_0^\infty w_\lambda \sigma_\lambda \, d\lambda$, $w_\lambda = w_\lambda(2854)$			
				Photocathode Type			
Manufacturer	Glass Number	Thickness	Color Series	Description	S1	S4	S11	S20
Corning	2540	stock	CS 7–56	Infrared	0.108	0.000	0.000	0.000
Corning	5113	½ stock	CS 5–58	Blue	0.004	0.126	0.103	0.055
Corning	2403	stock	CS 2–58	Deep red	0.788	0.114	0.112	0.257

the filter, I(no filter), is called the filter factor $T(t_\lambda, w_\lambda, \sigma_\lambda)$ and is given by

$$T(t_\lambda, w_\lambda, \sigma_\lambda) = I(\text{filter})/I(\text{no filter})$$
$$= \int_0^\infty t_\lambda w_\lambda \sigma_\lambda \, d\lambda \Big/ \int_0^\infty w_\lambda \sigma_\lambda \, d\lambda$$

where t_λ is the transmission of the filter at a given wavelength λ, and the notation $T(t_\lambda, w_\lambda, \sigma_\lambda)$ indicates that the filter factor is a function not only of the filter transmission t_λ but also of the detector response σ_λ and the source distribution w_λ. Typical filter factors are given in Table 5.

The ratio of emitted photocurrent with the filter, I(filter), to the flux in lumens $L(2854)$, incident on the filter (not on the cathode) from a 2854°K source is designated as S(photocathode+filter) and is given by

$$S(\text{photocathode+filter}) = I(\text{filter})/L(2854)$$
$$- S(2854)\, T(t_\lambda, 2854, \sigma_\lambda).$$

The magnitude of the luminous sensitivity, S(photocathode+filter), in amperes per lumen is used to specify cathode sensitivity, or more precisely, cathode-plus-filter sensitivity, over a selected spectral region, where the filter is chosen to restrict the flux incident on the photocathode to the desired region. The sensitivity, S(photocathode+filter), is then designated as the "infrared" sensitivity, or "red" sensitivity, or "blue" sensitivity, et cetera, depending on the predominant spectral region passed by the filter.

ELECTRODE DISSIPATION

After the electron stream has given up the useful component of its energy, the remainder is dissipated as heat in some suitable part of the tube. Five processes are commonly used to remove this heat. The amount which can be removed depends on the area available, the temperature differential, and, in the cases of forced cooling, the coolant flow.

TABLE 6—TYPICAL OPERATING DATA FOR COMMON TYPES OF COOLING.

Type	Average Cooling Surface Temperature (°C)	Specific Dissipation of Cooling Surface (watts/cm²)	Cooling-Medium Supply
Radiation	400–1000	4–10	
Water	30–150	30–110	0.25–0.5 gallon/minute/kilowatt
Forced air	150–200	0.5–1	50–150 feet³/minute/kilowatt
Evaporative	100–120	80–125	Water-, air-, or convection-cooled condenser. A water-cooled condenser would require 0.07–0.1 gallon/minute/kilowatt
Conduction	100–250	5–30	Heat sink operating at 50–100°C

In computing cooling-medium flow, a minimum velocity sufficient to assure turbulent flow at the dissipating surface must be maintained. The figures for specific dissipation (Table 6) apply to clean cooling surfaces and may be reduced to a small fraction of the values shown by heat-insulating coatings such as scale or dust.

Radiation Cooling

In a radiation-cooled system, that portion of the tube on which the heat is dissipated is allowed to reach a temperature such that the heat is radiated to the surroundings. The amount of heat which can be removed in this manner is given by

$$P = \epsilon_t \sigma (T^4 - T_0^4)$$

where P = radiated power in watts/centimeter², ϵ_t = total thermal emissivity of the surface, σ = Stefan-Boltzmann constant = 5.67×10^{-12} watt-centimeters^{-2} × degrees Kelvin^{-4}, T = temperature of radiating surface in degrees Kelvin, and T_0 = temperature of surroundings in degrees Kelvin. Total thermal emissivity varies with the degree of roughness of the surface of the material and the temperature. Values for typical surfaces are in Table 7.

TABLE 7—TOTAL THERMAL EMISSIVITY ϵ_t OF ELECTRON-TUBE MATERIALS.

Material	Temperature (°K)	Thermal Emissivity
Aluminum	450	0.1
Anode graphite	1000	0.9
Copper	300	0.07
Molybdenum	1300	0.13
Molybdenum, quartz-blasted	1300	0.5
Nickel	600	0.09
Tantalum	1400	0.18
Tungsten	2600	0.30

Water Cooling

For water cooling the water is circulated through a suitably designed structure. The amount of heat which can be removed by this process is given by

$$P = 264 Q_W (T_2 - T_1)$$

where P = power in watts, Q_W = flow in gallons per minute, and T_2, T_1 = outlet and inlet water temperatures in degrees Kelvin, respectively.

This same relationship is given in the nomogram of Fig. 6 with the temperature rise in degrees Fahrenheit or Celsius and the power in kilowatts.

Forced Air Cooling

With forced air cooling a stream of air is forced past a suitable radiator. The heat which can be removed by this process is given by

$$P = 169 Q_A [(T_2/T_1) - 1]$$

where Q_A = air flow in feet³/minute, other quantities as above.

Evaporative Cooling

A typical evaporative-cooled system consists of a tube with a specially designed anode immersed in a boiler containing distilled water. When power is dissipated on the anode, the water boils and the steam is conducted upward through an insulating pipe to a condenser. The condensate is then gravity fed back to the boiler, thus eliminating the pump required in a circulating water system.

For some transmitter applications the steam is directed downward to leave the space above the tube available for other components. Such a system requires a pump to return the condensate to the boiler, but even then the pump has to handle only about 0.05 of the amount of water required for a water-cooled system because of the exploitation of the latent heat of steam.

The size of the heat-exchanger equipment for an evaporative-cooled system is less than one-third of that required for a water-cooled system because of the greater mean temperature differential between the cooled liquid and the secondary coolant. Typical temperature differentials for the two systems are 75°C and 30°C, respectively.

The anode dissipation should not exceed 135 watts per square centimeter of external anode surface because at this point, often referred to as the "Leidenfrost" or "calefaction" point, the surface becomes completely covered with a sheath of vapor and the thermal conductivity between the anode and the cooling liquid drops to 30 watts per square centimeter, with resultant overheating of the anode. Special designs of the external anode surface (such as the "pineapple") allow up to 500 watts to be dissipated per square centimeter of internal anode surface.

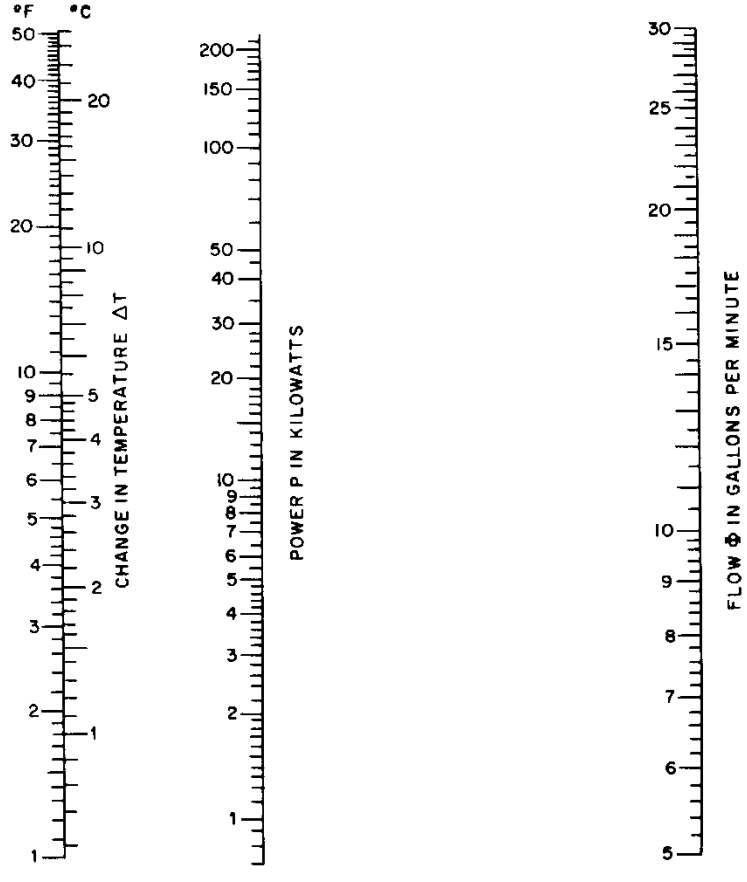

Fig. 6—Heat transfer in cooling water. $P=0.1466\Phi\Delta T$, for T in Fahrenheit.

Conduction Cooling

When an external heat sink is available, heat may be removed from the tube by conduction. Since the electrode where the heat appears is usually at an elevated potential, it is often necessary to conduct the heat through an electrical insulator.

Because of its relatively high thermal conductivity, beryllia ceramic can be used as a common insulator and thermal conductor between the anode of a tube and a heat sink.

Properties of beryllia:

Breakdown strength = 10 kV/mm
Dielectric constant = 6–8
Thermal conductivity = 2.62 watts/cm/°C at 20°C, 1.75 watts/cm/°C at 200°C
Dielectric loss factor = 4×10^{-5}
Tensile strength = 18 000 lbs/square inch
Compressive strength = 150 000 lbs/square inch.

The temperature drop in degrees Celsius across the beryllia ceramic is given by

$$t_1-t_2=dW_a/KA \quad \text{(for a parallel configuration)}$$

where t_1 = temperature of tube anode (typical maximum 250°C), t_2 = temperature of heat sink (typically 100°C), d = thickness of beryllia in cm, A = cross-sectional area of beryllia perpendicular to direction of heat flow, K = thermal conductivity of beryllia in watts/cm/°C, and W_a = power dissipated on anode in watts.

To the temperature drop across the beryllia ceramic must be added the temperature drop across the interfaces between the ceramic and the anode and heat sink, typically 20°C for clamped surfaces at a loading of 25 watts/cm².

Because of its toxic nature, care must be taken in handling and disposal of beryllia ceramic.

Grid Temperature

Operation of grids at excessive temperatures will result in one or more harmful effects: liberation of gas, high primary (thermal) emission, contamination of the other electrodes by deposition of grid material, and melting of the grid. Grid-current ratings should not be exceeded, even for short periods.

NOISE IN TUBES

There are several sources of noise in electron tubes*, some associated with the nature of electron emission and some caused by other effects in the tube.

Shot Effect

The electric current emitted from a cathode consists of a large number of electrons and consequently exhibits fluctuations which produce tube noise and set a limit to the minimum signal that can be amplified. The root-mean-square value of the fluctuating (noise) component of the plate current I_n is given in amperes by

$$I_n^2=2eI\Gamma^2\Delta f$$

where I = plate direct current in amperes, e = electron charge = 1.6×10^{-19} coulomb, Δf = bandwidth in hertz, and Γ^2 = space-charge reduction or smoothing factor. For temperature-limited cases, $\Gamma^2=1$. For space-charge-controlled regions

$$\Gamma^2=2kT_c\theta/\sigma eI$$

where k = Boltzmann's constant = 1.380×10^{-23} joule/degree Kelvin, T_c = cathode temperature in degrees Kelvin, g = conductance or transconductance in mhos, which relates the output signal current to the input signal voltage*, θ = a factor which in most practical cases is nearly equal to its asymptotic value of $3[1-(\pi/4)]=0.644$, and σ = a tube parameter, related to the amplification factor and electrode spacings, which is unity for diodes and varies between 0.5 and 1.0 for negative-grid tubes.

Partition Noise

Excess noise appears in multicollector tubes because of fluctuations in the division of the current between the different electrodes. In a grid-controlled tube, these fluctuations in current division reduce the effectiveness of the space-charge smoothing of the shot noise in the plate current. For a screen-grid tube, the root-mean-square noise currents in the cathode lead, the screen-grid lead, and the plate lead (I_{nk}, I_{nc2}, and I_n, respectively) are given by

$$I_{nk}^2=2eI_k\Gamma^2\Delta f$$

$$I_{nc2}^2=2eI_{c2}[(\Gamma^2I_{c2}+I)/I_k]\Delta f$$

$$I_n^2=2eI[(\Gamma^2I+I_{c2})/I_k]\Delta f$$

where I_k and I_{c2} are the cathode and screen-grid currents, respectively.

Flicker Effect

The mechanism is not completely understood but appears to depend on the field distribution in the surface layer of the cathode due to its porous structure. Because this same field distribution also will influence the cathode activity and temperature, flicker noise will depend on cathode activity and temperature in a complicated manner.

The flicker noise spectrum is usually of the form $f^{-\alpha}$ with α close to unity and thus is important only at low frequencies. The sensitivity of audio, subaudio, and direct-current amplifiers is limited by the flicker noise generated in the first tube.

Collision Ionization

Free gas ions can be generated by collisions with the electron stream. The electrons thus liberated and collected by the anode will appear as noise in the anode circuit. The ions that travel to the cathode will travel slowly through the po-

* For diodes, g is the conductance; for triode and pentode amplifiers, g is the transconductance g_m; and for triode or pentode mixers and converters, g is the conversion conductance g_c.

tential minimum and reduce the space charge, which in turn will reduce the space-charge smoothing effect. This also will increase the noise in the anode circuit.

Induced Noise

At high frequencies it is not necessary for electrons to reach an electrode for induced current to flow in the electrode leads. This noise is an important consideration in miniature tubes above 15 megahertz and becomes the principal limiting factor in low-noise amplifier design above about 100 megahertz. For microwave tubes, this is the dominant method by which beam noise is coupled to the output circuit.

Miscellaneous Noise

Other noise may be present due to microphonics, hum, leakage, charges on insulators, poor contacts, and secondary emission.

Evaluation of Tube Performance

There are two common ways of evaluating tube performance: equivalent noise input resistance value, and noise figure (or factor).

Equivalent Noise Input Resistance: A resistor generates an amount of thermal noise (also called Johnson noise or Brownian motion noise) given by

$$E_n^2 = 4kTR\Delta f$$

where E_n = the open-circuit root-mean-square fluctuating voltage measured across the resistor terminal in volts, T = resistor temperature in degrees Kelvin, and R = resistor resistance in ohms. The equivalent noise input resistance in ohms R_{eq} is defined as that value of resistance which, when connected to the input of the tube and held at room temperature, will double the output noise power. This can be expressed as

$$4kT_0R_{eq}\Delta f g^2 = 2eI\Gamma_{eff}^2\Delta f$$

or

$$R_{eq} = eI\Gamma_{eff}^2/2kT_0g^2$$

where $T_0 = 293°K$, Γ_{eff}^2 = the effective space-charge reduction factor to include partition noise effects, and g = the appropriate transconductance or conversion conductance as before. Practical approximations to R_{eq} are given in Table 8 for several tube functions.

Noise Figure: The noise figure of a tube is defined as the ratio of the available signal-to-noise ratio at the input to the signal-to-noise ratio at the output. It is usually given the symbol F and is always greater than unity. For a more-detailed discussion of noise figure refer to the chapter on "Radio Noise and Interference."

TABLE 8—APPROXIMATE EQUIVALENT NOISE RESISTANCES.

Function	Type	R_{eq}
Amplifying	Triode	$2.5/g_m$
	Pentode	$I/(I+I_{c2}) \times[(2.5/g_m)+(20I_{c2}/g_m^2)]$
Mixing	Triode	$4/g_c$
	Pentode	$I/(I+I_{c2})(4/g_c+20I_{c2}/g_c^2)$
Converting and mixing	Multigrid	$19I(I_k-I)/g_c^2I_k$

Microwave Tubes

The noise appearing in the output circuit of a microwave tube is due in part to induced noise from the beam. Also, some of the electrons may be intercepted by the radio-frequency structure (microwave cavity, slow-wave circuit, et cetera) giving rise to partition noise. In well-designed low-noise tubes, however, this latter effect is kept negligibly small.

For lossless linear beam tubes (traveling-wave amplifiers, klystron amplifiers, backward-wave amplifiers), the minimum obtainable noise figure F_{min} for one-dimensional single-velocity small-signal theory and high gain has been found to be given by

$$F_{min} = 1 + (2\pi/kT_0)(S-\pi)$$

where $S-\pi$ is the basic noise parameter and is established in the region of the potential minimum of the beam. If certain assumptions concerning the potential minimum are made, such as full shot noise and uncorrelated current and velocity fluctuations,* then values for S and π can be obtained. They are given as

$$\pi = 0$$

$$S = [1-(\pi/4)]^{1/2}(kT_c/\pi)$$

therefore

$$F_{min} = 1 + (4-\pi)^{1/2}(T_c/T_0).$$

For $T_c/T_0 = 4$, $F_{min} \approx 4$. The assumptions made are not entirely valid, as shown by the fact that noise figures of less than 4 have been obtained experimentally. At the present time values of S and π/S are obtained by measurement.

LOW- AND MEDIUM-FREQUENCY TUBES

This section applies particularly to triodes and multigrid tubes operated at frequencies where electron-inertia effects are negligible. Traditionally the vacuum envelope of such tubes has been of glass with metal, usually copper, for the anode in larger sizes. In recent years the trend has been toward ceramic in place of glass for the external insulating portions of such tubes. Figure 7 shows a typical construction of a medium-power transmitting tube.

Ceramic-envelope tubes have the following advantages over glass tubes.

(**A**) The radio-frequency loss P_{rf} in the seals of a tube is given by

$$P_{rf} = Kf^{5/2}R^{1/2}\mu^{1/2}$$

where K = constant, f = frequency, R = resistivity of the conducting material, and μ = permeability of the conducting material. In glass-to-metal seals, the metal is normally of a magnetic material such as Kovar. As Kovar has high resistivity and permeability, the radio-frequency losses at the seals are therefore high, and at high frequencies cracking and/or glass suck-in near the seals can result. With ceramic-to-metal seals this problem is minimized because the radio-frequency circulating currents at the seals flow through the metallizing and plating on the ceramic. The resistivity is low, and the permeability is unity.

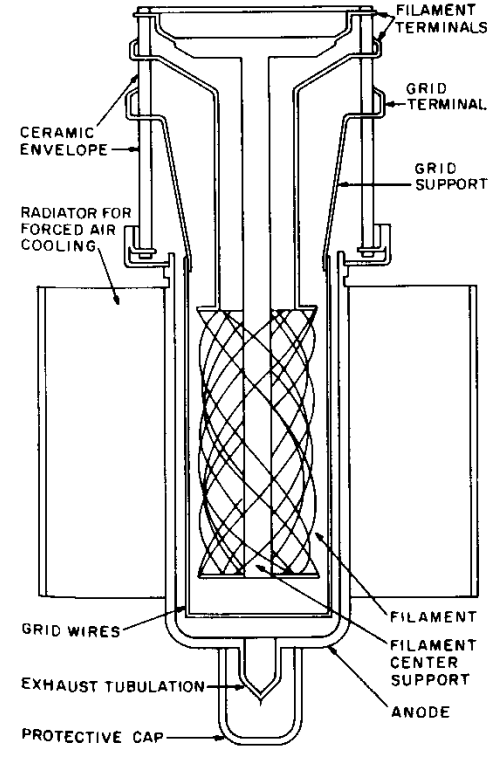

Fig. 7—Electrode arrangement of medium-power external-anode transmitting tube.

(**B**) Ceramics have a lower dielectric loss than glass. Furthermore the loss factor of glass rapidly rises with temperature. This leads to a "runaway" condition, glass suck-in, and hence severe limitation of maximum frequency of operation of glass tubes.

(**C**) The safe operating temperature of a ceramic-to-metal seal may be between 220 and 250 degrees Celsius as against 180 degrees Celsius for Kovar glass seals.

(**D**) High bakeout temperature of ceramic-envelope tubes during evacuation increases reliability and life.

(**E**) Ceramic tubes withstand higher thermal and mechanical shocks than those with glass envelopes. They can also be manufactured to closer dimensional tolerances.

Coefficients

Amplification factor μ: Ratio of incremental plate voltage to control-electrode voltage change at a fixed plate current with constant voltage on other electrodes

$$\mu = \left[\frac{\delta e_b}{\delta e_{c1}}\right]_{\substack{I_b, E_{c2}, \cdots E_{cn} \text{ constant} \\ r_l = 0}}$$

Transconductance s_m: Ratio of incremental plate current to control-electrode voltage change at constant voltage on other electrodes

$$s_m = \left[\frac{\delta i_b}{\delta e_{c1}}\right]_{\substack{E_b, E_{c2}, \cdots, E_{cn} \text{ constant} \\ r_l = 0}}$$

When electrodes are plate and control grid, the ratio is the mutual conductance g_m

$$g_m = \mu/r_p.$$

Variational (AC) Plate Resistance r_p: Ratio of incremental plate voltage to current change at constant voltage on other electrodes

$$r_p = \left[\frac{\delta e_b}{\delta i_b}\right]_{\substack{E_{c1}, \cdots, E_{cn} \text{ constant} \\ r_l = 0}}$$

Total (DC) Plate Resistance R_p: Ratio of total plate voltage to current for constant voltage on

TABLE 9—TUBE CHARACTERISTICS FOR UNIPOTENTIAL CATHODE AND NEGLIGIBLE SATURATION OF CATHODE.

Function	Parallel-Plane Cathode and Anode	Cylindrical Cathode and Anode
Diode anode current (amperes)	$G_1 e_b^{3/2}$	$G_1 e_b^{3/2}$
Triode anode current (amperes)	$G_2[(e_b+\mu e_c)/(1+\mu)]^{3/2}$	$G_2[(e_b+\mu e_c)/(1+\mu)]^{3/2}$
Diode perveance G_1	$2.3\times10^{-6}(A_b/d_b^2)$	$2.3\times10^{-6}(A_b/\beta^2 r_b^2)$
Triode perveance G_2	$2.3\times10^{-6}(A_b/d_b d_c)$	$2.3\times10^{-6}(A_b/\beta^2 r_b r_c)$
Amplification factor μ	$2.7 d_c[(d_b/d_c)-1]/[\rho \log(\rho/2\pi r_g)]$	$(2\pi d_c/\rho)[\log(d_b/d_c)/\log(\rho/2\pi r_g)]$
Mutual conductance g_m	$1.5G_2[\mu/(\mu+1)](E'_g)^{1/2}$	$1.5G_2[\mu/(\mu+1)](E'_g)^{1/2}$
	$E'_g=(E_b+\mu E_c)/(1+\mu)$	$E'_g=(E_b+\mu E_c)/(1+\mu)$

where A_b = effective anode area in square centimeters, d_b = anode-cathode distance in centimeters, d_c = grid-cathode distance in centimeters, β = geometric constant, a function of ratio of anode-to-cathode radius; $\beta^2 \approx 1$ for $r_b/r_k > 10$ (Fig. 9), ρ = pitch of grid wires in centimeters, r_g = grid-wire radius in centimeters, r_b = anode radius in centimeters, r_k = cathode radius in centimeters, and r_c = grid radius in centimeters.

Note:

These equations are based on theoretical considerations and do not provide accurate results for practical structures; however, they give a fair idea of the relationship between the tube geometry and the constants of the tube.

other electrodes

$$R_p=\left[\frac{E_b}{I_b}\right]_{\substack{E_{c1},\cdots,E_{cn}\ \text{constant}\\ r_l=0}}$$

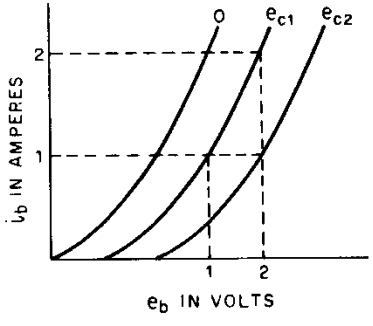

Amplification factor $\mu=(e_{b2}-e_{b1})/(e_{c2}-e_{c1})$
Mutual conductance $g_m=(i_{b2}-i_{b1})/(e_{c2}-e_{c1})$
Total plate resistance $R_p=e_{b2}/i_{b2}$
Variational plate resistance $r_p=(e_{b2}-e_{b1})/(i_{b2}-i_{b1})$.

Fig. 8—Graphic method of determining coefficients.

A useful approximation of these coefficients may be obtained from a family of anode characteristics, Fig. 8. Relationships between the actual geometry of a tube and its coefficients are given roughly in Table 9.

HIGH-FREQUENCY TRIODES AND MULTIGRID TUBES*

When the operating frequency is increased, the operation of triodes and multigrid tubes is affected

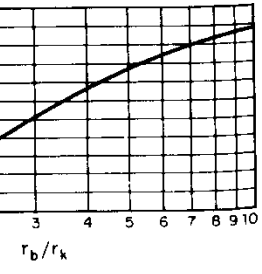

Fig. 9—Values of β^2 for values of $r_b/r_k<10$.

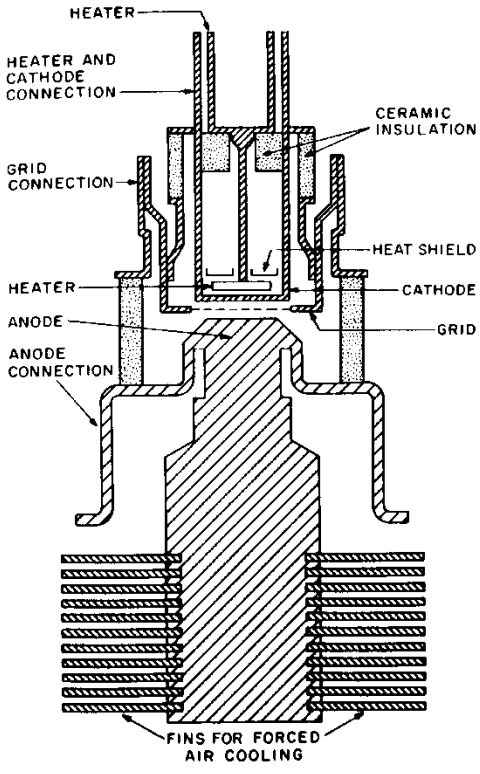

Fig. 10—Electrode arrangement of a small high-frequency external-anode triode.

by electron-inertia effects. The design features that distinguish the high-frequency tube shown in Fig. 10 from the lower-frequency tube (Fig. 7) are: reduced cathode-to-grid and grid-to-anode spacings, high emission density, high power density, small active and inactive capacitances, heavy terminals, short support leads, and adaptability to a cavity circuit.

Factors Affecting Ultra-High-Frequency Operation

Electron Inertia: The theory of electron-inertia effects in small-signal tubes has been formulated; no comparable complete theory is now available for large-signal tubes.

When the transit time of the electrons from cathode to anode is an appreciable fraction of one radio-frequency cycle:

(A) Input conductance due to reaction of electrons with the varying field from the grid becomes appreciable. This conductance, which increases as the square of the frequency, results in lowered gain, an increase in driving-power requirement, and loading of the input circuit.

(B) Grid-anode transit time introduces a phase lag between grid voltage and anode current. In oscillators, the problem of compensating for the phase lag by design and adjustment of a feedback circuit becomes difficult. Efficiency is reduced in both oscillators and amplifiers.

(C) Distortion of the current pulse in the grid-anode space increases the anode-current conduction angle and lowers the efficiency.

Electrode Admittances: In amplifiers, the effect of cathode-lead inductance is to introduce a conductance component in the grid circuit. This effect is serious in small-signal amplifiers because the loading of the input circuit by the conductance current limits the gain of the stage. Cathode-grid and grid-anode capacitive reactances are of small magnitude at ultra-high frequencies. Heavy currents flow as a result of these reactances and tubes must be designed to carry the currents without serious loss. Coaxial cavities are often used in the circuits to resonate with the tube reactances and to minimize resistive and radiation losses. Two circuit difficulties arise as operating frequencies increase:

(A) The cavities become physically impossible as they tend to take the dimensions of the tube itself.

(B) Cavity Q varies inversely as the square root of the frequency, which makes the attainment of an optimum Q a limiting factor.

Scaling Factors: For a family of similar tubes, the dimensionless magnitudes such as efficiency are constant when the parameter

$$\phi=fd/V^{1/2}$$

is constant, where f = frequency in megahertz, d = cathode-to-anode distance in centimeters, and V = anode voltage in volts.

Based on this relationship and similar considerations, it is possible to derive a series of factors that determine how operating conditions will vary as the operating frequency or the physical dimensions are varied (Table 10). If the tube is to be scaled exactly, all dimensions will be reduced inversely as the frequency is increased, and operating conditions will be as given in the "Size-Frequency Scaling" column. If the dimensions of the tube are to be changed but the operating frequency maintained, operation will be as in the "Size Scaling" column. If the dimensions are to be maintained but the operating frequency changed, operating conditions will be as in the "Frequency Scaling" column. These factors apply in general to all types of tubes.

TABLE 10—SCALING FACTORS FOR ULTRA-HIGH-FREQUENCY TUBES.

Quantity	Ratio	Size-Frequency Scaling	Size Scaling	Frequency Scaling
Voltage	V_2/V_1	1	d^2	f^2
Field	E_2/E_1	f	d	f^2
Current	I_2/I_1	1	d^2	f^2
Current density	J_2/J_1	f^2	d	f^2
Power	P_2/P_1	1	d^5	f^5
Power density	h_2/h_1	f^2	d^3	f^6
Conductance	G_2/G_1	1	d	f
Magnetic-flux density	B_2/B_1	f	1	f

d = ratio of scaled to original dimensions
f = ratio of original to scaled frequency

With present knowledge and techniques, it has been possible to reach certain values of power with conventional tubes in the ultra- and super-high-frequency regions. The approximate maximum values that have been obtained are plotted in Fig. 11.

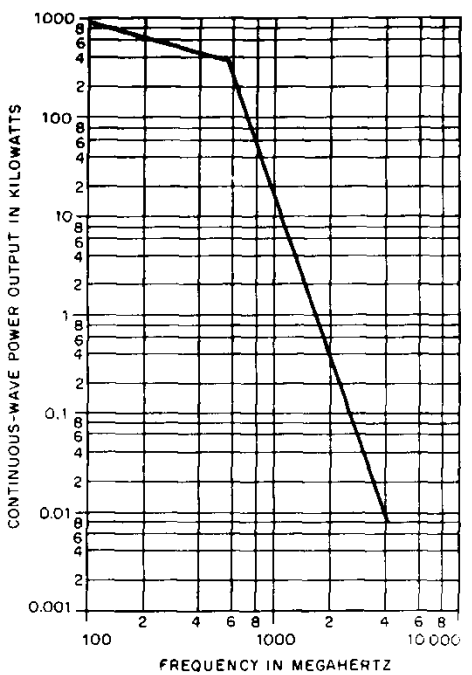

Fig. 11—Approximate maximum ultra-high-frequency continuous-wave power obtainable from a single triode or tetrode. These data are based on 1965 knowledge and techniques.

MICROWAVE TUBES*

The reduced performance of space-charge control tubes in the microwave region has fostered the development of other types of tubes for use as oscillators and amplifiers at microwave frequencies. Such tubes generally function on the basis of the modulation of the velocity of an electron stream rather than of its density. They may be roughly divided simply into linear beam devices and crossed-field devices. In the former the electron stream flows essentially linearly, often with a collimating magnetic field to counteract space-charge spreading; in the latter the electron stream follows a curved path under the action of orthogonal electric and magnetic fields. The linear beam devices are often referred to as *O*-type, while the crossed-field devices are referred to as *M*-type.

Terminology

Bunching: Any process that introduces a radio-frequency conduction-current component into a velocity-modulated electron stream as a direct result of the variation in electron transit time that the velocity modulation produces.

Cavity Resonator: Any region bounded by conducting walls within which resonant electromagnetic fields may be excited.

Circuit Efficiency: The ratio of (A) the power of the desired frequency delivered to the output terminals of the circuit of an oscillator or amplifier to (B) the power of the desired frequency delivered by the electron stream to the circuit.

Coherent-Pulse Operation: Method of pulse operation in which the phase of the radio-frequency wave is maintained through successive pulses.

Drift Space: In an electron tube, a region substantially free of externally applied alternating fields in which a relative repositioning of the electrons is determined by their velocity distributions and the space-charge forces.

Duty Cycle: The product of the pulse duration and the pulse repetition rate. It is also the ratio of the average power output to the peak power output.

External Q: The reciprocal of the difference between the reciprocals of the loaded and unloaded *Q*'s.

Frequency Pulling of an oscillator is the change in the generated frequency caused by a change of the load impedance.

Frequency Pushing of an oscillator is the change in frequency due to change in anode current (or in anode voltage).

Loaded Q of a specific mode of resonance of a system is the *Q* when there is external coupling to that mode. Note: When the system is connected to the load by means of a transmission line, the loaded *Q* is customarily determined when the line is terminated in its characteristic impedance.

Mode: One of the components of a general configuration of a vibrating system. A mode is characterized by a particular geometric pattern of the electromagnetic field and a resonant frequency (or propagation constant).

Noise Figure: The ratio in decibels of the total available output noise from an amplifier to the available noise which would be present at the output if the amplifier itself were noiseless, assuming a source temperature of 290°K.

Pulling Figure of an oscillator is the difference in megahertz between the maximum and minimum frequencies of oscillation obtained when the phase angle of the load-impedance reflection coefficient varies through 360 degrees, while the absolute value of this coefficient is constant and is normally equal to 0.20.

Pulse: Momentary flow of energy of such short time duration that it may be considered as an isolated phenomenon.

Pushing Figure of an oscillator is the rate of frequency pushing in megahertz per ampere or megahertz per volt.

Q: The *Q* of a specific mode of resonance of a system is 2π times the ratio of the stored electromagnetic energy to the energy dissipated per cycle when the system is excited in this mode.

Reflector: Electrode whose primary function is to reverse the direction of an electron stream. It is also called a *repeller*.

Reflex Bunching: Type of bunching that occurs when the velocity-modulated electron stream is made to reverse its direction by means of an opposing direct-current field.

Slow-Wave Structure: A microwave circuit, as used in beam-type microwave tubes, capable of propagating radio-frequency waves with phase velocities appreciably less than the velocity of light.

LINEAR BEAM TUBES

The principal types of linear beam tubes are the klystron, the traveling-wave amplifier, and the backward-wave oscillator.

Klystrons

A klystron* is an electron tube in which the following processes may be distinguished:

(A) Periodic variations of the longitudinal velocities of the electrons forming the beam in a region confining a radio-frequency field.

(B) Conversion of the velocity variation into conduction-current modulation by motion in a region free from radio-frequency fields.

(C) Extraction of the radio-frequency energy from the beam in another confined radio-frequency field.

The transit angles in the confined fields are made short ($\delta \doteqdot \pi/2$) so that there is no appreciable conduction-current variation while traversing them.

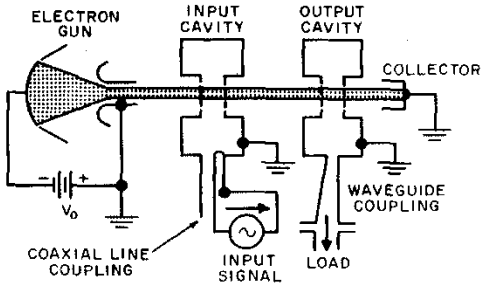

Fig. 12—Two-cavity klystron amplifier. *J. W. Gewartowski and H. A. Watson, "Principles of Electron Tubes," 1965: p. 296. Courtesy of D. Van Nostrand Company, Inc.*

Several variations of the basic klystron exist. Of these, the simplest is the 2-cavity amplifier or oscillator. The most important is the reflex klystron, used as a low-power oscillator. The multicavity high-power amplifier is also important.

Two-Cavity Klystron Amplifiers: An electron beam is formed in an electron gun and passed through the gaps associated with the two cavities (Fig. 12). After emerging from the second gap, the electrons pass to a collector designed to dissipate the remaining beam power without the production of secondary electrons. In the first gap, the electron beam is alternately accelerated and decelerated in succeeding half-periods of the radio-frequency cycle, the magnitude of the change in speed depending on the magnitude of the alternating voltage impressed on the cavity. The electrons then move in a drift space where there are no radio-frequency fields. Here, the electrons that were accelerated in the input gap during one half-cycle catch up with those that were decelerated in the preceding half-cycle, and a local increase of current density occurs in the beam. Analysis shows that the maximum of the current-density wave occurs at the position, in time and space, of those electrons that passed the center of the input gap as the field changed from negative to positive. There is therefore a phase difference of $\pi/2$ between the current wave and the voltage wave that produced it. Thus at the end of the drift space, the initially uniform electron beam has been altered into a beam showing periodic density variations. This beam now traverses the output gap and the variations in density induce an amplified voltage wave in the output circuit, phased so that the negative maximum corresponds with the phase of the bunch center. The increased radio-frequency energy has been gained by conversion from the direct-current beam energy.

The 2-cavity amplifier can be made to oscillate by providing a feedback loop from the output to the input cavity, but a much simpler structure results if the electron beam direction is reversed by a negative electrode, termed the reflector.

*Reflex Klystrons**: A schematic diagram of a reflex klystron is shown in Fig. 13. The velocity-modulation process takes place as before, but analysis shows that in the retarding field used to reverse the direction of electron motion, the phase of the current wave is exactly opposite to that in the 2-cavity klystron. When the bunched beam returns to the cavity gap, a positive field extracts maximum energy from the beam, since the direction of electron motion has now been reversed. Consideration of the phase conditions shows that for a fixed cavity potential, the reflex klystron will oscillate only near certain discrete values of reflector voltage for which the transit time measured from the gap center to the reflection point and back is given by

$$\omega\tau = 2\pi(N + \tfrac{3}{4})$$

where N is an integer called the mode number.

By varying the reflector voltage around the value corresponding with the mode center, it is possible to vary the oscillation frequency by a small percentage. This fact is made use of in providing automatic frequency control or in frequency-modulation transmission.

Reflex-Klystron Performance Data: The performance data for a reflex klystron are usually given in the form of a reflector-characteristic chart. This

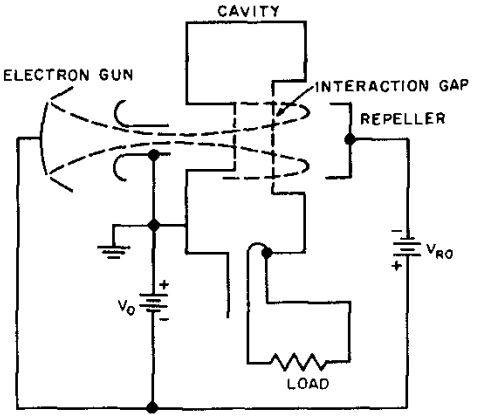

Fig. 13—Schematic of reflex klystron with power supply.

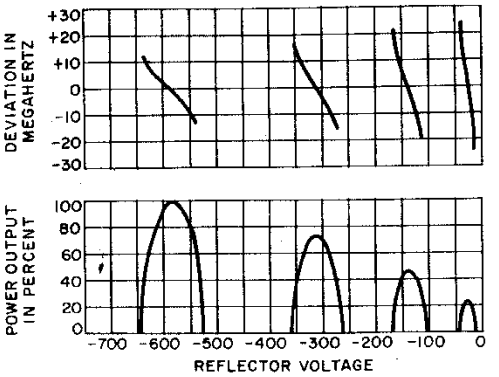

Fig. 14—Klystron reflector characteristic chart. *Courtesy of Sperry Gyroscope Company.*

chart displays power output and frequency deviation as a function of reflector voltage. Several modes are often displayed on the same chart. A typical chart is shown in Fig. 14.

There are two rather distinct classes of reflex klystrons in current large-scale manufacture (Table 11).

(**A**) Low-power tubes suitable for use in local-oscillator service, maser pumping, antenna-pattern testing, or similar applications. These tubes have power outputs in the range of 10 milliwatts to 1 to 2 watts. Typically, for local-oscillator service, a power of 10 to 100 milliwatts is necessary to operate crystal mixers with the required degree of isolation. For such applications as antenna testing or pumping of cryogenically cooled masers, power of 500 milliwatts to 2 watts is usually required. The electronic tuning range required is about 50 megahertz independent of center frequency, but the linearity of the Δf versus ΔV_r characteristic is relatively unimportant.

(**B**) Tubes as frequency modulators in microwave links. These usually require considerably greater power, up to about 10 watts, and the linearity of the Δf versus ΔV_r characteristic over a limited (for example 10-megahertz) excursion is of primary importance as this parameter determines the harmonic margins in the system. Second-harmonic margins of −96 decibels for deviations of 125 kilohertz have been observed; the third-harmonic margins are about −120 decibels.

Multicavity Klystrons: Multicavity klystrons* have been perfected for use in two rather different fields of application: applications requiring extremely high pulse powers and continuous-wave systems in which moderate powers (tens of kilowatts) are required. An example of the first application is a power source for nuclear-particle acceleration, while ultra-high-frequency television and troposcatter transmitters are examples of the latter.

A multicavity klystron amplifier is shown schematically in Fig. 15. The example shown has 3 cavities all coupled to the same beam. The radio-frequency input modulates the beam as before. The bunched beam induces an amplified voltage across the second cavity, which is tuned to the operating frequency. This amplified voltage remodulates the beam with a certain phase shift and the now more-strongly bunched beam excites a highly amplified wave in the output circuit.

TABLE 11—CLASSES OF REFLEX KLYSTRONS.

Frequency (MHz)	Power Output (mW)	Useful Mode Width Δf_{3db} (MHz)	Operating Voltage
	Local oscillators		
3 000	150	40	300
9 000	40	40	350
24 000	35	120	750
35 000	>15	50	2000
50 000	10–20	60–140	600
	Maser pumps		
35 000	500–1500	70	2000
45 000	500–1000	80	2000
	Frequency-modulation transmitters		
4 000	10 000	40	1100
7 000	10 000	37	750
9 000	6 000	60	500

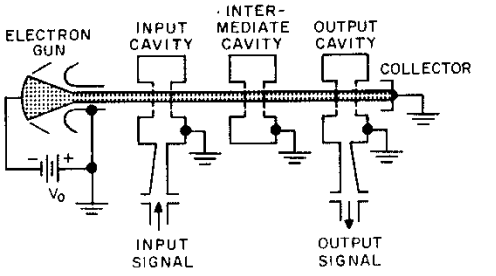

Fig. 15—Three-cavity klystron amplifier.

It is found that the optimum power output is obtained when the second cavity is slightly detuned. Moreover, when increased bandwidth is required, the second cavity may be loaded with a resultant lowering in overall gain. Modern multicavity klystrons use magnetically focused high-perveance beams, and under these conditions high gains, large power outputs, and reasonable values of efficiency are readily obtained.

Continuous-wave multicavity klystrons are available with outputs of around 10 kilowatts at frequencies up to 5000 megahertz. The efficiencies are of the order of 30 percent and the gains vary between 20 and 50 decibels, according to the number of cavities, bandwidth, et cetera. Pulsed tubes have been designed for outputs of 30 megawatts and with efficiencies of over 40 percent at frequencies near 3000 megahertz.

Traveling-Wave Tubes

The traveling-wave tube* differs from the klystron in that the radio-frequency field is not confined to a limited region but is distributed along a wave-propagating structure. A longitudinal electron beam interacts continuously with the field of a wave traveling along this wave-propagating structure. In its most common form it is an amplifier, although there are related types of tubes that are basically oscillators.

The principle of operation may be understood by reference to Fig. 16. An electron stream is produced by an electron gun, travels along the axis of the tube, and is finally collected by a suitable electrode. Spaced closely around the beam is a circuit, in this case a helix, capable of propagating a slow wave. The circuit is proportioned so that the phase velocity of the wave is small with respect to the velocity of light. In typical low-power tubes, a value of the order of one-tenth of the velocity of light is used; for higher-power tubes the phase velocity may be two or three times higher. Suitable means are provided to couple an external radio-

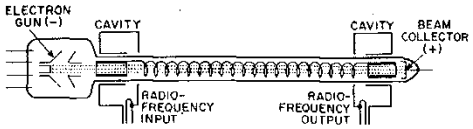

Fig. 16—Basic helix traveling-wave tube. The magnetic beam-focusing system between input and output cavities is not shown.

frequency circuit to the slow-wave structure at the input and output. The velocity of the electron stream is adjusted to be approximately the same as the axial phase velocity of the wave on the circuit.

When a wave is launched on the circuit, the longitudinal component of its field interacts with the electrons traveling in approximate synchronism with it. Some electrons will be accelerated and some decelerated, resulting in a progressive rearrangement in phase of the electrons with respect to the wave. The electron stream, thus modulated, in turn induces additional waves on the helix. This process of mutual interaction continues along the length of the tube with the net result that direct-current energy is given up by the electron stream to the circuit as radio-frequency energy, and the wave is thus amplified.

By virtue of the continuous interaction between a wave traveling on a broad-band circuit and an electron stream, traveling-wave tubes do not suffer the gain-bandwidth limitation of ordinary types of electron tubes. By proper circuit design, such tubes are made to have bandwidths of an octave in frequency, and even more in special cases.

The helix is an extremely useful form of slow-wave circuit because the impedance that it presents to the wave is relatively high and because, when properly proportioned, its phase velocity is almost independent of frequency over a wide range.

An essential feature of this type of tube is the approximate synchronism between the electron stream and the wave. For this reason, the traveling-wave tube will operate correctly over only a limited range in voltage. Practical considerations require that the operating voltages be kept as low as is consistent with obtaining the necessary beam input power; the voltage, in turn, dictates the phase velocity of the circuit. The electron velocity v in centimeters/second is determined by the accelerating voltage V in accordance with

$$v = 5.93 \times 10^7 V^{1/2}.$$

Figure 17 shows a typical relationship between gain and beam voltage. The gain G of a traveling-wave tube is given approximately by

$$G = A + BCN$$

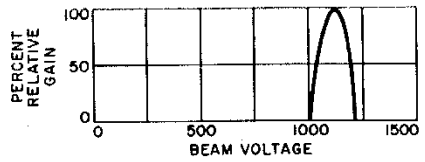

Fig. 17—Traveling-wave-tube gain versus accelerating voltage.

in decibels, where A = the initial loss due to the establishment of the modes on the helix and lies in the range from −6 to −9 decibels, B = a gain coefficient that accounts for the effect of circuit attenuation and space charge, C = a gain parameter that depends on the impedances of the circuit and the electron stream = $[(E^2/(\omega/v)^2P) \times (I_0/8V_0)]^{1/8}$, I_0 = beam current, V_0 = beam voltage, N = number of active wavelengths in tube = $(l/\lambda_0)(c/v)$, l = axial length of the helix, λ_0 = free-space wavelength, v = phase velocity of wave along tube, and c = velocity of light. The term $E^2/(\omega/v)^2P$ is a normalized wave impedance that may be defined in a number of ways.

In practice, the attenuation of the circuit will vary along the tube, and consequently the gain per unit length will not be constant. The total gain will be a summation of the gains of various sections of the tube.

Commonly, C is of the order of 0.02 to 0.2 in helix traveling-wave tubes. The gain of low- and medium-power tubes varies from 20 to 70 decibels with 30 decibels being a common value. The gain in a tube designed to produce appreciable power will vary somewhat with signal level when the beam voltage is adjusted for optimum operation. Figure 18 shows a typical characteristic.

To restrain the physical size of the electron stream as it travels along the tube, it is necessary to provide a focusing field, either magnetic or electrostatic, of a strength appropriate to overcome the space-charge forces that would otherwise cause

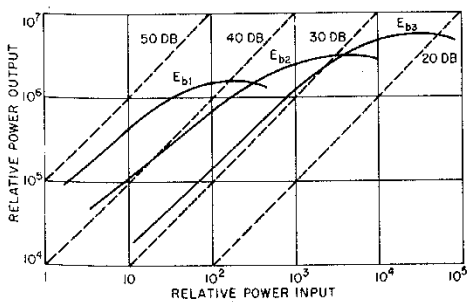

Fig. 18—Gain of traveling-wave tube as a function of input level and beam voltage. $E_{b1} < E_{b2} < E_{b3}$.

the beam to spread. Until fairly recently a longitudinal magnetic field supplied by a solenoid electromagnet was used for this purpose. Continuing demands for improved efficiency and reliability, and for weight and size reduction, however, have forced the development of permanent magnet-type focusing structures. At the present time, focusing by periodically reversing magnetic fields produced by permanent magnet structures is rapidly becoming predominant.

Several techniques for electrostatic containment of the electron stream have also been developed. Typical is the use of a bifilar helix slow-wave structure where an appropriate voltage difference between the helices provides, in effect, a distributed Einzel lens. Because of voltage breakdown problems as well as increased power supply requirements, electrostatic focusing has not yet proved practical for use in linear beam tubes.

Other types of slow-wave circuits in addition to the helix are possible, including a number of periodic structures. In general, such designs are capable of operation at higher power levels but at the expense of bandwidth.

Traveling-Wave-Tube Performance Data

Traveling-wave tubes are designed to emphasize particular inherent characteristics for specific applications. Three general classes are distinguished.

Low-Noise Amplifiers: Tubes of this class are intended for the first stage of a receiver and are proportioned to have the best possible noise figure. This requires that the random variations in the electron stream be minimized and that steps be taken also to minimize partition noise. Tubes have been made for commercial use with noise figures as low as 3 decibels in S-band and 6 decibels or less over the entire range from 1000 to 12 000 megahertz. Gains of from 20 to 35 decibels are typical. The maximum power output is generally not more than a few milliwatts. Performance of this order can be achieved with either permanent-magnet or electromagnet focusing structures. Recently a new class of tubes has been developed which offers medium-power performance (1 to 5 watts) with reasonable low-noise performance (noise figures of 10 to 14 decibels).

Intermediate Power Amplifiers: These tubes are intended to provide power gain under conditions where neither noise nor large values of power output are important. Gains of 30 or more decibels are customary and the maximum output power is usually in the range from 100 milliwatts to 1 watt.

Power Amplifiers: For this class of tubes, the application is usually the output stage of a transmitter; the power output, either continuous-wave

or pulsed, is of primary importance. Much active development continues in this area and the values of power obtainable are steadily increasing. At present, continuous-wave powers range from tens of kilowatts in the ultra-high-frequency region to more than 100 watts at 10 000 megahertz. Tubes especially designed for pulsed operation provide considerably higher power. Several megawatts of peak power have been achieved at 3000 megahertz. Efficiencies in excess of 30 percent have been obtained and this may be further enhanced by recently developed collector-depression techniques. Power gains of 30 to 50 decibels are normal.

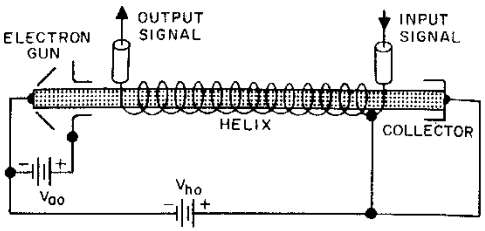

Fig. 19—A traveling-wave tube in operation as a backward-wave amplifier. A separate power supply connected to the anode permits beam-current control independent of the helix voltage.

Backward-Wave Oscillators

A member of the traveling-wave-tube family, the *O*-type backward-wave oscillator,* makes use of the interaction of the electron stream with a radio-frequency circuit wave whose phase and group velocities are 180° apart. The group velocity, and thus the direction of energy flow, is directly opposed to the direction of electron motion. Figure 19 shows schematically a backward-wave tube with connection to both ends of the slow-wave structure, so that operation as either oscillator or amplifier could be achieved. An electron beam is produced by the electron gun, traverses the slow-wave structure, and is dissipated in the collector structure. During its transit the beam is confined by a longitudinal magnetic field. With a beam current of sufficient magnitude, the beam-structure interaction will produce oscillations and microwave power will be delivered from the end of the structure adjacent to the electron gun. At beam-current levels below the "start-oscillation" value, a radio-frequency signal may be introduced at the collector end of the device and the tube will operate as an amplifier.

To improve interaction efficiency, electron beams with hollow cross sections are usually used. This places all the electrons as close as possible to the slow-wave structure in the region of maximum radio-frequency field. The reason here is that the strength of the -1 space harmonic field goes to zero on the axis. To produce this hollow-cross-section beam it is necessary to use magnetically confined electron flow from the cathode, and thus the electron gun is entirely immersed in the magnetic field.

O-type backward-wave devices are voltage tunable, with the frequency being porportional to the $\frac{1}{2}$ power of the cathode-helix voltage as well as dependent on the dimensions of the structure. Typically, tuning over full octave range is possible and in special cases a range of 2 or more octaves can be achieved. However, where confined limits are desired on power variation or other special characteristics, more-restricted frequency ranges may be necessary. Where full octave tuning is used, power output variation of 6 to 10 decibels across the range is usual. In most cases a separate control element in the gun permits adjustment of beam-current amplitude and thus provides control of power output. Oscillators of this type have very low pulling figures but the pushing figure is often substantial. Frequency stability is generally excellent, with the achievable value normally depending on power supply capabilities rather than inherent tube limitations.

O-type backward-wave oscillators are generally low-power devices, with 10 to 50 milliwatts being typical. However, in the range from 1 to 4 gigahertz up to several hundred milliwatts is feasible, while in the range from 50 to 100 gigahertz 5 to 10 milliwatts is relatively difficult to achieve reliably. Typical performance for low-power helix-type permanent-magnet-focused backward-wave oscillators is listed in Table 12.

TABLE 12—PERFORMANCE OF TYPICAL LOW-POWER BACKWARD-WAVE OSCILLATORS.

Frequency Range (GHz)	Tuning Voltage (V)	Cathode Current (mA)	Minimum Power Output (mW)
1.0–2.0	250–1150	15	100
2.0–4.0	300–1800	10	100
4.0–8.0	250–2400	12	25
5.3–11.0	245–2400	10	25
8.0–12.4	550–2400	10	25

Electron-Beam Parametric Amplifiers

Parametric amplification occurs through a time-varying or nonlinear parameter of the system. A simple mechanical example is a child pumping up a swing. He gives energy to the swing amplitude by raising and lowering his center of gravity at twice the swing frequency. The time-varying parameter is the effective length of the swing.

Parametric amplifiers differ from usual amplifiers in the frequency of the energy source; for parametric amplifiers the energy comes from a high-frequency source whereas for the usual amplifier it comes from a direct-current source. There normally are 3 frequencies associated with parametric amplifiers: the signal frequency f_s; the energy source or pump frequency f_p; and the difference or idler frequency $f_i = f_p - f_s$. Although no energy is supplied at f_i, a circuit must be provided to support this frequency. Four-frequency parametric amplifiers, where the fourth frequency is a second idler or a second pump frequency, have been made. The advantage of this device is that the pump frequency (frequencies) can be lower than the signal frequency. The disadvantage is that a fourth circuit must be provided. Two-frequency (degenerate) parametric amplifiers, in which $f_p = 2f_s$ so that $f_i = f_s$, are the common form of the electron-beam devices. (The child in the swing is a version of the degenerate parametric amplifier.) The advantage of the degenerate parametric amplifier is that only 2 circuits need to be provided—1 for the signal frequency and 1 for the pump frequency. The disadvantage is that the phasing between the signal and pump must be adjusted precisely. In each of the foregoing cases, the ratios of the powers at the several frequencies are governed by the Manley–Rowe relations.*

The parametric amplifier's principal virtue is its low-noise behavior. It has this feature in common with the maser to which it bears a superficial resemblance.

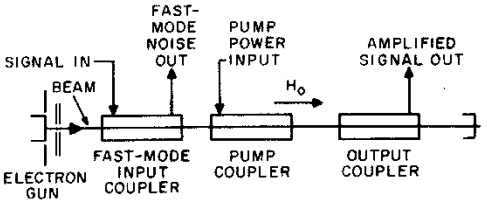

Fig. 20—Block diagram of *O*-type parametric amplifier.

Electron-beam parametric amplifiers are, for the most part, linear beam (*O*-type) devices, although crossed-field (*M*-type) devices have been built.* The usual *O*-type amplifier, such as the traveling-wave tube, uses the coupling between a circuit and the slow space-charge wave on the beam to obtain gain. Since this wave carries negative kinetic power, it is not possible to couple the noise on this wave out of the beam. For parametric amplification, it is necessary to use either the fast space-charge wave or the fast cyclotron wave. Because these waves carry positive kinetic power, it is possible (theoretically) to couple all the noise on these waves out of the beam.

A block diagram of an *O*-type parametric amplifier is shown in Fig. 20. A microwave tube version of this block diagram is shown in Fig. 21. This device has 20-decibel gain at 4140 megahertz with a bandwidth of 67 megahertz and a double-channel noise figure of 2.4 decibels. The tube uses the fast

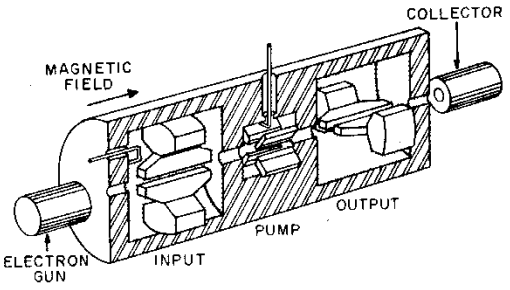

Fig. 21—Cross section of a microwave *O*-type parametric amplifier.

cyclotron wave, and the input and output are microwave forms of the Cuccia coupler.*

Crossed-Field Tubes

The earliest type of crossed-field tube† was the magnetron oscillator. The carcinotron oscillator and the crossed-field amplifier have been developed more recently. Crossed-field tubes generally operate with higher conversion efficiencies than linear beam devices, making them especially attractive for high-power applications.

Magnetrons

A magnetron‡ is a high-vacuum tube containing a cathode and an anode, the latter usually divided into two or more segments. A constant magnetic field modifies the space-charge distribution and the current-voltage relations. In modern usage, the term "magnetron" refers to the magnetron oscillator in which the interaction of the electronic space charge with the resonant system converts direct-current power into alternating-current power, usually at microwave frequencies.

Many forms of magnetrons have been made in the past and several kinds of operation have been employed. The type of tube that is now almost universally employed is the multicavity magnetron generating traveling-wave oscillations. It possesses the advantages of good efficiency at high frequencies, capability of high outputs either in pulsed or continuous-wave operation, moderate magnetic-field requirements, and good stability of operation. A section through the basic anode structure of a typical magnetron is shown in Fig. 22.

In magnetrons, the operating frequency is determined by the resonant frequency of the separate cavities arranged around the central cylindrical cathode and parallel to it. A high direct-current potential is placed between the cathode and the cavities, and radio-frequency output is brought out through a suitable transmission line or waveguide usually coupled to one of the resonator cavities. Under the action of the radio-frequency voltages across these resonators and the axial magnetic field, the electrons from the cathode form a bunched space-charge cloud that rotates around the tube axis, exciting the cavities and maintaining their radio-frequency voltages.

Magnetron Performance Data

The performance data for a magnetron are usually given in terms of two diagrams, the performance chart and the Rieke diagram.

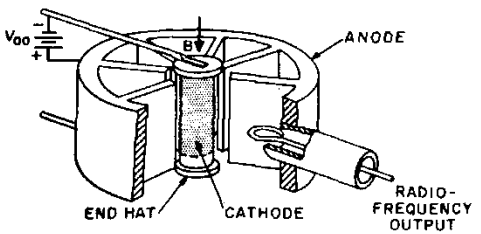

Fig. 22—Magnetron oscillator.

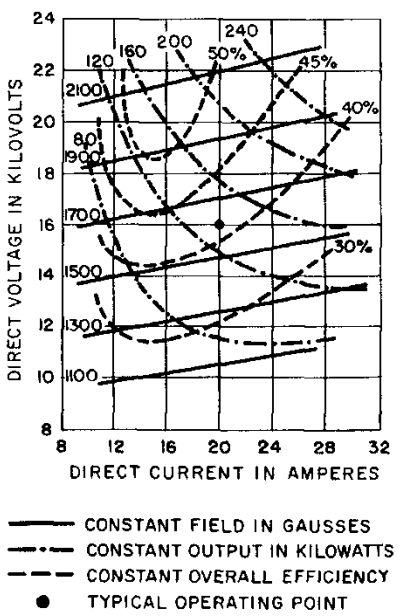

Fig. 23—Performance chart for pulsed magnetron.

Performance Chart: This is a plot of anode current along the abscissa and anode voltage along the ordinate of rectangular-coordinate paper. For a fixed typical tube load, pulse duration, pulse-repetition rate, and setting of the tuner of tunable tubes; lines of constant magnetic field, power output, efficiency, and frequency may be plotted over the complete operating range of the tube. Regions of unsatisfactory operation are indicated by cross hatching. For tunable tubes, it is customary to show performance charts for more than one setting of the tuner. In the case of magnetrons with attached magnets, curves showing the variation of anode voltage, efficiency, frequency, and power output with change in anode current are given. A typical chart for a magnetron having 8 resonators is given in Fig. 23.

Rieke Diagram: This shows the variation of power output, anode voltage, efficiency, and frequency with changes in the voltage standing-wave ratio and phase angle of the load for fixed typical operating conditions such as magnetic field, anode current, pulse duration, pulse-repetition rate, and the setting of the tuner for tunable tubes. The Rieke diagram is plotted on polar coordinates, the radial coordinate being the reflection coefficient measured in the line joining the tube to the load, and the angular coordinate being the angular distance of the voltage standing-wave minimum from a suitable reference plane on the output terminal. On the Rieke diagram, lines of constant frequency, anode voltage, efficiency, and output may be drawn (Fig. 24).

Magnetrons for pulsed operation have been built to deliver peak powers ranging from 3 megawatts at 3000 megahertz to 100 kilowatts at 30 000 megahertz. Continuous-wave magnetrons having outputs ranging from 1 kilowatt at 3000 megahertz to a few watts at 30 000 megahertz have been produced. Operation efficiencies up to 60 percent at 3000 megahertz are obtained, falling to 30 percent at 30 000 megahertz.

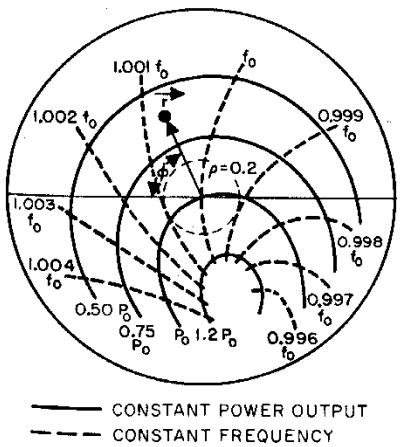

Fig. 24—Rieke diagram.

Carcinotron

The carcinotron is an *M*-type backward-wave oscillator in which the electron stream traverses the tube and interacts with the fields on the slow-wave structure under conditions where the electric and magnetic fields are perpendicular to each other. Figure 25 shows schematically a linear version of the carcinotron. In the electron gun, current is drawn from the cathode when the accelerator voltage is applied. Because of the presence of the magnetic field, directed as shown, the electron paths are curved approximately 90° so that they enter the interaction region between the slow-wave structure and the sole. If the voltages and the magnetic field strength are proper, the electrons will travel along a path approximately parallel to the structure until they reach the collector.

Although Fig. 25 shows a linear arrangement, carcinotrons are conventionally designed in a circular arrangement to conserve magnet size and weight. In this arrangement, the sole approximates the appearance of the cathode of a magnetron and the slow-wave structure is in the position of the magnetron anode, but neither the sole nor the structure are re-entrant.

The carcinotron performance is similar to that of the *O*-type backward-wave oscillator but it offers several of the advantages of crossed-field devices. High-efficiency operation is possible with

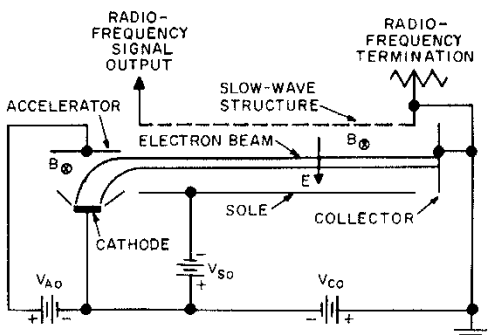

Fig. 25—Linear version of an *M*-carcinotron oscillator.

values of 20 to 30 percent being readily obtained. This efficiency capability makes the carcinotron useful as a high-power device with continuous-wave capabilities of hundreds of watts through X-band. Its construction is such as to permit direct scaling to very-high frequencies, with several milliwatts of power having been achieved at frequencies beyond 300 gigahertz.

The carcinotron, like the *O*-type backward-wave oscillator, is voltage-tunable with the oscillation frequency being approximately directly proportional to the cathode slow-wave-structure voltage. This linear relationship simplifies the associated electronic tuning circuit considerably. Frequency pushing is also considerably lower than in *O*-type backward-wave oscillators. The *M*-type carcinotron has the disadvantage, however, that it is relatively noisy, with spurious power output often not more than 10 to 15 decibels below the main signal output.

In addition to obvious usage as high-power tunable signal sources, carcinotrons with their high noise may be used as electronic countermeasure jamming sources.

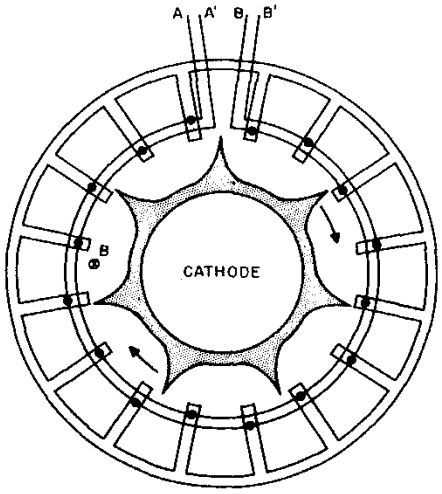

Fig. 26—Schematic drawing of a crossed-field amplifier.

Crossed-Field Amplifiers

Crossed-field amplifiers as a general class of tubes are mechanically quite similar to the crossed-field oscillator or magnetron. As may be seen from Fig. 26, the major difference is that the slow-wave structure is not re-entrant whereas in the magnetron both the beam and the circuit are re-entrant.

Referring to Fig. 26, voltage and magnetic field are applied as for the magnetron. A radio-frequency signal is applied to the structure and progresses in a clockwise direction toward the output terminal. Current spokes, produced in the cathode-circuit region by the radio-frequency electric fields, also progress in a clockwise direction synchronously with the circuit wave. The interaction between the beam and circuit wave results in a growing of the circuit wave and thus gain. If desired, interaction with a backward mode may also be accomplished with this device.

Since the beam is re-entrant, the crossed-field amplifier will oscillate if the circuit gain becomes high. Gain is usually limited to 10 to 15 decibels. If only a portion of the circumference is used for the slow-wave structure and a drift area is left between the two ends of the structure, the feedback mechanism is disrupted and gains of 15 to 20 decibels may be realized.

The power output of the crossed-field amplifier is essentially independent of the radio-frequency drive signal and it thus operates as a saturated amplifier. This characteristic makes it unsuitable for amplifying amplitude-modulated signals.

Crossed-field amplifiers offer the advantage of relatively high efficiency, 40 to 60 percent or even higher, and they may be designed to provide very high peak output powers. Their disadvantages are their low gain, limited bandwidth, high noise, and saturated-amplifier characteristic.

GAS TUBES

Ionization

A gas tube is an electron tube in which the pressure of the contained gas is such as to affect substantially the electrical characteristics of the tube. Such effects are caused by collisions between moving electrons and gas atoms. These collisions, if of sufficient energy, may dislodge an electron from the atom, thereby leaving the atom as a positive ion. The electron space charge is effectively neutralized by these positive ions and comparatively high free-electron densities are easily created.

Table 13—Ionization Properties of Gases.

Gas	Ionization Energy (volts)	Collision Probability P_c
Helium	24.5	12.7
Neon	21.5	17.5
Nitrogen	16.7	37.0
Hydrogen (H_2)	15.9	20.0
Argon	15.7	34.5
Carbon monoxide	14.2	23.8
Oxygen	13.5	34.5
Krypton	13.3	45.4
Water vapor	13.2	55.2
Xenon	11.5	62.5
Mercury	10.4	67.0

Table 13 gives the energy in electron-volts necessary to produce ionization. The column P_c is the kinetic-theory collision probability per centimeter of path length for an electron in a gas at 15° Celsius at a pressure of 1 millimeter of mercury. The collision frequency is given by

$$f_c = vP_c\rho$$

where f_c = collisions per second, P_c = collision probability in collisions per centimeter per millimeter of pressure, and ρ = gas pressure in millimeters of mercury.

Characteristics of Gas Tubes

Gas tubes may be generally divided into two classes, depending on whether the cathode is hot or cold and thus on the mechanism by which electrons are supplied.

Hot-Cathode Gas Tubes: The electrons in the hot-cathode gas tube are produced thermionically. The voltage drop across such tubes is that required to produce ionization of the gas and is generally a few tens of volts. The current conducted by the tube depends primarily on the emission capability of the cathode. Figure 27 shows the effect of the ionized gas on the voltage distribution in a hot-cathode tube.

Cold-Cathode Gas Tubes: The electrons in a cold-cathode tube are produced by bombardment of the cathode by ions and/or by the action of a localized high electric field. The voltage drop across such a tube is higher than in the hot-cathode tube because of this mechanism of electron generation, and the current which can flow is limited. Figure 28 shows the effect of tube geometry and gas pressure on the voltage required to initiate the discharge.

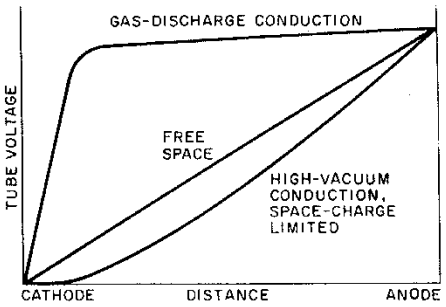

Fig. 27—Voltage distribution between plane parallel electrodes showing effect of space-charge neutralization in a hot-cathode gas tube.

Figure 29 shows a typical volt-ampere characteristic of a cold-cathode discharge. Cold-cathode gas tubes may be divided into two categories, depending on the region of this characteristic in which they operate.

Glow Discharge Tubes require a drop of several hundred volts across the tube and operate in region II. The current is of the order of tens of milliamperes.

Arc Discharge Tubes operate in region III. They are not, strictly speaking, cold-cathode tubes since the current is drawn from a localized spot on the cathode which is consequently heated and provides a large thermionic current. The voltage drop is thus lowered. Such a tube is capable of conducting currents of thousands of amperes at voltage drops of tens of volts. Mercury-pool cathodes are used

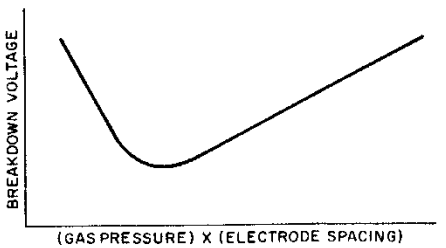

Fig. 28—Effect of gas pressure and tube geometry on gap voltage required for breakdown in a cold-cathode gas tube.

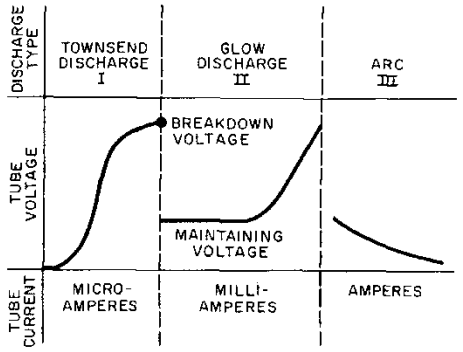

Fig. 29—Typical volt-ampere characteristic of cold-cathode gas discharge.

in one common form of arc discharge tube, supplying the electron current from an arc spot on the mercury-pool surface. The mercury vapor evaporated from the surface provides the gas atmosphere which is ionized.

Power Applications of Gas Tubes

Power Rectifier and Control Tubes: Mercury-vapor rectifiers, thyratrons, and ignitrons employ the very high current-carrying capacity of gas discharge tubes with low power losses for rectification and control in high-power equipment. The operation of mercury-vapor tubes depends on temperature insofar as tube voltage drop and peak inverse voltages are concerned (Fig. 30).

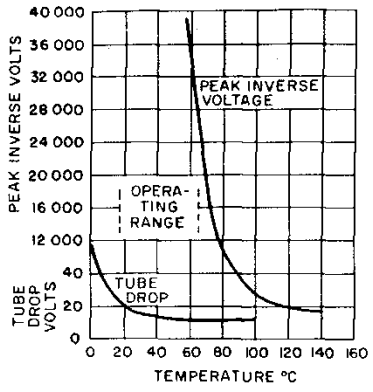

Fig. 30—Tube drop and arc-back voltages as a function of the condensed mercury temperature in a hot-cathode mercury-vapor tube.

Hydrogen Thyratrons are hot-cathode hydrogen-filled triodes designed for use as electronic switching devices where short anode delay time is important. In pulsing service they are capable of switching tens of megawatts at voltages of tens of kilovolts. Anode delay time and time jitter are in the nanosecond range, and the tubes do not depend on ambient temperature for proper operation. Hydrogen thyratrons are also used in crowbar applications to protect other circuit components against fault voltages or currents and are capable of handling peak currents of several-thousand amperes.

Triggered Spark Gaps are cold-cathode gas tubes operating in the arc discharge region III. The gaps contain two high-power electrodes and a trigger electrode which is generally fired through a step-up pulse transformer by a simple low-energy pulse. The gaps are used as electronic switching devices for peak currents of tens of thousands of amperes and voltages of tens of kilovolts. They can discharge stored energies of several thousand joules and are used for energy transfer in exploding-bridge-wire circuits, gas plasma discharges, spark chambers, and Kerr cells. They are also used in crowbar applications for fast-acting protection of other circuit components against fault voltages and currents. Before conduction the gap presents a low capacitance and a very high impedance to the circuit. After triggering, when the gap is conducting, the impedance drops to a few ohms or less.

Voltage Regulators of the glow discharge type take advantage of the volt-ampere characteristic in region II, where the voltage is nearly independent of the current. They operate at milliamperes and up to a few hundred volts.

Voltage regulators of the corona discharge type operate at currents of less than a milliampere and at voltages up to several thousand volts.

Microwave Applications of Gas Tubes

Noise Sources: Gas discharge devices possess a highly stable and repeatable effective noise temperature when in the fired condition. This feature provides a convenient and accurate means for determining noise figure. The microwave energy radiated from a gas discharge plasma is coupled into a radio-frequency transmission line with which it is used. The amount of radio-frequency power available from a gas discharge tube depends mainly on the nature of the gas fill, the geometric characteristic of the discharge tube, and the electron temperature of the positive column or plasma. The design parameter which most strongly determines the noise temperature is the type of gas employed. Any of the noble gases may be used in a noise source. In practice, however, only two or three are normally used:

Gas	$F=\mathrm{ENR(dB)}$
Helium	21.0
Neon	18.5
Argon	15.3

When referring to a noise source or generator, the ratio of its noise power output to thermal noise power is called the Excess Noise Ratio (ENR).

$$F=\mathrm{ENR}=\frac{[(T_2/T_0)-1]-Y[(T_1/T_0)-1]}{Y-1}$$

where Y = ratio of the noise output power of the receiver with the noise generator ON, to that with the noise generator OFF, $T_0=290°\mathrm{K}$, T_1 = temperature (in degrees K) of the termination, and T_2 = effective noise temperature (in degrees K) of the noise generator in the fired condition. The expression $[(T_2/T_0)-1]$ is termed the excess noise power of the noise source. When $T_1=T_0=290°\mathrm{K}$

$$\mathrm{ENR}=[(T_2/T_0)-1]/(Y-1)$$

$$\mathrm{ENR\,(dB)}=10\log_{10}\mathrm{ENR}.$$

The effective temperature of the noise source is equal to the temperature of the discharge only if the coupling of the transmission line to the discharge is complete. Otherwise there is a reduction in the noise power output which can best be determined by measuring the fired and unfired insertion loss of the unit at the frequency of interest. The relation between these factors is given by

$$[(T_e/T_0)-1]/[(T_2/T_0)-1]=1-(L_u/L_f)$$

where $[(T_e/T_0)-1]$ is the effective excess noise power of the generator, $[(T_2/T_0)-1]$ is the excess noise power, and L_u and L_f are the insertion losses in the unfired and fired conditions, respectively. This correction should be subtracted from the apparent measured noise figure.

Noise figure is always measured with reference to a standard temperature of 290°K (T_0). If the ambient temperature (T_1) of the noise-generator termination differs from the standard temperature, the noise figure calculated must be corrected. To find the correction factor, substitute the ambient temperature of the noise-generator termination for T_1 in the following equation and add the temperature factor (F_T) to the noise figure calculated.

$$F_T=[Y/(Y-1)][(T_1/T_0)-1].$$

TR Tubes: Transmit-receive tubes are gas discharge devices designed to isolate the receiver section of radar equipment from the transmitter during the period of high power output. A typical TR tube and its circuit are illustrated in Fig. 31.

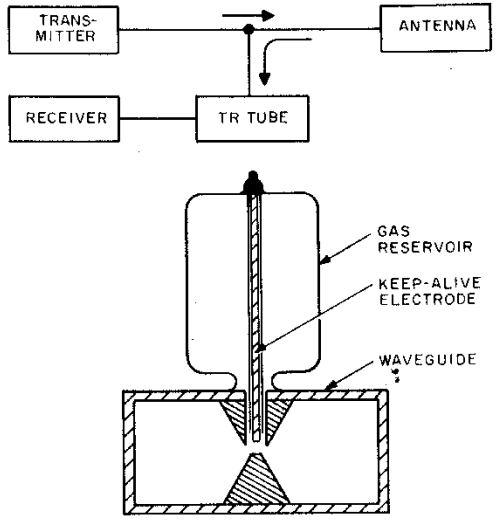

Fig. 31—Diagram of a TR tube and circuit.

The cones in the waveguide form a transmission cavity tuned to the transmitter frequency and the tube conducts received low-power-level signals from the antenna to the receiver. When the transmitter is operated, however, the high-power signal causes gas ionization between the cone tips, which detunes the structure and reflects all the transmitter power to the antenna. The receiver is protected from the destructively high level of power and all of the available transmitter power is useful output.

Microwave Gas Discharge Circuit Elements: Because of the high free-electron density, the plasmas of gas discharges are capable of strong interaction with electromagnetic waves in the microwave region. In general, microwave phase shift and/or absorption result. If used in conjunction with a magnetic field, these effects can be increased and made nonreciprocal. Phase shift is a result of the change in dielectric constant caused by the plasma according to

$$\epsilon_p/\epsilon_0=1-(0.8\times10^{-4}N_0/f_s^2)$$

where ϵ_p = dielectric constant in plasma, ϵ_0 = dielectric constant in free space, N_0 = electron density in electrons/centimeter^3, and f_s = signal frequency in megahertz.

Absorption of microwave energy results when electrons, having gained energy from the electric field of the signal, lose this energy in collisions with the tube envelope or neutral gas molecules. This absorption is a maximum when the frequency of collisions is equal to the signal frequency and the absolute magnitude is proportional to the free-electron density.

LIGHT-SENSING AND -EMITTING TUBES

Radiometry and Photometry

Radiometric and photometric* systems are generally based on the concept of radiated flux, where flux is defined as the total amount of radiation passing through a unit area per unit time.

If a flux is measured in terms of its thermal heating ability, the most common unit is the watt and the resultant measurement system is called radiometry.

If a flux is measured in terms of its ability to stimulate the standard photopic human eye, the resultant unit is the lumen, and the resultant measurement system is called photometry.

A third choice for the measurement of flux is the number of photons per unit time.

These three choices, in conjunction with the MKS† system of units, lead to the three mutually compatible systems of units shown in Table 14. Table 15 gives equivalents between units in different photometric measurement systems.

Flux Units: The number of lumens dL_λ and the number of photons per second dN_λ associated with a monochromatic flux dW_λ in watts are given by

$$dL_\lambda = 680 E_\lambda \, dW_\lambda$$

and

$$dN_\lambda = (\lambda/hc)\, dW_\lambda$$

where 680 = number of lumens per watt of radiation at the peak photopic eye response, E_λ = normalized (to unity maximum) photopic human eye response (Fig. 32), λ = wavelength of the monochromatic radiation (meters), h = Planck's constant $\simeq 6.6\times10^{-34}$ (joule-second), and c = velocity of light $\simeq 3.0\times10^{8}$ (meters per second).

The number of lumens L and the number of photons per second N between the wavelength units of λ_3 to λ_4 associated with a distributed spectral radiation source having a wattage W between the wavelength limits, λ_1 and λ_2, are given by

$$L/W = 680 \int_0^\infty E_\lambda w_\lambda \, d\lambda \Big/ \int_{\lambda_1}^{\lambda_2} w_\lambda \, d\lambda$$

and

$$Nhc/W = \int_{\lambda_3}^{\lambda_4} \lambda w_\lambda \, d\lambda \Big/ \int_{\lambda_1}^{\lambda_2} w_\lambda \, d\lambda$$

where

$$W = w_{\lambda\,\max} \int_{\lambda_1}^{\lambda_2} w_\lambda \, d\lambda$$

† Meter, kilogram, second.

and where $w_{\lambda\max}$ = maximum spectral density in watts per unit wavelength in the spectral band between λ_1 and λ_2, and w_λ = relative spectral distribution of the radiation source on thermal-energy basis, normalized to a maximum value of unity. Some typical w_λ spectral distributions are shown in Fig. 32.

Optical Imaging: In an optical lens system of flux-gathering diameter D_f in meters, focal length f in meters, and optical transmittance T, the ratio $f/D_f = n_f$ is called the f-number of the lens. If the surface of an object of radiance or luminance B in flux units per steradian per meter^2 is imaged by this system with a linear magnification m, and assuming Lambertian emittance characteristics over the solid angle subtended by the optical system, the image will be subjected to an irradiance or illuminance I_L in flux units per meter^2 given by

$$I_L = \pi BT/[4n_f^2(m+1)^2 + m^2].$$

For objects at infinity, $m=0$, and

$$I_L(\text{object at infinity}) = \pi BT/4n_f^2.$$

If the irradiance (or illuminance) I_L in flux units per meter^2 is allowed to fall on a nonabsorbing Lambertian diffusing surface, the resultant image radiance (or luminance) B_i in flux units per steradian per meter^2 is given by

$$\Pi B_i = I_L.$$

Any desired method of measuring flux units, such as watts, lumens, or photons/second (Table 14), can be selected for expressing the object radiance (or luminance) B in flux units steradian^{-1} meter^{-2} and the irradiance (or illuminance) I_L in flux units meter^{-2} in these relationships. Thus, a radiance B in watt steradian^{-1} meter^{-2} would be paired with an irradiance I_L in watt meter^{-2}, a luminance B in lumen steradian^{-1} meter^{-2} with an illuminance I_L in lumen meter^{-2}, and a radiance B in photon second^{-1} steradian^{-1} meter^{-2} with an irradiance I_L in photon second^{-1} meter^{-2}.

Any spectral distribution modifications, if present, would be included in the numerical magnitude of the lens transmission T, defined as the ratio of the total output flux from the optical system to the corresponding input flux.

Selection of appropriate alternative pairs of luminance and illuminance units when the flux units are not explicitly stated (first column of Table 15) must be made with care. Thus candle centimeter^{-2} (or stilb) would be paired with phot, candle meter^{-2} (or nit) with lux, and candle foot^{-2} with footcandle. Even greater difficulty arises when the factor Π in the preceding relationships is absorbed or included in the units of luminance. Thus the product ΠB in apostilb would be paired with I_L in lux, the product ΠB in lambert with

TABLE 14—COMPATIBLE SYSTEMS OF RADIATION UNITS.

Parameter	Radiometric System	Photometric System	Photon System
Flux	watt	lumen	photon sec^{-1}
Source intensity	watt ster^{-1}	lumen ster^{-1}	photon sec^{-1} ster^{-1}
Irradiance (or illuminance)*	watt m^{-2}	lumen m^{-2}	photon sec^{-1} m^{-2}
Emittance	watt m^{-2}	lumen m^{-2}	photon sec^{-1} m^{-2}
Radiance (or luminance)*	watt ster^{-1} m^{-2}	lumen ster^{-1} m^{-2}	photon sec^{-1} ster^{-1} m^{-2}
Energy	watt sec	lumen sec	photon

* The terms *illuminance* and *luminance* (sometimes *brightness*) are commonly substituted for *irradiance* and *radiance*, respectively, when reference is made to a photometric system of radiation units.

TABLE 15—PHOTOMETRIC EQUIVALENTS.

Photometric Unit	Equivalent Unit Based on the Lumen (lm) as the Unit of Flux	Equivalent Lumen-MKS Unit
	Source Intensity, C	
1 candle (Note 1)	1 lm ster^{-1} (Note 2)	1 lm ster^{-1} (Note 2)
1 candela	1 lm ster^{-1}	1 lm ster^{-1}
1 int. candle (Note 1)	1 lm ster^{-1} (Note 2)	1 lm ster^{-1} (Note 2)
1 Hefner candle	0.92 lm ster^{-1}	0.92 lm ster^{-1}
1 candlepower (Note 1)	1 lm ster^{-1} (Note 2)	1 lm ster^{-1} (Note 2)
	Surface Luminance, B	
1 candle cm^{-2}	1 lm ster^{-1} cm^{-2}	10^4 lm ster^{-1} m^{-2}
1 candle m^{-2}	1 lm ster^{-1} m^{-2}	1 lm ster^{-1} m^{-2}
1 candle in^{-2}	1 lm ster^{-1} in^{-2}	1.55×10^3 lm ster^{-1} m^{-2}
1 candle ft^{-2}	1 lm ster^{-1} ft^{-2}	10.8 lm ster^{-1} m^{-2}
1 nit	10^{-4} lm ster^{-1} cm^{-2}	1 lm ster^{-1} m^{-2}
1 stilb	1 lm ster^{-1} cm^{-2}	10^4 lm ster^{-1} m^{-2}
1 apostilb	π^{-1} lm ster^{-1} m^{-2}	π^{-1} lm ster^{-1} m^{-2}
1 lambert	π^{-1} lm ster^{-1} cm^{-2}	$10^4\,\pi^{-1}$ lm ster^{-1} m^{-2}
1 millilambert	$10^{-3}\,\pi^{-1}$ lm ster^{-1} cm^{-2}	$10\pi^{-1}$ lm ster^{-1} m^{-2}
1 footlambert	π^{-1} lm ster^{-1} ft^{-2}	$10.8\pi^{-1}$ lm ster^{-1} m^{-2}
	Illuminance of a Surface, I_L	
1 lux	1 lm m^{-2}	1 lm m^{-2}
1 phot	1 lm cm^{-2}	10^4 lm m^{-2}
1 milliphot	10^{-3} lm cm^{-2}	10 lm m^{-2}
1 footcandle	1 lm ft^{-2}	10.8 lm m^{-2}
	Energy, U	
1 talbot	1 lm sec	1 lm sec

Notes:

1. Unit becoming obsolete.
2. For a discussion of small differences in source intensity definitions and magnitudes a standard textbook on photometry should be consulted

I_L in phot, the product ΠB in millilambert with I_L in milliphot, and the product ΠB in footlambert with I_L in footcandle. These difficulties are avoided by the use of the compatible systems of radiation units shown in Table 14.

Typical Approximate Illumination Values at the Earth's Surface:

Sun at zenith$\simeq 10^4$ footcandles
$\simeq 10^5$ lumen meter^{-2}
Full moon$\simeq 3\times 10^{-2}$ footcandles
$\simeq 3\times 10^{-1}$ lumen meter^{-2}.

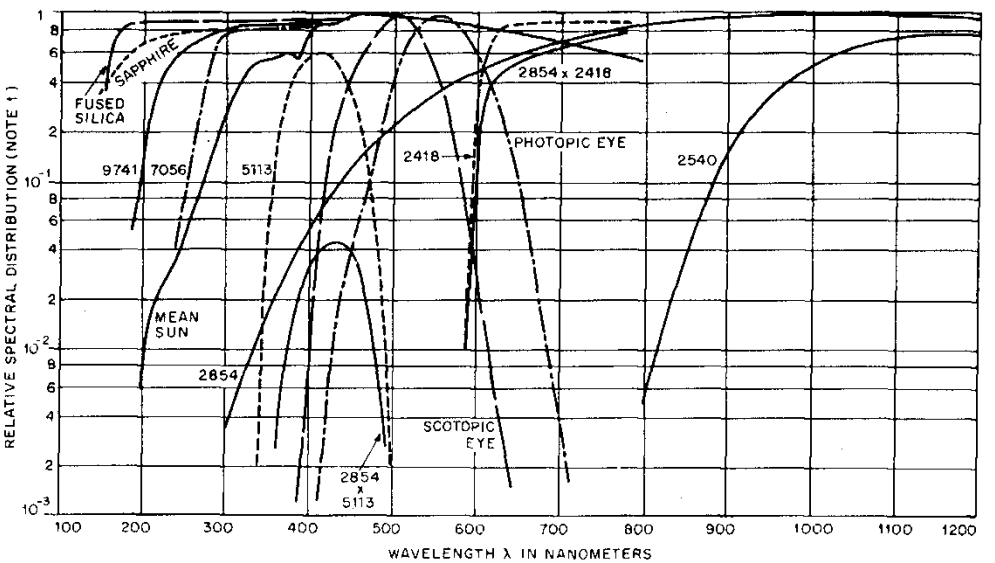

Fig. 32—Useful spectral distributions.

Fused silica: transmission through polished "Suprasil" (1 millimeter thick)

Sapphire: transmission through polished Sapphire (1 millimeter thick)

9741: transmission through polished Corning 9741 glass (1 millimeter thick)

7056: transmission through polished Corning 7056 glass (1 millimeter thick)

Mean sun: mean solar distribution at Earth's surface

5113: transmission through polished Corning 5113 filter (CS-5-58) (half-stock thickness)

2854×5113: product of 5113 curve and 2854 curve

2854: spectral density distribution of 2854°K color-temperature tungsten lamp

Scotopic eye: relative response of dark-adapted eye

Photopic eye: standard eye response

2418: transmission through polished Corning 2418 filter (CS-2-62) (stock thickness)

2854×2418: product of 2854 and 2418 curves

2540: transmission through polished Corning 2540 filter (CS-7-56) (stock thickness)

Note: "Relative spectral distribution" designates the relative radiant-energy density distribution w_λ for sources, the relative visual stimulation for equi-energy inputs for the eye response, and the spectral transmission t_λ for windows and filters. The transmission characteristics of individual filter and window samples can be expected to depart appreciably from these typical values.

Typical Approximate Brightness Values:

	footlamberts	lm ster^{-1}m^{-2}
Highlights, 35-millimeter movie	$\simeq 4$	$\simeq 100$
Page brightness for reading fine print	$\simeq 10$	$\simeq 3\times 10^2$
November football field	$\simeq 50$	$\simeq 1.5\times 10^3$
Surface of moon seen from Earth	$\simeq 1.5\times 10^3$	$\simeq 5\times 10^4$
Summer baseball field	$\simeq 3\times 10^3$	$\simeq 10^5$
Surface of 40-watt frosted lamp bulb	$\simeq 8\times 10^3$	$\simeq 2.5\times 10^5$
Crater of carbon arc	$\simeq 4.5\times 10^7$	$\simeq 10^9$
Sun seen from Earth	$\simeq 5.2\times 10^8$	$\simeq 1.5\times 10^{10}$

Photoconductivity

Photoconductivity* is the increase in electrical conductivity of a material which takes place when the material is illuminated with infrared, visible, or ultraviolet light.

The absorption of light is a quantum process in which electrons are excited to higher energy levels. Ordinarily, the excited electrons are more mobile than unexcited electrons. Photoconductivity is commonly analyzed in terms of the number and mobility of the excited electrons in an electron conduction band and of electron vacancies or "holes" in a lower-energy valence band. To maintain a steady current, both types of current carriers must be generated in the volume of the material, or else charge carriers must enter the photoconductor at one of the electrodes. Many photoconductors make "ohmic" contacts with their electrodes. These serve as practically unlimited reservoirs of mobile electrons, free to enter the photoconductor volume. Even in these photoconductors the steady dark current is usually limited to a low value by a build-up of a space-charge-potential barrier in the photoconductor.

At the same time that mobile photoelectrons are excited (thermally or optically) in the interelectrode volume, positive charges must also be generated; these compensate the charge of the photoelectrons in such a way that a "photocurrent" can be superimposed on the small space-charge-limited "dark" current originating at the electrode. If the positive charges are immobile, then long after the photoelectron has passed through the photoconductor into the anode, the immobile positive charges may remain to support a photocurrent of electrons, drawing on the reservoir of electrons at the cathode. This will continue until the immobile "holes" or impurity centers are neutralized by recombination with some of the mobile electrons. Since the recombination lifetime may be much longer than the electron transit time between electrodes, the number of "photoelectrons" transported across the photoconductor may be much larger than the rate of generation of photoelectrons in the photoconductor volume. This ratio of photocurrent to generation rate is called the photoconductive gain.

The photoconductive gain of a pure material can often be greatly increased by addition of localized traps lying near the conducting band. Since these are in thermal equilibrium with the conducting band, they serve as an additional reservoir of the charge carriers. This can increase both the response time and the sensitivity by a large factor.

Practically all materials are photoconductors in the sense that light of the correct wavelengths will generate current carriers. However, in many materials the photoconductivity is not detectable by ordinary measurements, either because of very short carrier lifetimes or because of a large dark current. The useful photoconductors, characterized by comparatively long lifetimes and low dark currents, have most of their charge carriers immobile (in the dark). Light of the proper energy can excite these carriers through the forbidden energy regions into the conduction bands. The long-wavelength limit of photoconductivity at low temperatures is approximately given by

$$\lambda_{max}=hc/E_g$$

where E_g is the forbidden band gap, h is Planck's constant, and c is the velocity of light. For wavelengths longer than 5 microns, this equation gives a band gap smaller than $\frac{1}{4}$ volt. Photoconductors with such small energy gaps are usually cooled to reduce the dark conductivity due to thermal excitation of carriers across the gap.

A commonly used figure of merit for photoconductors is the detectivity D^*, defined as the signal-to-noise ratio at a given chopping frequency with an amplifier bandwidth of 1 hertz for a photodetector of 1 square centimeter, divided by the light flux in watts. Detectivities for several typical photoconductors at room temperature are shown in Fig. 33. The photoconductors with long-

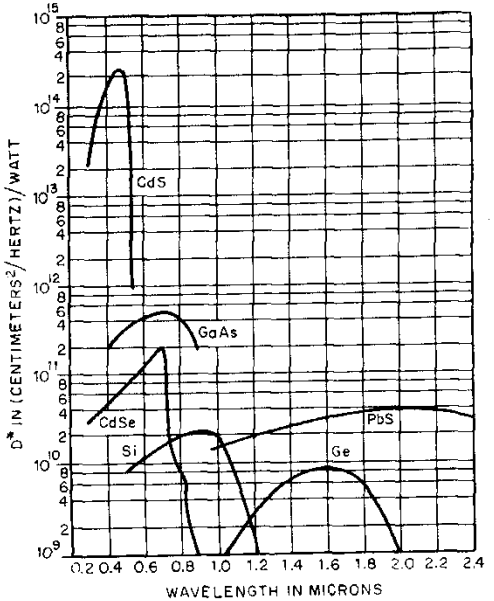

Fig. 33—Detectivity for some typical photoconductors at room temperature.

wavelength cutoffs will be considerably more sensitive if they are cooled below room temperature.

Phosphors

Fluorescent screens* are used in various electron devices such as image tubes, cathode-ray tubes, and storage cathode-ray tubes to convert electron energy into radiant energy. These viewing screens are comprised of many small-diameter (2 to 3 microns) phosphor crystals which emit light when bombarded by high-energy electrons. The spectral response of a phosphor screen is determined by its chemical and physical composition, deposition methods, and the tube processing procedures. Phosphor screens with given output characteristics have been categorized and assigned type numbers. Typical absolute spectral-response characteristics of aluminized phosphor screens are shown in Fig. 34.

Phosphor Efficiency: Over a rather wide range of magnitudes, the ratio U/q of total radiated energy U into a 2π solid angle, to exciting electron charge q for typical aluminized phosphor screens, Fig. 35, is independent of excitation time, beam-current magnitude, and bombarded area.

Consequently the ratio W/I of average total radiated flux W to average exciting current I is also independent of the magnitude of the average current I, the peak current I_{max}, and the bombarding area, and may therefore be used to describe the flux-generating properties of raster-scanned as well as steady-state excited phosphor screens. Experimentally, it is found that the ratio W/I is not a linear function of electron beam voltage V, as might be expected if the phosphor converts the beam energy IV linearly into radiated flux, but behaves in general as shown in Fig. 36, with an offset energy component IV_k followed by an approximately linear dependence on the added energy $I(V-V_k)$ over the usual working voltage range, $V_{min}<V<V_{max}$.

The flux-generating properties of a phosphor screen behaving in the above manner are therefore approximately described by

$$W/I=\mathcal{E}_w(V-V_k), \qquad \text{for } V_{min}<V<V_{max}$$

where W = average output flux (watts), I = average exciting electron beam current (amperes), $\mathcal{E}_w$ = dimensionless phosphor efficiency ratio [radiated watts per exciting electron beam watts (watts watt^{-1})], V = electron beam voltage, V_k = extrapolated offset knee voltage (Fig. 36), and V_{min}, V_{max} = limits of operating electron beam voltage.

The offset knee voltage V_k for typical aluminized phosphor screens has a magnitude between 1 and 3 kilovolts, and may be attributed primarily to electron beam power losses in penetrating the aluminizing layer plus possible inert-phosphor-particle coatings.

The average monochromatic radiant flux output per unit wavelength dw_λ from a phosphor screen at wavelength λ under these conditions is given by

$$dw_\lambda=\mathcal{E}_\lambda I(V-V_k)$$

where

$$\mathcal{E}_w=\int_0^\infty \mathcal{E}_\lambda\, d\lambda=\mathcal{E}_{\lambda\,max}\int_0^\infty w_\lambda\, d\lambda$$

$\mathcal{E}_\lambda$ = spectral density distribution of the phosphor efficiency or "spectral efficiency" [(watts meter^{-1}) watt^{-1}]

$\mathcal{E}_{\lambda\,max}$ = maximum spectral power density efficiency [(watts meter^{-1}) watt^{-1}]

w_λ = normalized relative power density of the radiant energy spectrum.

Typical values of the "spectral efficiency" $\mathcal{E}_\lambda$ are plotted in Fig. 34 for a number of commonly

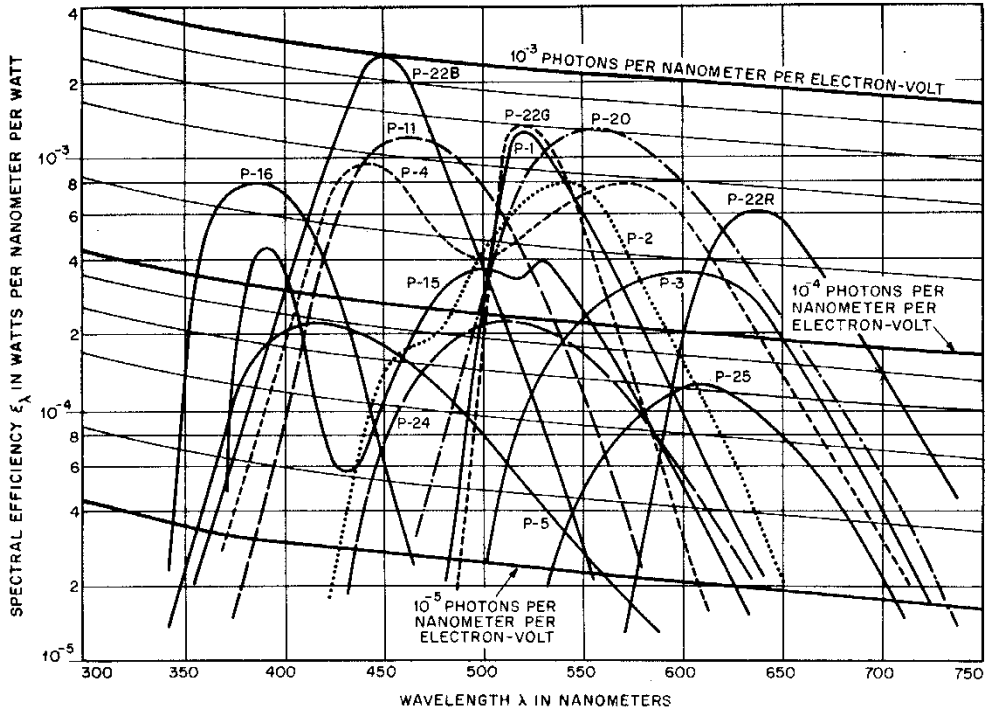

Fig. 34—Typical absolute spectral response characteristics of aluminized phosphor screens.

Phosphor Screen P Number	Chemical Composition	Fluorescent Color	Persistence Classification	Typical Peak Wavelength (nanometers)	Typical Luminous Equivalent $\mathcal{E}_L/\mathcal{E}_w$ (radiated lumens per radiated watt)	Typical Absolute Efficiency $\mathcal{E}_w$ (radiated watts per watt excitation)	Typical Quantum Yield Factor Y (photons per electron-volt)
P1	Zn_2SiO_4:Mn	Yellow-green	Med.	525	520	0.06	0.026
P2	ZnS:Cu	Yellow-green	Med.	533	460	0.07	0.03
P3	$Zn_3BeSi_2O_{19}$:Mn	Yellow-orange	Med.	603	380	0.041	0.02
P4	ZnS:Ag+ZnCdS:Ag	White	Med. short	459	290	0.15	0.067
	(all sulfide type)						
	(silicate-sulfide type)	White	Med.	450	290	—	—
	(silicate type)	White	Med.	410	240	—	—
P5	$CaWO_4$:W	Blue	Med. short	417	90	0.025	0.009
P6	ZnS:Ag+ZnCdS:Ag	White	Short	565	340	—	—
P7	ZnS:Ag on ZnCdS:Cu	White	Med. short	440	280	—	—
		(White decay)	Long	—	—	—	—
P10	KCl	(dark trace)	Long	—	—	—	—
P11	ZnS:Ag(Ni)	Blue	Med. short	460	140	0.10	0.038
P12	$ZnMgF_2$:Mn	Orange	Long	590	410	—	—
P13	$MgSiO_3$:Mn	Red-orange	Med.	640	140	—	—

Fig. 34—Continued.

Phosphor Screen P Number	Chemical Composition	Fluorescent Color	Persistence Classification	Typical Peak Wavelength (nanometers)	Typical Luminous Equivalent $\mathcal{E}_L/\mathcal{E}_w$ (radiated lumens per radiated watt)	Typical Absolute Efficiency $\mathcal{E}_w$ (radiated watts per watt excitation)	Typical Quantum Yield Factor Y (photons per electron-volt)
P14	ZnS:Ag+ZnCdS:Cu	Purple-blue	Med. short	440	250	—	—
		(Yel.-or. decay)	Med.	—	—	—	—
P15	ZnO:Zn	Green	Short	390	250	0.051	0.02
P16	$CaMgSiO_3$:Ce	UV-blue	Very short	380	25	0.049	0.015
P17	ZnO+ZnCdS:Cu	Blue-white	Short	550	350	—	—
		(Yellow decay)	Long	—	—	—	—
P18	$CaMgSiO_3$:Ti+P3	White	Med.	410	230	—	—
P19	$KMgF_2$:Mn	Orange	Long	590	390	0.0002	—
P20	ZnCdS:Ag	Yellow-green	Med.	560	480	0.14	0.063
P21	MgF_2:Mn	Red-orange	Med.	610	360	—	—
P22B	ZnS:Ag	Blue	Short	450	55	0.15	0.055
P22G	Zn_2SiO_4:Mn	Green	Med.	525	530	0.06	0.025
P22R	$Zn_3(PO_4)_2$:Mn	Red	Med.	645	150	0.05	0.022
P23	P4 type	White	Med. short	570	320	—	—
P24	ZnO:Zn (Special)	Green	Short	510	360	0.026	0.011
P25	$CaSiO_3$:Pb, Mn	Orange	Med.	610	320	0.013	0.006
P26	ZnF	Orange	Very long	590	410	—	—
P27	$Zn_3(PO_4)_2$:Mn	Red-orange	Med.	635	60	—	—
P28	ZnS:Ag, Cu	Green-yellow	Long	550	500	—	—
P29	P2 & P25 type	—	—	—	—	—	—
P31	ZnS:Cu	Green	Med. short	522	230	0.22	—

Notes:

Since the response characteristics of phosphor screens depend on such variable parameters as chemical composition, particle size, deposition methods, and the tube processing procedures, considerable departure from the data given on this chart is to be expected for individual screen samples.

With the exception of efficiency and quantum yield factor, the data are based primarily on JEDEC Publication No. 16 entitled "Optical Characteristics of Cathode-Ray-Tube Screens."

Efficiency and quantum yield factor data on phosphor screen types shown in the figure are derived directly from experimental measurements. For the remaining phosphors, data from various published sources, primarily phosphor manufacturers, have been extrapolated to the stated units of measurement whenever possible.

Phosphor excitation is expressed in terms of the power dissipated by the electron beam in the phosphor layer proper, with corrections for power losses to the aluminum layer coating and to the glass substrate in the case where the electron beam completely penetrates the phosphor layer. Expressing the phosphor excitation in this manner minimizes the variations of efficiency ratings with accelerating potential. The ratings given are most accurate in the region from 8 kV to 12 kV. Typical phosphor screen dead voltages, as a result of the aluminum coating, can be expected to be on the order of 1 kV to 3 kV.

Radiant output is expressed in terms of the total flux leaving the phosphor exit window. Luminance characteristics may be calculated from the data given provided a radiating area is also specified and assuming a cosine-law radiance distribution (approximately valid only).

Input current levels are restricted to the linear response region for each phosphor with respect to both average and peak current densities.

Quantum yield factors are tabulated in terms of photons per electron-volt, making it possible to multiply the listed numerical factor by the selected effective excitation voltage to give the quantum yield in photons per electron.

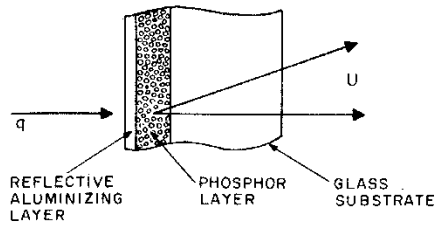

Fig. 35—Aluminized phosphor-screen construction.

used JEDEC-registered phosphor materials. The apparently redundant designation (watts meter^{-1}) watt^{-1} (or the equivalent) is retained in Fig. 34 and in this text to emphasize the fact that watt watt^{-1} refers to ratios of radiated watts to effective exciting electron beam wattage. The spectral distributions shown in Fig. 34 refer only to the first fast component of phosphor emission and ignore the slower less-intense excitation levels occurring in some phosphors.

If the total flux output is measured in lumens L instead of watts, then the corresponding relationships are

$$L/I=\mathcal{E}_L(V-V_k), \qquad \text{for } V_{\min}<V<V_{\max}$$

$$dL_\lambda=\mathcal{E}_{L\lambda}I(V-V_k)$$

$$\mathcal{E}_L=\int_0^\infty \mathcal{E}_{L\lambda}\,d\lambda$$

where the subscript L indicates the use of lumens for measuring the flux. Phosphor efficiency $\mathcal{E}_L$ in lumens watt^{-1} and spectral efficiency $\mathcal{E}_{L\lambda}$ in (lumens meter^{-1}) watt^{-1} are related to their corresponding absolute values $\mathcal{E}$ and $\mathcal{E}_\lambda$ by

$$\mathcal{E}_{L\lambda}=680E_\lambda\mathcal{E}_\lambda$$

and

$$\mathcal{E}_L=680\mathcal{E}_w\int_0^\infty w_\lambda E_\lambda\,d\lambda \Big/ \int_0^\infty w_\lambda\,d\lambda$$

where 680 = luminous equivalent of monochromatic radiation in lumen watt^{-1} at the peak eye-response wavelength, and E_λ = relative photopic eye response.

Some typical values of the dimensionless "spectral-matching-factor ratio"

$$\int_0^\infty w_\lambda E_\lambda\,d\lambda \Big/ \int_0^\infty w_\lambda\,d\lambda$$

appearing in these relationships are given in Table 4.

If the total flux output is measured in photons second^{-1} instead of watts or lumens, then the corresponding relationships are

$$N/n_e=Y(V-V_k)$$

$$dN_\lambda=y_\lambda n_e(V-V_k)$$

$$Y=\int_0^\infty y_\lambda\,d\lambda$$

where N = total number of output photons, n_e = total number of triggering input electrons, Y = "quantum yield factor" (photons electron-volt^{-1}), dN_λ = number of photons per unit wavelength (photons meter^{-1}), and y_λ = spectral efficiency (photons meter^{-1}) electron-volt^{-1} (shown on curved coordinate scales of Fig. 34).

The "quantum yield factor" Y, tabulated in Fig. 34 for the listed typical phosphor behavior, is useful in predicting the quantum yield N/n_e of a phosphor screen for an effective exciting electron beam voltage $V-V_k$ according to the above equation.

For a phosphor screen radiating according to Lambert's Cosine Law (often approximately, but not exactly, valid), the radiance B in (watts ster^{-1}) meter^{-2} and the luminance B_L in (lumens ster^{-1}) meter^{-2} is given by

$$\pi B=\mathcal{E}_w J(V-V_k)$$

$$\pi B_L=\mathcal{E}_L J(V-V_k)$$

where J = exciting current density (amperes meter^{-2}).

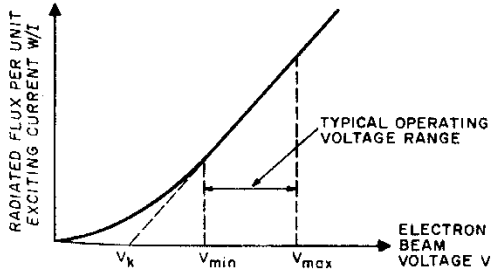

Fig. 36—Typical phosphor-screen behavior.

LIGHT-SENSING TUBES

Image Tubes and Image Intensifiers

An image tube* is an optical-image-in to optical-image-out electron tube device, combining an input

photocathode and an output phosphor screen such that photoelectrons emitted from each point on the photocathode subsequently excite a corresponding individual image "point" on the phosphor screen. Various focusing means, including magnetic and electrostatic electron lenses, may be used to assure maximum point-to-point correlation between the input and output images. The principal operating requirements are a lens to form the input image and a high-voltage supply, typically 5–25 kilovolts, to provide sufficient electron beam energy to excite the output phosphor screen.

If means are provided within the image tube to amplify the photoelectrons before they strike the output phosphor screen, or if the tube without such means produces a much brighter output image than the input image would produce on a diffusing screen, the tube is commonly called an image-intensifier tube.

Image-intensifier tubes are used to amplify the brightness of a faint input image for better visual or photographic viewing, whereas image tubes without amplification are used to convert radiation from one spectral region to another (image conversion) or to perform such control operations as optical shuttering by programing the applied high voltage.

The total output flux w_o in watts exiting (through 2Π steradians) from the phosphor-screen faceplate of an image intensifier tube for an input monochromatic flux dW_λ in watts at a wavelength λ is given by

$$dW_o = s_\lambda G \mathcal{E}_w (V - V_k)\, dW_\lambda$$
$$= G_\lambda\, dW_\lambda$$

where G_λ = monochromatic wattage gain of the image intensifier tube at a wavelength λ = ratio of the total output flux dW_o in watts to the input monochromatic flux dW_λ in watts, s_λ = radiant sensitivity of the input photocathode in amperes per watt (Fig. 5), G = internal current gain ratio of the image intensifier tube = ratio of the current bombarding the output phosphor screen to the corresponding photocurrent leaving the input photocathode, $\mathcal{E}_w$ = absolute phosphor screen efficiency = ratio of the total radiated flux in watts to the exciting electron beam power in watts dissipated in the particles of the output phosphor screen (Fig. 34), V = energy of the electron beam in volts bombarding the output phosphor screen, and V_k = extrapolated knee voltage of the output phosphor screen (Fig. 36).

If the phosphor screen radiates flux according to Lambert's Law (usually only approximately valid), the corresponding output image radiance R_o in watt steradian^{-1} meter^{-2} is given by

$$R_o = G_{\lambda_1} I_{\lambda_1} / \Pi m^2$$

where I_{λ_1} = input image irradiance on the photocathode in watt meter^{-2} at the wavelength λ_1 and m = differential magnification ratio of the image tube = output incremental image size divided by the corresponding input incremental image size.

For a spectrally distributed input flux having a known relative spectral distribution w_λ and a known total radiated power $W_{\lambda_1\lambda_2}$ in watts between the wavelength limits λ_1 and λ_2, the resulting total output flux W_o in watts exiting from the image tube is given by

$$W_o = s_{\lambda\,\max}\left(\int_0^\infty \sigma_\lambda w_\lambda\, d\lambda \Big/ \int_{\lambda_1}^{\lambda_2} w_\lambda\, d\lambda\right) \times G\mathcal{E}_w (V - V_k) W_{\lambda_1\lambda_2}$$
$$= G_{\lambda_1\lambda_2} W_{\lambda_1\lambda_2}$$

where $s_{\lambda\,\max}$ = peak radiant sensitivity of the input photocathode in amperes per watt, σ_λ = relative radiant sensitivity of the input photocathode as a function of wavelength λ normalized to unity maximum, w_λ = relative spectral distribution of the power density spectrum of the input flux normalized to unity maximum, and $G_{\lambda_1\lambda_2}$ = wattage gain of the image tube for the relative spectral distribution w_λ and the wavelength limits λ_1 and λ_2. Typical values for the magnitude of the dimensionless spectral-matching-factor ratio

$$\int_0^\infty \sigma_\lambda w_\lambda\, d\lambda \Big/ \int_{\lambda_1}^{\lambda_2} w_\lambda\, d\lambda$$

are found in Table 4.

The total output flux L_o in lumens exiting from an image tube, corresponding to the total output flux W_o in watts, can be computed from the flux conversion relationships given in the section on Radiometry and Photometry, or from the following relationship

$$L_o = s_{\lambda\,\max}\left(\int_0^\infty \sigma_\lambda w_\lambda\, d\lambda \Big/ \int_0^\infty E_\lambda w_\lambda\, d\lambda\right) \times G\mathcal{E}_w \left(\int_0^\infty E_\lambda w_{o\lambda}\, d\lambda \Big/ \int_0^\infty w_{o\lambda}\, d\lambda\right)(V - V_k) L_i$$
$$= G_L L_i$$

where G_L = luminous gain of the image intensifier tube = ratio of the output flux in lumens to the corresponding input flux in lumens for the spectral input distribution w_λ, E_λ = standard tabulated average relative photopic eye response (Table 4), $w_{o\lambda}$ = relative spectral density distribution of the output flux, and L_i = input flux in lumens. The typical values of the dimensionless spectral matching factors given in Table 4 can be used to determine the magnitude of the dimensionless integral ratios appearing in these relationships.

For the special case where the input flux $L_i(2854)$ in lumens is generated by a 2854°K color-temperature tungsten-filament lamp, the output flux $L_o(2854)$ in lumens is given by

$$L_o(2854) = S(2854) G \mathcal{E}_w \left(\int_0^\infty w_{o\lambda} E_\lambda\, d\lambda \Big/ \int_0^\infty w_{o\lambda}\, d\lambda\right) \times (V - V_k) L_i(2854)$$
$$= G_L(2854) L_i(2854)$$

where $G_L(2854)$ = luminous gain of the image intensifier for 2854°K tungsten-lamp radiation, and $S(2854)$ = luminous sensitivity of the input photocathode for 2854°K tungsten-lamp radiation. The magnitude of the luminous gain $G_L(2854)$ is commonly used to characterize the image intensification properties of an image intensifier tube.

If the output phosphor screen radiates flux according to Lambert's Law (usually only approximately valid), the output image luminance (or brightness) B_o in lumen steradian^{-1} meter^{-2} is given by

$$B_o = G_L I_i / \pi m^2$$

where G_L = luminous gain of the image intensifier for the particular input spectral distribution w_λ, I_i = input illuminance (or illumination) on the photocathode in lumen meter^{-2} for the spectral distribution w_λ, and m = differential magnification ratio of the image tube = output incremental image size divided by the corresponding input incremental image size.

Internal current gain G of an image intensifier tube can be obtained by the use of an internal sandwich electrode, in which an auxiliary or sandwich photocathode is mounted in close proximity to and following an auxiliary or sandwich phosphor. Photoelectrons from the input photocathode of the tube are then imaged onto this sandwich phosphor screen and the flux from this screen is coupled to the sandwich photocathode, generating an enhanced photocurrent. The current gain ratio G of this sandwich phosphor–photocathode combination, defined as the ratio of output photocurrent to input photocurrent, is given by

$$G = s_{\lambda\,\max,\,\mathrm{sand}} \left(\int_0^\infty w_{\lambda(\mathrm{sand})} \sigma_{\lambda(\mathrm{sand})}\, d\lambda \Big/ \int_0^\infty w_{\lambda(\mathrm{sand})}\, d\lambda\right) \mathcal{E}_{w,\,\mathrm{sand}} (V_{\mathrm{sand}} - V_{k,\,\mathrm{sand}}) \gamma$$

where $s_{\lambda\,\max,\,\mathrm{sand}}$ = peak monochromatic responsivity of the sandwich photocathode in ampere watt^{-1}, $w_{\lambda(\mathrm{sand})}$ = relative spectral distribution of the flux emitted by the sandwich phosphor screen, $\sigma_{\lambda(\mathrm{sand})}$ = the relative spectral distribution of the sandwich photocathode, $\mathcal{E}_{w,\,\mathrm{sand}}$ = absolute efficiency of the sandwich phosphor screen in watt watt^{-1}, V_{sand} = electron beam energy in volts bombarding the sandwich phosphor screen, $V_{k,\,\mathrm{sand}}$ = extrapolated knee voltage in volts for the sandwich phosphor screen, and γ = optical coupling efficiency of the sandwich electrode = ratio of the flux falling onto the sandwich photocathode to the corresponding flux emitted by the sandwich phosphor screen. Typical values of the dimensionless ratio of the two integrals appearing in this relationship are given in Table 4.

The combination of a phosphor screen and a photocathode to produce current gain G can also be achieved by optically coupling the output flux from one image tube to the input of a second tube.

Resolution in image tubes and image intensifier tubes is a subjective parameter describing the number of pairs of equally spaced illuminated and unilluminated bars per unit distance at the photocathode imaged onto the input photocathode surface which can just be distinguished visually by a trained observer under stated test conditions.

Distortion is a parameter describing any change in the geometric shape of the output image compared with the input image. Radially increasing magnification leads to "pincushion" distortion, radially decreasing magnification leads to "barrel" distortion, and radially changing image rotation leads to "S" distortion.

Vacuum Photodiodes

The combination of a photocathode and an anode electrode for collecting the emitted photocurrent in an evacuated envelope is called a vacuum photodiode. A positive anode potential sufficient to assure collection of all emitted photoelectrons (that is, to "saturate" the diode phototube) is normally required, the tube then acting as a constant-current generator (Fig. 37). The power supply potential V_B must assure sufficient anode potential in the presence of a voltage drop in the load resistor R_L.

Under these conditions the total anode output current I_a, neglecting all noise fluctuations, is given by

$$I_a = I_s + I_b + I_d + I_L$$

where I_s = emitted photocathode signal current, I_b = emitted photocathode photocurrent due to stray background flux, I_d = photocathode therm-

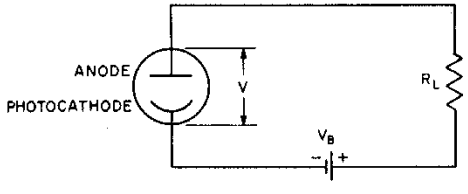

Fig. 37—Photodiode circuit.

ionic dark current, and I_L = residual dark current (leakage, etc.).

The instantaneous value of the signal current I_s will follow the instantaneous signal flux input magnitude from direct current up to an upper frequency limit (commonly 200–2000 megahertz) set by the transit-time spread of the electrons crossing the gap between cathode and anode, and including induced displacement currents during transit.

For steady-state or slowly varying input flux rates, the total noise current output i_n from the diode and load resistor is given by

$$i_n^2 = 2e\Delta f(I_s + I_b + I_d) + (4kT\Delta f/R_L) + i_L^2$$

where e = the electron charge = 1.6×10^{-19} coulomb, Δf = noise-current measurement bandwidth, k = Boltzmann factor = 1.38×10^{-23} joule per °K, T = absolute temperature of the load resistor (°K), R_L = load resistance (ohms), and i_L = residual dark noise current (from leakage, stray pickup, etc.).

To increase the absolute level of the noise voltage generated by the noise current i_n so that tube noise predominates over the noise voltage of the subsequent amplifiers or indicating circuits, and to suppress load-resistor noise relative to tube noise, large values of the load resistor (of the order of 10^7–10^9 ohms) are commonly used.

For a plane-parallel vacuum photodiode, the space-charge-limited output current $I_{a(\max)}$ in amperes for a given applied cathode-to-anode potential difference V in volts is given by

$$I_{a(\max)} = 2.33\times10^{-6}\, AV^{3/2}/d^2$$

where A = uniformly emitting emission area (meters^2), and d = anode–cathode spacing (meters).

In practice, linear output currents up to approximately half of this maximum limit can be obtained.

For a plane-parallel vacuum phototube, the output anode current I_A as a function of time t for an ultra-short exciting light pulse is given by

$$I_A = (2QRC/T^2)[(t/RC) + \exp(-t/RC) - 1] \quad \text{for } 0 < t < T$$

$$I_A = (2QRC/T^2)[(T/RC) + \exp(-I/RC) - 1] \times \exp[-(t-T)/RC] \quad \text{for } t \geq T$$

and

$$T = d(2m/\text{eV})^{1/2} = (3.37\times10^{-6})\; d/(V)^{1/2} \text{ seconds}$$

where T = transit time of the charge from cathode to anode (seconds), V = cathode-to-anode potential (volts), C = total capacitance including external circuit capacitance, R = load resistance, and Q = total charge.

Gas Photodiodes

In diode phototubes not containing a high vacuum, ionization by collision of electrons with neutral molecules may occur so that more than one electron reaches the anode for each originally emitted photoelectron. This "gas amplification factor" has a value of between 3 and 5; a higher factor causes instabilities. Gas-tube operation is restricted to frequencies below about 10 000 hertz.

Photomultipliers

The combination of a photocathode and a secondary-emission electron multiplier is called a photomultiplier.* Emitted photoelectrons from the photocathode are directed under the influence of a suitable electrode, often called the "focus electrode," to the surface of a secondary-emitting electrode, the "first dynode." Subsequently emitted secondary electrons, increased in number by the effective secondary-emission ratio σ_1, are then directed to the secondary-emitting surface of a subsequent dynode by an appropriate electric field for further multiplication. Continuing this process for n successive dynodes and collecting the multiplier charge at an output electrode called the "anode" or "collector," leads to a charge or current amplification G given by

$$G = \sigma^n, \quad \text{for} \quad \sigma_1 = \sigma_2 = \sigma_3 \cdots = \sigma$$

where gains as high as 10^5–10^9 are commonly achieved in 10-stage to 16-stage multipliers.

Output Current: Disregarding all noise fluctuations of the output current, and assuming operation within the usual linear-response region, a photomultiplier acts as a constant-current source generating an output current I_o given by

$$I_o = I_s + I_b + I_d$$
$$= G\epsilon I_{ks} + G\epsilon I_{kb} + G\epsilon I_{kd} + I_{ad}$$

where I_s = anode signal current due to an incident signal flux to be detected, I_b = anode current due to any background flux simultaneously present on the photocathode, I_d = anode dark current, G = current gain of the electron multiplier, ϵ = collection efficiency (ratio of current entering the electron multiplier to emitted photocathode current), I_{ks} = photocathode signal current due to an incident signal flux to be detected, I_{kb} = photocathode current generated by any background flux simultaneously present on the photocathode, I_{kd} = photocathode dark current, and I_{ad} = component of anode dark current I_d not originating from the photocathode.

The output signal current I_s follows the instantaneous value of the input signal flux from direct current up to an upper frequency limit (typically 20–200 megahertz) established by the response time or "transit-time spread" (typically 1–10 nanoseconds).

The ratio of the output signal current I_s in amperes to the triggering input flux L in lumens is called the anode luminous sensitivity A in amperes/lumen and is given by

$$A = I_s/L = G\epsilon I_{ks}/L = G\epsilon S$$

where S = photocathode luminous sensitivity in amperes/lumen (Table 3).

The value of the input flux L_D in lumens giving an output anode current just equal to the anode dark current I_d is called the "equivalent anode-dark-current input" or, more precisely, the luminous equivalent of the anode dark current and is given by

$$L_D = I_d/A = I_d/G\epsilon S.$$

Signal and Noise: Noise fluctuations of the output current in photomultipliers can be divided into two classes: *dark noise*, occurring in the absence of input flux; and *noise-in-signal*, including "quantum" noise resulting from the inherent quantum nature of the input flux as well as uncontrolled fluctuations of that flux. The presence of an appreciable, in fact often predominant, noise-in-signal current component in photomultipliers depending on the instantaneous signal current magnitude requires caution in applying noise concepts to photomultipliers, and may lead to erroneous conclusions regarding photomultiplier behavior, particularly for a modulated flux input.

For a steady-state unmodulated flux input, the total noise current i_n flowing in the load resistance R is given by

$$i_n^2 = 2eGK\Delta f(I_s + I_b + G\epsilon I_{kd}) + i_r^2 + (4kT\Delta f/R)$$

where K = photomultiplier noise factor, Δf = noise bandwidth of the noise-current measuring circuits (hertz), i_r = residual photomultiplier anode dark noise current, excluding dark current emission from the photocathode (amperes), $(4kT\Delta f/R)^{1/2}$ = Johnson-Nyquist noise current in the load resistance R (amperes), k = Boltzmann's constant, 1.38×10^{-23} joule/°K, and T = absolute temperature of the load resistance (°K).

For photomultipliers with a constant gain per stage σ in the first few stages of the electron multiplier, the noise factor K may be estimated from

$$K = \sigma/(\sigma - 1).$$

The luminous equivalent of the anode dark noise current is called the equivalent noise input, abbreviated as ENI and defined as "the peak-to-peak value of a square-wave-chopped flux input which gives an rms value for the fundamental component of the output current just equal to the rms value of the dark noise current measured for a 1-hertz bandwidth." The ENI in lumens is given by

$$\text{ENI} = \frac{\pi(2)^{-1/2}(2eGK\epsilon I_{kd} + i_r^2(1 \text{ hertz}) + 4kT/R)^{1/2}}{G\epsilon S}$$

where the factor $\pi(2)^{-1/2}$ converts peak-to-peak flux magnitude to equivalent rms magnitude of the fundamental component, and the notation i_r^2 (1 hertz) indicates that the residual dark noise current i_r excluding photocathode dark noise current is to be evaluated for a 1-hertz bandwidth.

Photomultipliers as Scintillation and Single-Electron Counters

In combination with suitable scintillating material, typically thallium-activated NaI crystals, photomultipliers are extensively used to detect the single flashes of light generated by the scintillating material on bombardment by a single triggering particle, typically a gamma ray from a nuclear disintegration process. If the scintillating material generates an average of N photons per disintegration incident on the effective photocathode of peak quantum efficiency $Y_{\max}$, the resultant average charge pulse Q_A appearing in the anode circuit (disregarding all photons or electrons producing no output charge) will be given by

$$Q_A = NY_{\max}\alpha Ge$$

where α is a spectral matching factor describing the relative match between the scintillator spectral output and the cathode sensitivity. (Refer to section on photoemission.)

Because of the random statistical fluctuations of cathode quantum efficiency $Y_{\max}$ and electron-multiplier gain G, as well as in the number of effective photons N generated by the scintillator, the anode charge Q_A will vary in magnitude from pulse to pulse, introducing ambiguity in the determination of the average magnitude of N, which in turn is used to determine the energy of the triggering input particle, for example the gamma ray. The ratio of the spread of the amplitude of individually observed values of the charge Q_A

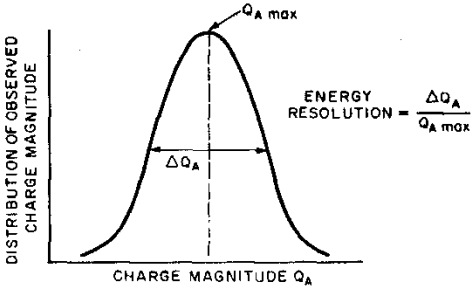

Fig. 38—Energy resolution of photomultiplier.

at half maximum to the most probable value $Q_{A(max)}$ is called the "energy resolution" of the photomultiplier-plus-scintillator combination and is commonly 7–10% minimum. (See Fig. 38.)

If the input flux has no time-coherent groups of photons, as it does in scintillation detection, photoelectrons are emitted singly at random emission times from the photocathode and also generate an average output charge Q_A given by

$$Q_A = Ge$$

where all photons or electrons generating no output pulse are disregarded in measuring G and computing Q_A. Assuming sufficiently large gain G and sufficiently low generation of dark pulses of similar charge amplitude, the individual anode pulses of charge amplitude Ge can be detected and counted individually, the photomultiplier then acting as a single-electron counter.

Image Dissectors

Principle of Operation: The image dissector* is a specialized electronically deflectable photomultiplier. Inside its evacuated envelope, a photocathode emits electrons in proportion to the illumination from an optical image incident on it. These image electrons are accelerated and focused into a plane containing a defining aperture. By means of deflection coils or plates, the resulting electron image is moved across this plane and a sampling of electrons passes through the aperture. These electrons impinge on the secondary-emitting surface of a dynode where, on the average, they give rise to 3 to 5 secondary electrons. These secondary electrons pass, in turn, to the next in a series of dynodes where their number is further multiplied. Depending on the number of the dynodes of the electron multiplier chain, their quality, and their applied potentials, a single electron passing through the defining aperture typically produces 10^5 to 10^7 electrons at the multiplier output anode. An example of a modern image dissector is shown schematically in Fig. 39.

To a first approximation, the resolution properties of an image dissector are determined solely by the geometric size and shape of the dissecting aperture. The predicted falloff in peak-to-peak signal modulation m for a dissector with various aperture sizes and shapes scanning a bar pattern input of increasing spatial density R in line pairs per meter is shown in Fig. 40.

A lower limit on the effective aperture size of an image dissector occurs because of the finite emission energy of photoelectrons. The combination of a finite average lateral emission energy component V_{ro} in volts with a finite average axial emission energy component V_{zo} leads to an electron image on the dissector aperture plate (for a point optical input image) which is blurred according to an approximately Gaussian current density distribution called the "point-spread function" of the electron lens of the image dissector. For a magnetically focused image dissector with a uniform electric accelerating field over a distance L_1 in meters between the photocathode and an electron-transmissive mesh followed by an electric-field-free drift and deflection space (Fig. 39) of length L_2 in meters prior to the aperture plate, the full width at half maximum W of the resulting point-spread function at the aperture plate in meters is given by

$$W \simeq 1.23 L_1 \frac{(V_{ro}V_{zo})^{1/2}}{V_a}\left[1+0.42\,\frac{L_2-2L_1}{L_1}\left(\frac{\bar{V}_{zo}}{V_a}\right)^{1/2}\right]$$

where V_a is the beam energy in volts within the drift and deflection space. To maintain this minimum (focused) beam size at the aperture requires a solenoidal magnetic field strength B in weber meter^{-2} given by

$$B = \pi n(2mV_a)^{1/2}/L(e)^{1/2}$$

where n = number of beam loops between cathode and aperture plate = 1, 2, 3, $\cdots$, m = mass of the electron = 9.1×10^{-31} kilogram, and e = electron charge = 1.6×10^{-19} coulomb.

Given a dissector with the minimum useful aperture size (approximately one beamwidth W in diameter), the resulting maximum value of the spatial pattern density R_{max} in line pairs per meter which can be detected at a modulation ratio $m \simeq 0.05$ is given by

$$R_{max} \simeq 0.7/W.$$

Signal: For an input photocathode illuminance I_L in lumen meter^{-2}, the output signal current I_o from an image dissector is given by

$$I_o = StaGI_L$$

where S = photocathode luminous sensitivity in ampere lumen^{-1}, t = mesh transmission including collection efficiency losses between photocathode and first dynode = ratio of the current transmitted by the mesh to the current incident on the mesh, a = effective aperture area measured at the photo-

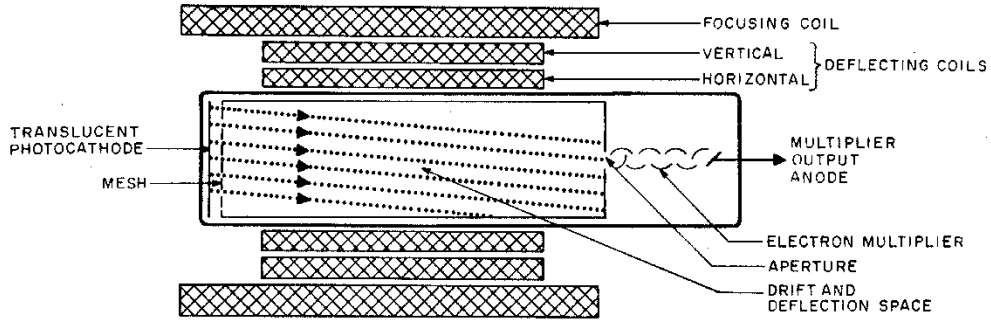

Fig. 39—Image dissector.

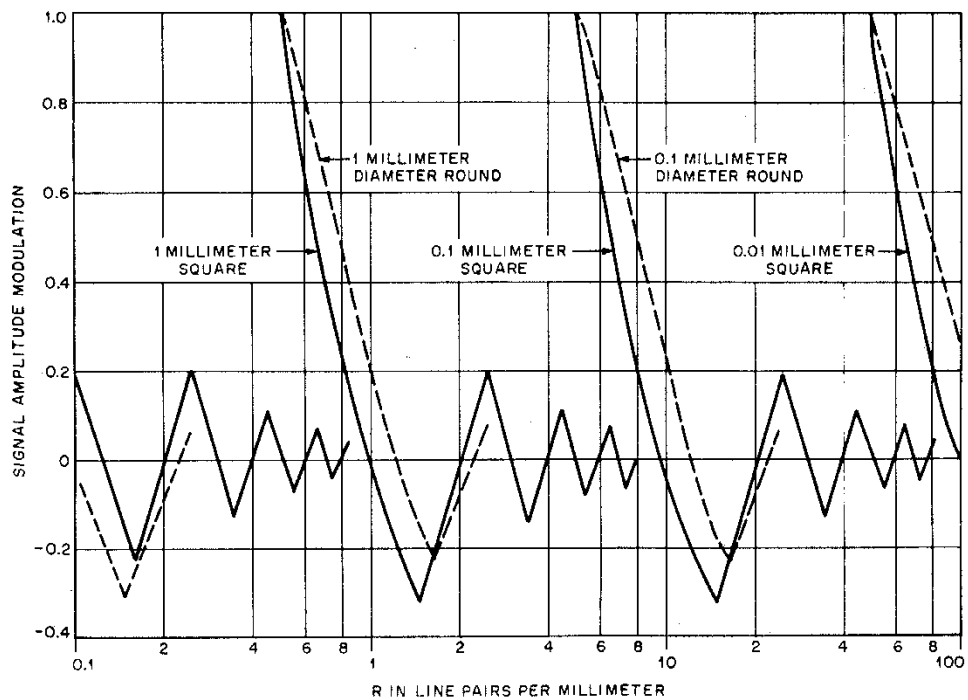

Fig. 40—Bar-pattern spatial density.

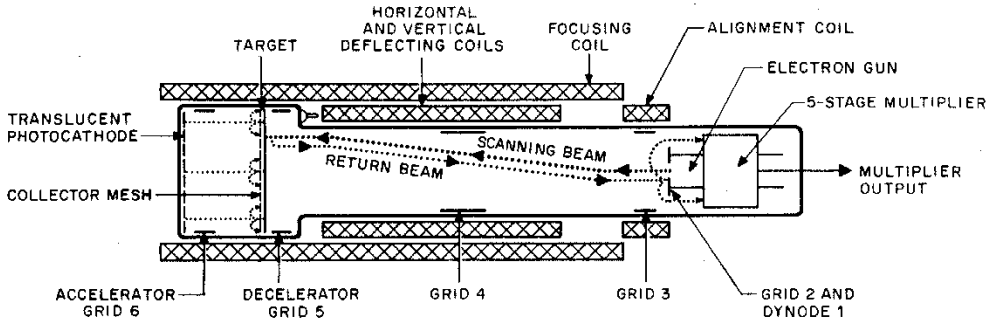

Fig. 41—Image orthicon

cathode surface (and thus compensating for possible electron optical magnification changes within the dissector), and G = electron multiplier current gain. The luminous sensitivity S pertains to the particular spectral distribution characteristic of the incident flux. If other units are used to measure the incident illuminance, for example watt meter^{-2} or photon second^{-1} meter^{-2}, the emitted photocathode current density SI_L in the above relationship may be computed according to the methods described in the section on Photoemission.

Noise: At the usual input illuminance levels necessary for satisfactory signal-to-noise-ratio performance of dissectors, dark noise (unlike all other conventional camera tubes) is completely negligible in magnitude. The total noise output current i_n in amperes is caused exclusively by the shot-noise fluctuations of the photocurrent emitted by the photocathode of the dissector and entering the dissector aperture, modified by statistically fluctuating gain processes within the electron multiplier. If the total output current is due to the incident signal illuminance I_L, the output noise current is given by

$$i_n^2 = 2eKGI_o\Delta f$$
$$= 2eKG^2StaI_L\Delta f$$

where K = the multiplier noise factor $\simeq \sigma/(\sigma-1)$, σ = average gain per stage of the electron multiplier, e = electron charge = 1.6×10^{-19} coulomb, and Δf = noise measurement bandwidth in hertz.

The signal-to-noise power ratio S/N under these conditions is given by

$$S/N = I_o^2/i_n^2 = StaI_L/2eK\Delta f.$$

Dynamic Range: The upper limit to input light level is established either by maximum space-charge-limited current in the final stages of the electron multiplier, by the maximum cathode-current density consistent with desired cathode lifetime, or by excessive current in the multiplier bleeder resistors. The lower limit is set usually by "shot noise" in the signal.

Image Orthicons

The image orthicon* is the camera tube most widely used for live commercial television. This fact derives from its high sensitivity, its close spectral-sensitivity match to the human eye, and its relatively fast response. Good-quality commercial television pictures can be generated by an image orthicon viewing a 5-to-20-footlambert ($\simeq$15–50 lumen steradian^{-1} meter^{-2}) scene through an F/5.6 lens. The image orthicon is generally available with either S-10 or S-20 spectral response (see Fig. 5), and is capable of 500 picture elements per raster height (9.9 line pairs/millimeter) at 30% video-amplitude response.

Principle of Operation: In the image section, a light image incident on the translucent photocathode liberates photoelectrons into the adjacent vacuum region in proportion to the light intensity (gamma is unity) on each element of the cathode. These photoelectrons are accelerated toward and magnetically focused onto the surface of a thin semiconducting target (Fig. 41). Electrons strike this target with sufficient energy to liberate a larger number of secondary electrons (typically 5) for each incident primary. The secondary electrons are collected by a mesh closely spaced from the target membrane. Hence, by depletion of electrons from the thin membrane, incremental areas become positive in proportion to the number of photoelectrons striking each element. In cases of high-light-level operation, parts of the target may become charged to target (collector) mesh potential, and saturation charge results. This phenomenon accounts for the so-called "knee" in the signal-vs-illumination transfer curve (Fig. 42).

Because the target membrane is very thin, of the order of microns, a charge distribution pattern formed on the image-section surface appears nearly simultaneously and identically on the scanning-section surface.

In the scanning section, an electron gun generates a highly apertured electron beam from a fraction to tens of microamperes in intensity. A solenoidal magnetic-focus coil and saddle-type deflection coils surrounding the scan section focus this beam on the insulator target and move it across the target. Scan-beam electrons impinge on the target at very low velocity, giving rise to relatively few secondary electrons. The target acts somewhat as a retarding field electrode and reflects a large number of the beam electrons that have less than average axial velocity. These two phenomena, small but finite secondary emission and reflection of slow beam electrons, limit scan-beam modulation to a maximum of about 30% at high light levels, and to 2 orders less at threshold. As will be shown later, the large unmodulated return beam current is the primary source of noise in the image orthicon.

Another problem created by the retarding-field aspect of low-velocity target scanning appears when the deflected beam does not strike the target normally. Since the entire beam-velocity component normal to the surface is now reduced by the cosine of the angle of incidence, the effective beam impedance is greatly increased. To overcome this problem, the decelerating field between grids 4 and 5 is shaped such that the electron beam always approaches normal to the plane of the target at a low velocity. If the elemental area on the target is positive, then electrons from the scanning beam deposit until the charge is neutralized. If the elemental area is at cathode potential (corresponding to a dark picture area), no electrons are deposited. In both cases the excess beam electrons are turned back and focused into a 5-stage electron multiplier. The charges existing on either side of the semiconductive target membrane will, by conductivity, neutralize each other in less than one frame time. Electrons turned back at the target form a return beam that has been amplitude-modulated in accordance with the charge pattern of the target.

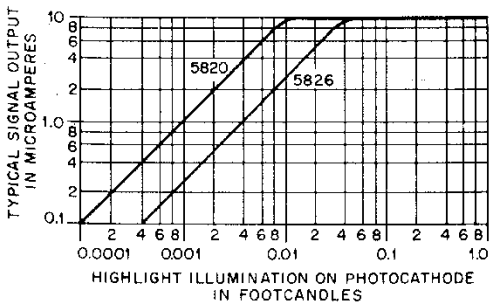

Fig. 42—Basic light-transfer characteristic for type *5820* and *5826* image orthicons. The curves are for small-area highlights illuminated by tungsten light, white fluorescent light, or daylight.

The return beam is redirected by the deflection and focus fields toward the electron gun where it originated. Atop the electron gun, and forming the final aperture for that gun, is a flat, secondary-emitting surface comprising the first dynode of the electron multiplier. The return beam strikes this surface, generating secondary electrons in a ratio of approximately 4:1.

Grid 3 facilitates a more complete collection by dynode 2 of the secondary electrons emitted from dynode 1. The gain of the multiplier is high enough that in operation the limiting noise is the shot noise of the returned electron beam rather than the input noise of the video amplifier.

Signal and Noise: Typical signal output current for tube types *5820* and *5826* are shown in Fig. 42. The tubes should be operated so that the highlights on the photocathode bring the signal output slightly over the knee of the signal-output curve.

The spectral response of the types *5820* and *5826* is shown in Fig. 43. Note that when a Wratten 6 filter is used with the tube, a spectral curve closely approximating that of the human eye is obtained.

From the standpoint of noise, the total television system can be represented as shown in Fig. 44, where I_s = signal current, I_n = total image-orthicon noise current, E_{nt} = thermal noise in R_1, E_{ns} = shot noise in the input amplifier tube, R_1 = input load, C_1 = total input shunt capacitance, and R_t = shot-noise equivalent resistance of the input amplifier = $2.5/g_m$ for triode or cascode input = $[I_b/(I_b+I_c)][(2.5/g_m)+(20I_{c2}/g_m^2)]$ for pentode input, with g_m = transconductance of input tube or cascode combination, I_b = amplifier direct plate current, and I_c = amplifier direct screen-grid current.

The noise added per stage is

$$\Delta n = [\sigma/(\sigma-1)]^{1/2}$$

where σ = stage gain in the multiplier. For a total multiplier noise figure to be directly usable, it must be referred to the first-dynode current, therefore, for 5 multiplier stages

$$\overline{\Delta N} = \Delta n^2 + \frac{\Delta n^2}{\sigma^2} + \frac{\Delta n^2}{\sigma^4} + \frac{\Delta n^2}{\sigma^5} + \frac{\Delta n^2}{\sigma^8}$$

where ΔN = electron-multiplier noise factor referred to multiplier input.

After combining all noise sources

$$\frac{S}{N}=\frac{I_s}{\left\{F\left[2eIk_m^2+4kT\left(\frac{1}{R_1}+\frac{R_t}{R_1^2}+\frac{\omega^2C_1^2R_t}{3}\right)\right]\right\}^{1/2}}$$

where S/N = signal-to-noise ratio, F = bandwidth in hertz, e = electron charge = 1.6×10^{-19} coulomb, I = image-orthicon beam current, k_m = electron-multiplier noise factor, referred to multiplier output = $m\Delta N$, k = Boltzmann's constant = 1.38×10^{-23} joule/degree Kelvin, T = absolute temperature in degrees Kelvin, and $\omega=2\pi f$ in hertz.

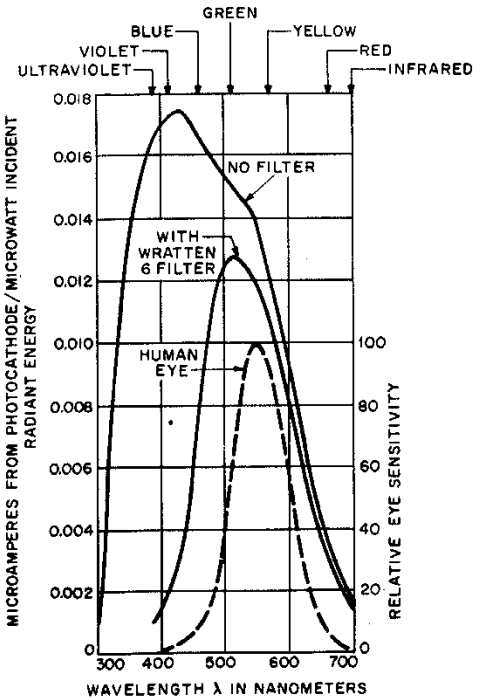

Fig. 43—Spectral sensitivity of image orthicon.

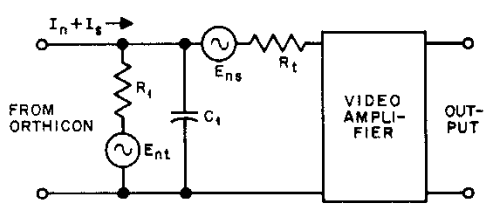

Fig. 44—Equivalent circuit for noise in orthicon and first amplifier stage.

The signal current is an alternating-current signal superimposed on a larger direct beam current. This can be thought of as a modulation of the beam current. Properly adjusted tubes obtain as much as 30-percent modulation.

$$I_s=mMI$$

where m = multiplier gain and M = percentage modulation. If S/N is now rewritten

$$\frac{S}{N}=\frac{I_s}{\left[4kTF\left(\frac{2eI_sm\Delta N^2}{4kTM}+\frac{1}{R_1}+\frac{R_t}{R_1^2}+\frac{\omega^2C_1^2R_t}{3}\right)\right]^{1/2}}.$$

In typical television operation, the thermal noise of the load resistor and the shot noise of the first amplifier can be neglected.

Focusing and Scanning Fields: The electron optics of the scanning section of the tube are quite complicated and space does not permit the inclusion of the complete equations. A simple relationship between the strength of the magnetic focusing field and the magnetic deflection field is given below.

The image orthicon is usually operated with multiple-node focus in the scanning section. Working at a multiple-node focus not only demands more focus current but also more deflection current. Note the deflection path in Fig. 45. Let H = horizontal dimension of scanned area or target, L = effective length of horizontal deflection field, H_d = horizontal deflection field (peak-to-peak value), and H_f = focusing field. Then

$$H_d=H_fH/L$$

for the image orthicon, $H\approx1.25$ inches, and $L\approx4$ inches. Thus $H_f\approx75$ gauss, and $H_d\approx23$ gauss.

Vidicons

The vidicon* is a small television camera tube that is used primarily for industrial television,

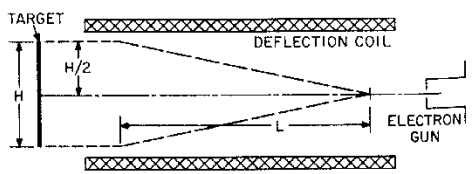

Fig. 45—Deflection in image orthicon.

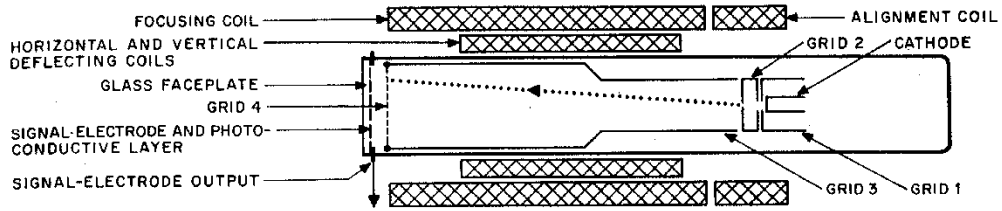

Fig. 46—Vidicon construction.

space applications, and studio film pickup because of its small size and simplicity.

As shown in Fig. 46, the tube consists of a signal electrode composed of a transparent conducting film on the inner surface of the faceplate; a thin layer (a few microns) of photoconductive material deposited on the signal electrode; a fine mesh screen (grid 4) located adjacent to the photoconductive layer; a focusing electrode (grid 3) connected to grid 4; and an electron gun.

Principle of Operation: Each elemental area of the photoconductor can be likened to a leaky capacitor with one plate electrically connected to the signal electrode that is at some positive voltage (usually about 20 volts) with respect to the thermionic cathode of the electron gun and the other plate floating except when commutated by the electron beam. Initially, the gun side of the photoconductive surface is charged to cathode potential by the electron gun, thus leaving a charge on each elemental capacitor. During the frame time, these capacitors discharge in accordance with the value of their leakage resistance, which is determined by the amount of light falling on that elemental area. Hence, there appears on the gun side of the photoconductive surface a positive-potential pattern corresponding to the pattern of light from the scene imaged on the opposite surface of the layer. Even those areas that are dark discharge slightly, since the dark resistivity of the material is not infinite.

The electron beam is focused at the surface of the photoconductive layer by the combined action of the uniform magnetic field and the electrostatic field of grid 3. Grid 4 serves to provide a uniform decelerating field between itself and the photoconductive layer such that the electron beam always approaches the surface normally and at a low velocity. When the beam scans the surface, it deposits electrons where the potential of the elemental area is more positive than that of the electron-gun cathode. At this moment the electrical circuit is completed through the signal-electrode circuit to ground. The amount of signal current which flows depends on the amount of discharge in the elemental capacitor, which in turn depends on the amount of light falling on this area.

Alignment of the beam is accomplished by a transverse magnetic field produced by external coils located at the base end of the focusing coil.

Deflection of the beam is accomplished by the transverse magnetic fields produced by external deflecting coils.

Signal and Noise: Since the vidicon acts as a constant-current generator as far as signal current is concerned, the value of the load resistor is determined by band-pass and noise considerations in the input circuit of the video amplifier. Unlike the image orthicon, vidicon signal current is removed at the target, and only that portion of the scan beam actually involved in the target discharge contributes shot noise. Moreover, electron-beam contributions to noise are minimal for low-light portions of the scene.

The primary noise associated with vidicon operation is seldom scan-beam shot noise. Where the signal current is less than 1 microampere and the band pass is relatively wide, the principal noise in the system is contributed by the input circuit and the first stage of the video amplifier. To minimize the thermal noise of the load resistor, its resistance is made much higher than flat-band-pass considerations would indicate, since signal voltage increases directly and noise voltage increases as the square root. To correct for attenuation of the signal with increasing frequency, the amplitude response of the video amplifier frequently employs high-frequency boost of the following form, where C_1 and R_1 refer to Fig. 47.

$$G=G_0(1+4\pi^2F^2C_1^2R_1^2)^{1/2}/R_1.$$

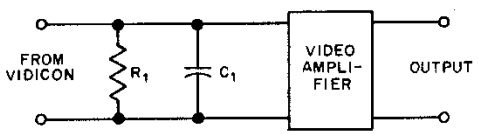

Fig. 47—Input circuit for first-stage amplifier in vidicon circuit.

A representative plot of amplitude response as a function of the number of television lines (per raster height) is shown in Fig. 48.

The vidicon has somewhat more lag or image persistence than the image orthicon. This is the result of two factors. To obtain high-sensitivity surfaces, the photoconductive decay time is made as long as tolerable, since quantum efficiency is limited by the ratio of effective carrier lifetime to carrier transit time across the photoconductor. A second source of lag is simply the *RC* time constant of the target recharging circuit; that is, the target capacitance and the beam impedance.

The spectral response of most commercial vidicons, designated S-18, is more actinic than the human eye. Figure 49 compares these responses with the spectrum of a 2854°K tungsten source.

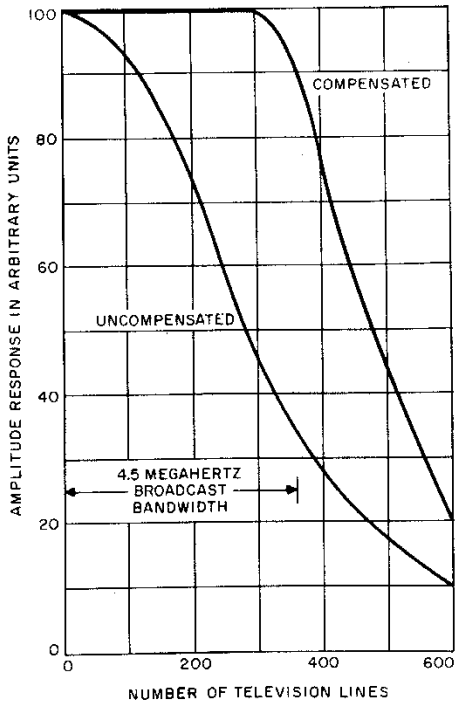

Fig. 48—Vidicon resolution, showing uncompensated and compensated horizontal responses. Highlight signal-electrode microamperes=0.35; test pattern=transparent square-wave resolution wedge; 80 television lines=1-megahertz bandwidth.

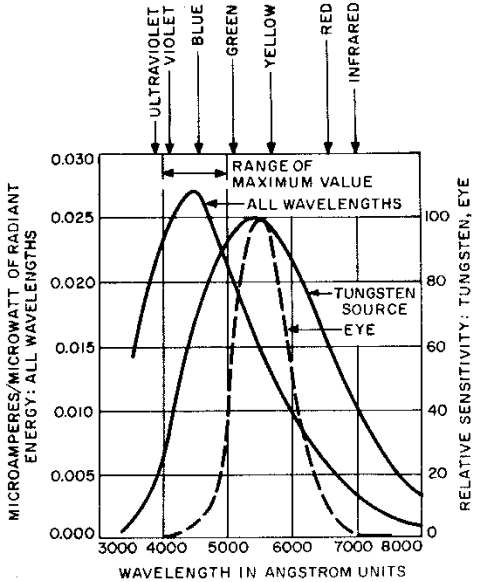

Fig. 49—Spectral response of vidicon.

Variations of the Vidicon

Interest in optical guidance and surveillance from air and spacecraft has given rise to a wide variety of vidicon camera tubes. To treat these variations in detail becomes encyclopedic, but the following gives some indication of the choices now available to the user.

Effective Sensitivity: True photoconductive tubes now offer sensitivities of 150–200 nanoamperes for ½-footcandle illumination with 20 nanoamperes dark current. Improved methods of deposition of photoconductors have made possible higher voltage operation without objectionable dark shading. Special devices using junction effects promise even better sensitivity.

Spectral Response: Available photoconductors, taken as a whole, provide sensitivity over the entire visible range with usual (7056) glass windows. Quartz window tubes offer useful sensitivity to below 2000 angstrom units. Numerous applications of direct excitation of photoconductors by X-radiation have been reported. High-velocity electron excitation (bombardment-induced conductivity) is also in use.

Size and Deflection: Vidicons are available in sizes ranging from ½ inch to 2 inches in diameter. Various combinations of deflection and focus are available.

Storage: A number of manufacturers have produced vidicons with long storage characteristics. Many are merely long-lag tubes; however, a few rely on high-resistivity materials or barrier layers to retain stored charge through minimal dark current. One such device, once exposed properly to a scene, regenerates the scene through readout over a period of the order of half an hour.

LIGHT-EMITTING TUBES

Cathode-Ray Tubes

A cathode-ray tube* is a vacuum tube in which an electron beam, deflected by applied electric and/or magnetic fields, indicates by a trace on a fluorescent screen the instantaneous value of the actuating voltages and/or currents. A typical high-intensity cathode-ray tube with post-deflection acceleration is shown in Fig. 50.

Principle of Operation: The function of the cathode-ray tube is to convert an electrical signal into a visual display. The tube contains an electron-gun structure (to provide a narrow beam of electrons) and a phosphor screen (refer to section on Phosphor Screens). The electron beam is directed to the phosphor screen and strikes it, causing light to be emitted in a small area or spot in proportion to the intensity of the electron beam. The beam intensity varies as a function of the electrical signal which is applied to the control element in the electron gun.

The electrical signal that controls the beam intensity corresponds to the desired picture information; therefore, in modulating the electron beam the individual picture elements can be reproduced on the phosphor screen in the same degree of black or white as in the original picture. Although one element is not enough to reproduce a picture, the same process is carried out for all picture elements in successive order, and each element is positioned correctly on the phosphor screen to reproduce the entire picture. Means are provided either internally or externally of the tube for positioning or deflecting the electron beam over the phosphor-screen area in some systematic fashion to reproduce the entire picture as a visual output.

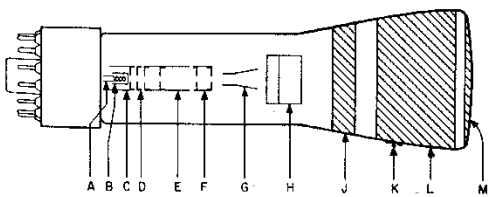

Fig. 50—Electrode arrangement of typical electrostatic focus and deflection cathode-ray tube. A—heater, B—cathode, C—control electrode, D—screen grid or pre-accelerator, E—focusing electrode, F—accelerating electrode, G—deflection-plate pair, H—deflection-plate pair, J—conductive coating connected to accelerating electrode, K—intensifier-electrode terminal, L—intensifier electrode (conductive coating on glass), M—fluorescent screen.

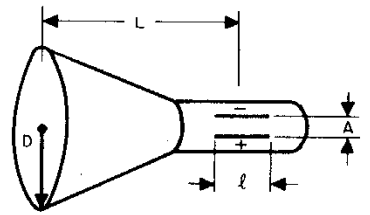

Fig. 51—Electrostatic deflection.

Electric-Field Deflection: Deflection is proportional to the deflection voltage, inversely proportional to the accelerating voltage, and in the direction of the applied field (Fig. 51). For structures using straight and parallel deflection plates, it is given by

$$D = E_d L l / 2 E_a A$$

where D = deflection in centimeters, E_a = accelerating voltage, E_d = deflection voltage, l = length of deflection plates or deflecting field in centimeters, L = length from center of deflecting field to screen in centimeters, and A = separation of plates.

Magnetic-Field Deflection: Deflection is proportional to the flux or the current in the coil, inversely proportional to the square root of the accelerating voltage, and at right angles to the direction of the applied field (Fig. 52). Deflection is given by

$$D = 0.3LlH/(E_a)^{1/2}$$

where H = flux density in gauss, and l = length of deflecting field in centimeters.

Deflection Sensitivity: The deflection sensitivity is linear up to the frequency where the phase of the deflecting voltage begins to reverse before an electron has reached the end of the deflecting field.

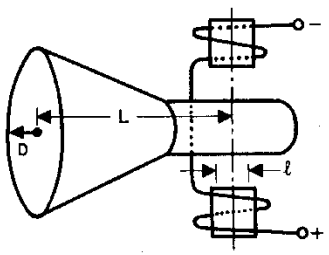

Fig. 52—Magnetic deflection.

Beyond this frequency, sensitivity drops off, reaching zero and then passing through a series of maxima and minima as $n = 1, 2, 3, \cdots$. Each succeeding maximum is of smaller magnitude.

$$D_{zero} = n\lambda(v/c)$$

$$D_{max} = (2n-1)(\lambda/2)(v/c)$$

where D = deflection in centimeters, v = electron velocity in centimeters/second, c = velocity of light $\approx 3 \times 10^{10}$ centimeters/second, and λ = free-space wavelength in centimeters.

Magnetic Focusing: There is more than one value of current that will focus, and best focus is at the minimum value. For an average coil $IN = 220\,(V_0 d/f)^{1/2}$ = ampere-turns, V_0 = accelerating voltage in kilovolts, d = mean diameter of coil, f = focal length, and d and f are in the same units.

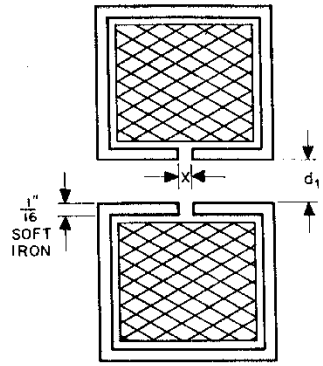

Fig. 53—Magnetic focusing.

A well-designed shielded coil will require fewer ampere-turns.

Figure 53 is an example of good shield design, where

$$x = d_1/20.$$

Storage Cathode-Ray Tubes

The storage cathode-ray tube* produces a visual display of controllable duration. The tube has two electron guns, a phosphor viewing screen, and two fine-mesh metal screens. One of the electron guns is referred to as the writing gun and the other as the flooding gun. The web of one screen is coated on the gun side with a thin dielectric material to form a surface on which the electron beam stores information, and the other screen serves as an electron collector. A typical storage cathode-ray tube is shown in Fig. 54.

Principle of Operation: The writing gun emits a pencil-like electron beam which is intensity modulated by the information to be stored. The information is in the form of an electrical input signal. The storage surface is scanned by this high-resolution beam which actually strikes this surface. A positive-charge image, corresponding in value to the input signal pattern, is imposed on the storage surface where it remains until it decays or is erased. The storage screen forms an array of elemental electron guns, with each mesh hole considered as a control element of one of the guns. After the desired information has been stored on the storage mesh, the entire surface is flooded by an electron beam from the flooding gun. The value of positive charge deposited at each mesh aperture controls the amount of flooding beam current that can pass through the mesh aperture to the phosphor viewing screen. The current that passes through the mesh strikes the phosphor viewing screen, where a light output is observed in proportion to the bombarding-current density and the energy with which the electrons strike the phosphor. In other words, a grey scale is reproduced in the stored image. After the stored information has been observed or recorded, it is erased from the storage surface by flooding the storage surface with low-velocity electrons. Thus a net negative charge is deposited on each elemental area of the storage surface until flooding cathode potential is reached. The storage surface is then prepared for storing a new image.

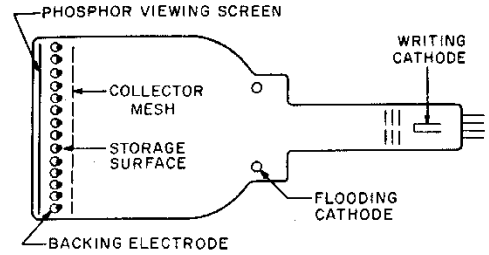

Fig. 54—Construction of storage cathode-ray tube.

Barrier-Grid Storage Tube

The barrier-grid storage tube is a form of cathode-ray tube in which information can be stored as an electrostatic charge. There is no visual display, since both the input and the output signals are electrical. The operation of this tube is closely similar to that of the storage cathode-ray tube. The tube (Fig. 55) consists of an electron gun for writing in and reading out the information, a curved target on which the information is stored, a collector electrode, and an associated electron optical system for focusing the signal electrons onto the collector electrode.

Principle of Operation: The target of the barrier-grid storage tube consists essentially of an array of elemental capacitors, which are charged or discharged by the action of the electron beam from the electron gun. During the write operation, an electrical signal (such as a video signal) is applied to a control electrode of the electron gun, which electrode in turn modulates the electron beam generated by the gun. This modulated beam is scanned across the target, and the information is stored on the target in the form of a pattern of charged areas. During the read cycle an unmodulated electron beam is scanned across the target. As this reading beam approaches each elemental charged area on the target, electrons leave the area and are attracted to the collector. This current constitutes the output signal.

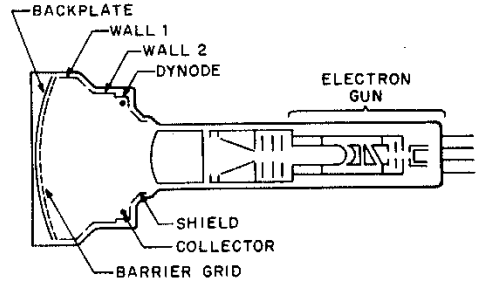

Fig. 55—Construction of barrier-grid storage tube.

Scan Converter

The scan converter is a tube in which information can be stored as an electrostatic charge. In the scan converter there is no visual display; its output as well as its input are electrical signals. The tube (Fig. 56) consists of two electron guns on opposite ends of the tube on the same axis, a

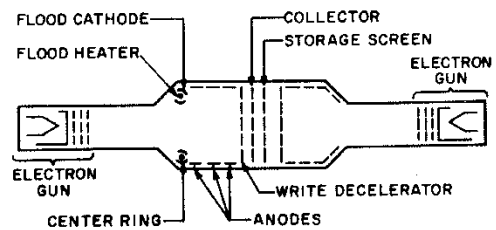

Fig. 56—Construction of scan converter.

collector mesh, and a storage screen comprised of a fine-mesh metal screen coated with a dielectric material serving as the storage surface. The holes of the screen remain open. Each electron gun directs a beam of electrons to the common storage mesh. Each beam is scanned over the storage surface by its own deflection system. One beam writes and the other reads, and it is possible for both modes of operation to occur simultaneously.

Principle of Operation: An electrical input signal, corresponding to the information to be stored, is applied to the writing gun. This signal controls the intensity of the electron beam which deposits or writes a pattern of electrostatic charge on the storage surface. This written information is read out in the form of an electrical output signal by the reading gun. The value of charge that has been deposited at each mesh aperture of the storage screen controls the amount of writing-beam current that can pass through the screen to the collector. The output signal thus varies as a function of the charge stored at each point on the storage screen. Either of the electron beams may be used to erase a stored picture after it has been read out thousands of times.

ELECTRON-TUBE CIRCUITS

APPLICATIONS OF ELECTRON TUBES

The advent of transistors is limiting the use of vacuum tubes to special applications. The voltage-handling capabilities of electron tubes satisfy the requirements for high-power oscillator, amplifier, and certain pulse service applications. Tubes are used in the high-power stages of radio and similar transmitters, as modulators of high-power radio-frequency amplifiers, and for specific conditions as pulse generators for radar and other pulse service equipment. Transistors and other semiconductor devices have largely replaced tubes in low-power applications.

CLASSIFICATION

It is common practice to differentiate between types of vacuum-tube circuits, particularly amplifiers, on the basis of the operating regime of the tube.

Class-A: Grid bias and alternating grid voltages such that plate current flows continuously throughout electrical cycle ($\theta_p = 360$ degrees).

Class-AB: Grid bias and alternating grid voltages such that plate current flows appreciably more than half but less than entire electrical cycle ($360° > \theta_p > 180°$).

Class-B: Grid bias close to cutoff such that plate current flows only during approximately half of electrical cycle ($\theta_p \approx 180°$).

Class-C: Grid bias appreciably greater than cutoff so that plate current flows for appreciably less than half of electrical cycle ($\theta_p < 180°$).

A further classification between circuits in which positive grid current is conducted during some portion of the cycle, and those in which it is not, is denoted by subscripts 2 and 1, respectively. Thus a class-AB_2 amplifier operates with a positive swing of the alternating grid voltage such that positive electronic current is conducted and accordingly in-phase power is required to drive the tube.

GENERAL DESIGN

For quickly estimating the performance of a tube from catalog data, or for predicting the characteristics needed for a given application, the ratios given below may be used.

Table 1 gives correlating data for typical operation of tubes in the various amplifier classifications. From the table, knowing the maximum ratings of a tube, the maximum power output, currents, voltages, and corresponding load impedance may be estimated. Thus, taking for example a type F-124-A water-cooled transmitting tube as a class-C radio-frequency power amplifier and oscillator—the constant-current characteristics of which are shown in Fig. 1—published maximum ratings are as follows.

DC plate voltage:

$$E_b = 20\,000 \text{ volts}$$

DC grid voltage:

$$E_c = 3000 \text{ volts}$$

DC plate current:

$$I_b = 7 \text{ amperes}$$

RF grid current:

$$I_g = 50 \text{ amperes}$$

Plate input:

$$P_i = 135\,000 \text{ watts}$$

Plate dissipation:

$$P_p = 40\,000 \text{ watts.}$$

Maximum conditions may be estimated as follows. For $\eta = 75$ percent

$P_i = 135\,000$ watts

$E_b = 20\,000$ volts.

Power output $P_o = \eta P_i = 100\,000$ watts.
Average dc plate current $I_b = P_i / E_b = 6.7$ amperes.

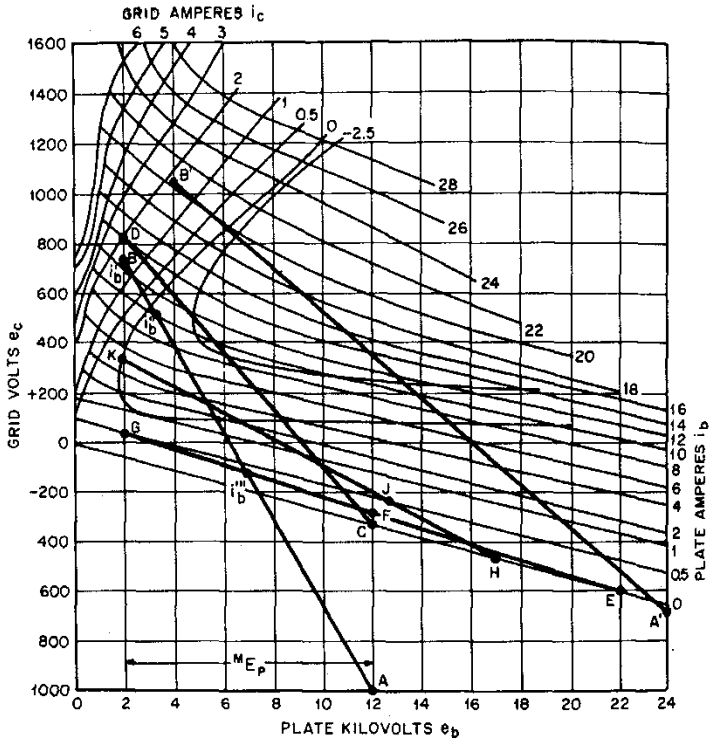

Fig. 1—Constant-current characteristics with typical load lines AB—class C, CD—class B, EFG—class A, and HJK—class AB.

From tabulated typical ratio $^{M}i_b/I_b=4$, instantaneous peak plate current $^{M}i_b=4I_b=27$ amperes.*

The rms plate alternating-current component, taking ratio $I_p/I_b=1.2$

$$I_p=1.2I_b=8 \text{ amperes.}$$

The rms value of the plate alternating-voltage component from the ratio $E_p/E_b=0.6$ is $E_p=0.6E_b=12\,000$ volts.

The approximate operating load resistance R_l is now found from

$$R_l=E_p/I_p=1500 \text{ ohms.}$$

An estimate of the grid drive power required may be obtained by reference to the constant-current characteristics of the tube and determination of the peak instantaneous positive grid current $^{M}i_c$ and the corresponding instantaneous total grid voltage $^{M}e_c$. Taking the value of grid bias E_c for the given operating condition, the peak alternating grid drive voltage is

$$^{M}E_g=(^{M}e_c-E_c)$$

from which the peak instantaneous grid drive power is

$$^{M}P_c=\,^{M}E_g\,^{M}i_c.$$

An approximation to the average grid drive power P_g, necessarily rough due to neglect of negative grid current, is obtained from the typical ratio

$$I_c/^{M}i_c=0.2$$

of dc to peak value of grid current, giving

$$P_g=I_cE_g=0.2\,^{M}i_cE_g \text{ watt.}$$

Plate dissipation P_p may be checked with published values since

$$P_p=P_i-P_o.$$

It should be borne in mind that combinations of published maximum ratings as well as each individual maximum rating must be observed. Thus, for example in this case, the maximum dc plate operating voltage of 20 000 volts does not permit operation at the maximum dc plate current of 7 amperes since this exceeds the maximum plate input rating of 135 000 watts.

Plate load resistance R_l may be connected directly in the tube plate circuit, as in the resistance-coupled amplifier, through impedance-matching elements as in audio-frequency transformer coupling, or effectively represented by a loaded parallel-resonant circuit as in most radio-frequency amplifiers. In any case, calculated values apply only to effectively resistive loads, such as are normally closely approximated in radio-frequency amplifiers. With appreciably reactive loads, operating currents and voltages will in general be quite different and their precise calculation is quite difficult.

The physical load resistance present in any given setup may be measured by audio-frequency or radio-frequency bridge methods. In many cases, the proper value of R_l is ascertained experimentally as in radio-frequency amplifiers that are tuned to the proper minimum dc plate current. Conversely, if the circuit is to be matched to the tube, R_l is determined directly as in a resistance-coupled amplifier or as

$$R_l=N^2R_s$$

in the case of a transformer-coupled stage, where N is the primary-to-secondary voltage transformation ratio. In a parallel-resonant circuit in which the output resistance R_s is connected directly in one of the reactance legs

$$R_l=X^2/R_s=L/CR_s=QX$$

where X is the leg reactance at resonance (ohms), L and C are leg inductance in henries and capacitance in farads, respectively, and $Q=X/R_s$.

*In this discussion, the superscript M indicates the use of the maximum or peak value of the varying component, i.e., $^{M}i_b$=*maximum* or peak value of the alternating component of the plate current.

Table 1—Typical Amplifier Operating Data. Maximum Signal Conditions—Per Tube.

Function	Class A	Class B af (p-p)	Class B rf	Class C rf
Plate efficiency η (percent)	20–30	35–65	60–70	65–85
Peak instantaneous to dc plate current ratio $^{M}i_b/I_b$	1.5–2	3.1	3.1	3.1–4.5
RMS alternating to dc plate current ratio I_p/I_b	0.5–0.7	1.1	1.1	1.1–1.2
RMS alternating to dc plate voltage ratio E_p/E_b	0.3–0.5	0.5–0.6	0.5–0.6	0.5–0.6
DC to peak instantaneous grid current $I_c/^{M}i_c$		0.1–0.25	0.1–0.25	0.1–0.25

GRAPHIC DESIGN METHODS

When accurate operating data are required, more-precise methods must be used. Because of the nonlinear nature of tube characteristics, graphic methods usually are most convenient and rapid. Examples of such methods are given below.

A comparison of the operating regimes of class A, AB, B, and C amplifiers is given in the constant-current characteristics graph of Fig. 1. The lines corresponding to the different classes of operation are each the locus of instantaneous grid e_c and plate e_b voltages, corresponding to their respective load impedances.

For radio-frequency amplifiers and oscillators having tuned circuits giving an effectively resistive load, plate and grid tube and load alternating voltages are sinusoidal and in phase (disregarding transit time), and the loci become straight lines.

For amplifiers having nonresonant resistive loads, the loci are in general nonlinear except in the distortionless case of linear tube characteristics (constant r_p), for which they are again straight lines.

Thus, for determination of radio-frequency performance, the constant-current chart is convenient. For solution of audio-frequency problems, however, it is more convenient to use the (i_b—e_c) transfer characteristics of Fig. 2 on which a dynamic load line may be constructed.

Methods for calculation of the most important cases are given below.

Class-C Radio-Frequency Amplifier or Oscillator

Draw straight line from A to B (Fig. 1) corresponding to chosen dc operating plate and grid voltages, and to desired peak alternating plate and grid voltage excursions. The projection of AB on the horizontal axis thus corresponds to $^{M}E_p$. Using Chaffee's 11-point method of harmonic analysis, lay out on AB points

$$e_p'=\,^{M}E_p$$

$$e_p''=0.866\,^{M}E_p$$

$$e_p'''=0.5\,^{M}E_p$$

to each of which correspond instantaneous plate currents i_b', i_b'', and i_b''' and instantaneous grid currents i_c', i_c'', and i_c'''. The operating currents

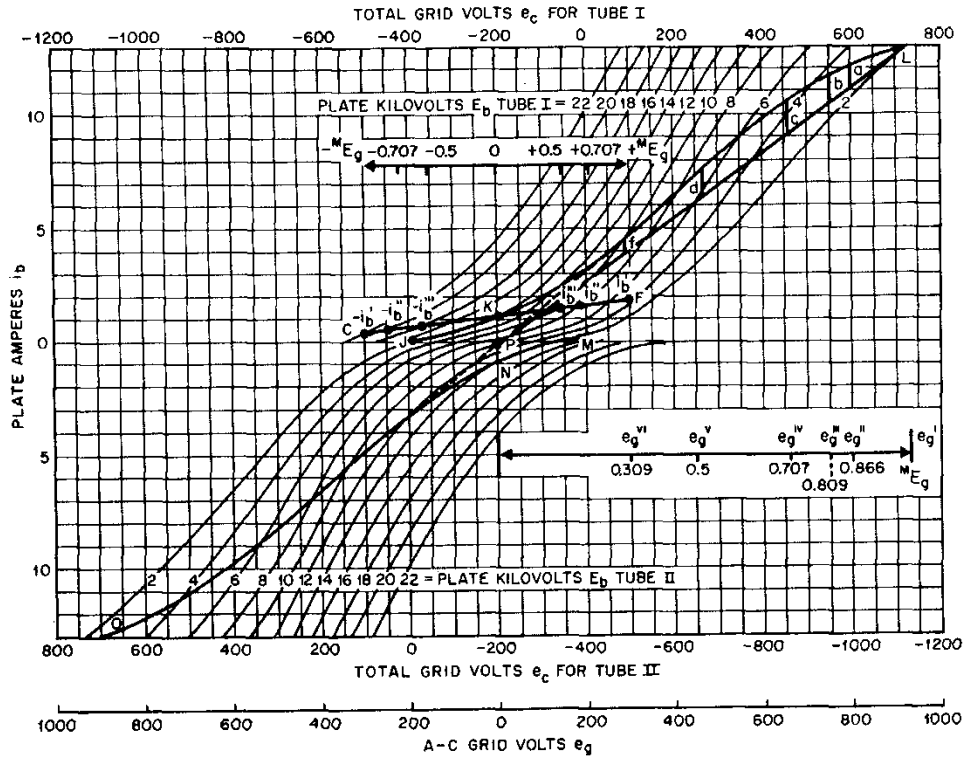

Fig. 2—Transfer characteristics i_b versus e_b with class A_2—CKF and class B—OPL load lines.

are obtained from

$$I_b=[i_b'+2i_b''+2i_b''']/12$$

$$I_c=[i_c'+2i_c''+2i_c''']/12$$

$$^{M}I_p=[i_b'+1.73i_b''+i_b''']/6$$

$$^{M}I_g=[i_c'+1.73i_c''+i_c''']/6.$$

Substitution of the above in the following give the desired operating data.

Power output $P_o=(^{M}E_p\ ^{M}I_p)/2$

Power input $P_i=E_bI_b$

Average grid excitation power $P_g=(^{M}E_g\ ^{M}I_g)/2$

Peak grid excitation power $^{M}P_c=^{M}E_gi_c'$

Plate load resistance $R_l=^{M}E_p/^{M}I_p$

Grid bias resistance $R_c=E_c/I_c$

Plate efficiency $\eta=P_o/P_i$

Plate dissipation $P_p=P_i-P_o$.

The above procedure may also be applied to plate-modulated class-C amplifiers. Taking the above data as applying to carrier conditions, the analysis is repeated for $^{crest}E_b=2E_b$ and $^{crest}P_o=4P_o$ keeping R_l constant. After a cut-and-try method has given a peak solution, it will often be found that combination fixed and self grid biasing as well as grid modulation are indicated to obtain linear operation.

TABLE 2—CLASS-C RF AMPLIFIER DATA FOR 100-PERCENT PLATE MODULATION.

Symbol	Preliminary	Detailed	
	Carrier	Carrier	Crest
E_b (volts)	12 000	12 000	24 000
$^{M}E_p$ (volts)	10 000	10 000	20 000
E_c (volts)	—	−1 000	−700
$^{M}E_g$ (volts)	—	1 740	1 740
I_b (amp)	2.9	2.8	6.4
$^{M}I_p$ (amp)	4.9	5.1	10.2
I_c (amp)	—	0.125	0.083
$^{M}I_g$ (amp)	—	0.255	0.183
P_i (watts)	35 000	33 600	154 000
P_o (watts)	25 000	25 500	102 000
P_g (watts)	—	220	160
η (percent)	75	76	66
R_l (ohms)	2 060	1 960	1 960
R_c (ohms)	—	7 100	7 100
E_{cc} (volts)	—	−110	−110

To illustrate the preceding exposition, a typical amplifier calculation is given below.

Operating requirements (carrier condition):

$E_b=12\ 000$ volts

$P_o=25\ 000$ watts

$\eta=75$ percent.

Preliminary calculation (refer to Tables 1 and 2):

$E_p/E_b=0.6$

$E_p=0.6\times12\ 000=7200$ volts

$^{M}E_p=1.41\times7200=10\ 000$ volts

$I_p=P_o/E_p$

$I_p=25\ 000/7200=3.48$ amperes

$^{M}I_p=4.9$ amperes

$I_p/I_b=1.2$

$I_b=3.48/1.2=2.9$ amperes

$P_i=12\ 000\times2.9=35\ 000$ watts

$^{M}i_b/I_b=4.5$

$^{M}i_b=4.5\times2.9=13.0$ amperes

$R_l=E_p/I_p=7200/3.48=2060$ ohms.

Complete Calculation: Lay out carrier operating line AB on constant-current graph, Fig. 1, using values of E_b, $^{M}E_p$, and $^{M}i_b$ from preliminary calculated data. Operating carrier bias voltage E_c is chosen somewhat greater than twice cutoff value (1000 volts) to locate point A.

The following data are taken along AB.

$i_b'=13$ amp

$i_b''=10$ amp

$i_b'''=0.3$ amp

$i_c'=1.7$ amp

$i_c''=-0.1$ amp

$i_c'''=0$ amp

$E_c=-1000$ volts

$e_c'=740$ volts

$^{M}E_p=10\ 000$ volts.

From the equations, complete carrier data as follows are calculated.

$^{M}I_p=[13+1.73\times10+0.3]/6=5.1$ amp

$P_o=(10\ 000\times5.1)/2=25\ 500$ watts

$I_b=[13+2\times10+2\times0.3]/12=2.8$ amp

$P_i=12\ 000\times2.8=33\ 600$ watts

$\eta=(25\ 500/33\ 600)\times100=76$ percent

$R_l=(10\ 000/5.1)=1960$ ohms

$I_c=[1.7+2(-0.1)]/12=0.125$ amp

$^{M}I_g=[1.7+1.7(-0.1)]/6=0.255$ amp

$P_g=(1740\times0.255)/2=220$ watts.

Operating data at 100-percent positive modulation crests are now calculated knowing that here

$$E_b=24\ 000\text{ volts}\quad R_l=1960\text{ ohms}$$

and for undistorted operation

$$P_o=4\times25\ 500=102\ 000\text{ watts}$$

$$^{M}E_p=20\ 000\text{ volts.}$$

The crest operating line A'B' is now located by trial so as to satisfy the above conditions, using the same equations and method as for the carrier condition.

It is seen that to obtain full-crest power output, in addition to doubling the alternating plate voltage, the peak plate current must be increased. This is accomplished by reducing the crest bias voltage with resultant increase of current conduction period but lower plate efficiency.

The effect of grid secondary emission to lower the crest grid current is taken advantage of to obtain the reduced grid-resistance voltage drop required. By use of combination fixed and grid resistance bias, proper variation of the total bias is obtained. The value of grid resistance required is given by

$$R_c=-(E_c-^{crest}E_c)/(I_c-^{crest}I_c)$$

and the value of fixed bias by

$$E_{cc}=E_c-(I_cR_c).$$

Calculations at carrier and positive crest together with the condition of zero output at negative crest give sufficiently complete data for most purposes. If accurate calculation of audio-frequency harmonic distortion is necessary, the above method may be applied to the additional points required.

Class-B Radio-Frequency Amplifiers

A rapid approximate method is to determine by inspection from the tube characteristics (i_b-e_b) the instantaneous current, i_b' and voltage e_b' corresponding to peak alternating voltage swing from operating voltage E_b.

AC plate current:

$$^{M}I_p=i_b'/2$$

DC plate current:

$$I_b=i_b'/\pi$$

AC plate voltage:

$$^{M}E_p=E_b-e_b'$$

Power output:

$$P_o=[(E_b-e_b')i_b']/4$$

Power input:

$$P_i=E_b i_b'/\pi$$

Plate efficiency:

$$\eta=(\pi/4)[1-(e_b'/E_b)].$$

Thus $\eta\approx 0.6$ for the usual crest value of ${}^{M}E_p\approx 0.8E_b$.

The same method of analysis used for the class-C amplifier may also be used in this case. The carrier and crest condition calculations, however, are now made from the same E_l, the carrier condition corresponding to an alternating-voltage amplitude of ${}^{M}E_p/2$ such as to give the desired carrier power output.

For greater accuracy than the simple check of carrier and crest conditions, the radio-frequency plate currents ${}^{M}I_p'$, ${}^{M}I_p''$, ${}^{M}I_p'''$, ${}^{M}I_p{}^{0}$, $-{}^{M}I_p'''$, $-{}^{M}I_p''$, and $-{}^{M}I_p'$ may be calculated for seven corresponding selected points of the audio-frequency modulation envelope $+{}^{M}E_g$, $+0.707\,{}^{M}E_g$, $+0.5\,{}^{M}E_g$, 0, $-0.5\,{}^{M}E_g$, $-0.707\,{}^{M}E_g$, and $-{}^{M}E_g$, where the negative signs denote values in the negative half of the modulation cycle. Designating

$$S'={}^{M}I_p'-(-{}^{M}I_p')$$

$$D'={}^{M}I_p'+(-{}^{M}I_p')-2\,{}^{M}I_p{}^{0}$$

the fundamental and harmonic components of the output audio-frequency current are obtained as

$${}^{M}I_{p1}=(S'/4)+[S''/2(2)^{1/2}]\ \text{(fundamental)}$$

$${}^{M}I_{p2}=(5D'/24)+(D''/4)-(D'''/3)$$

$${}^{M}I_{p3}=(S'/6)-(S'''/3)$$

$${}^{M}I_{p4}=(D'/8)-(D''/4)$$

$${}^{M}I_{p5}=(S'/12)-[S''/2(2)^{1/2}]+(S'''/3)$$

$${}^{M}I_{p6}=(D'/24)-(D''/4)+(D'''/3).$$

This detailed method of calculation of audio-frequency harmonic distortion may, of course, also be applied to calculation of the class-C modulated amplifier, as well as to the class-A modulated amplifier.

Class-A and AB Audio-Frequency Amplifiers

Approximate equations assuming linear tube characteristics:

Maximum undistorted power output

$${}^{M}P_o=({}^{M}E_p\,{}^{M}I_p)/2$$

when plate load resistance

$$R_l=r_p\left[\frac{E_c}{({}^{M}E_p/\mu)-E_c}-1\right]$$

and negative grid bias

$$E_c=({}^{M}E_p/\mu)[(R_l+r_p)/(R_l+2r_p)]$$

giving maximum plate efficiency

$$\eta={}^{M}E_p\,{}^{M}I_p/8E_bI_b.$$

Maximum maximum undistorted power output

$${}^{MM}P_o={}^{M}E^2{}_p/16r_p$$

when

$$R_l=2r_p \qquad E_c=\tfrac{3}{4}({}^{M}E_p/\mu).$$

An exact analysis may be obtained by use of a dynamic load line laid out on the transfer characteristics of the tube. Such a line is CKF of Fig. 2, which is constructed about operating point K for a given load resistance r_l from

$$i_b{}^{S}=[(e_b{}^{R}-e_b{}^{S})/R_l]+i_b{}^{R}$$

where R, S, etc., are successive conveniently spaced construction points.

Using the seven-point method of harmonic analysis, plot instantaneous plate currents i_b', i_b'', i_b''', i_b, $-i_b'''$, $-i_b''$, and $-i_b'$ corresponding to $+{}^{M}E_g$, $+0.707\,{}^{M}E_g$, $+0.5\,{}^{M}E_g$, 0, $-0.5\,{}^{M}E_g$, $-0.707\,{}^{M}E_g$, and $-{}^{M}E_g$, where 0 corresponds to the operating point K. In addition to the equations given under class-B radio-frequency amplifiers

$$I_b\ \text{average}=I_b+(D'/8)+(D''/4)$$

from which complete data may be calculated.

Class-AB and B Audio-Frequency Amplifiers

Approximate equations assuming linear tube characteristics give (referring to Fig. 1, line CD) for a class-B audio-frequency amplifier

$${}^{M}I_p=i_b'$$

$$P_o={}^{M}E_p\,{}^{M}I_p/2$$

$$P_i=(2/\pi)E_b\,{}^{M}I_p$$

$$\eta=(\pi/4)\,({}^{M}E_p/E_b)$$

$$R_{pp}=4({}^{M}E_p/i_b')=4R_l.$$

Again an exact solution may be derived by use of the dynamic load line JKL on the (i_b-e_c) characteristic of Fig. 2. This line is calculated about the operating point K for the given R_l (in the same way as for the class-A case). However, since two tubes operate in phase opposition in this case, an identical dynamic load line *MNO* represents the other half cycle, laid out about the operating bias abscissa point but in the opposite direction (see Fig. 2).

Algebraic addition of instantaneous current values of the two tubes at each value of e_c gives the composite dynamic characteristic OPL for the two tubes. Inasmuch as this curve is symmetrical about point P, it may be analyzed for harmonics along a single half-curve PL by the Mouromtseff 5-point method. A straight line is drawn from P to L and ordinate plate-current differences a, b, c, d, f between this line and curve, corresponding to e_g'', e_g''', $e_g{}^{IV}$, $e_g{}^{V}$, and $e_g{}^{VI}$, are measured. Ordinate distances measured upward from curve PL are taken positive.

TABLE 3—DESIGN INFORMATION FOR 3 CLASSES OF AMPLIFIERS.

Grounded-Cathode	Grounded-Grid	Grounded-Plate or Cathode-Follower
Circuit schematic		
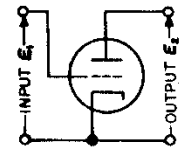	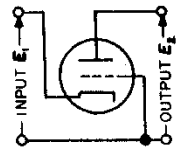	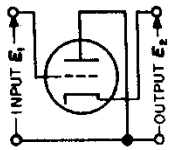
Equivalent circuit, alternating-current component, class-A operation		
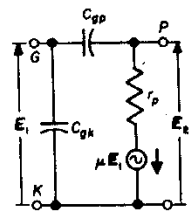	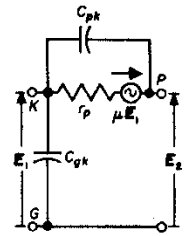	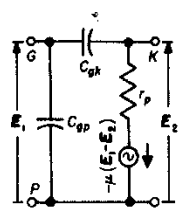
Voltage gain **A** for output load impedance Z_2; $\mathbf{A}=\mathbf{E}_2/\mathbf{E}_1$		
$\mathbf{A}=-\mu Z_2/(r_p+Z_2)$ $=-g_m[r_pZ_2/(r_p+Z_2)]$	$\mathbf{A}=(1+\mu)[Z_2/(r_p+Z_2)]$	$\mathbf{A}=\mu Z_2/[r_p+(1+\mu)Z_2]$
neglecting C_{gp} (Z_2 includes C_{pk})	neglecting C_{pk} (Z_2 includes C_{gp})	neglecting C_{gk} (Z_2 includes C_{pk})
Input admittance; $Y_1=\mathbf{I}_1/\mathbf{E}_1$		
$Y_1=j\omega[C_{gk}+(1-\mathbf{A})C_{gp}]$	$Y_1=j\omega[C_{gk}+(1-\mathbf{A})C_{pk}]$ $+[(1+\mu)/(r_p+Z_2)]$	$Y_1=j\omega[C_{gp}+(1-\mathbf{A})C_{gk}]$
Equivalent generator seen by load at output terminals		
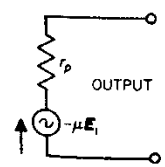	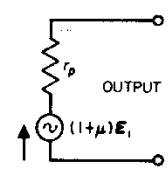	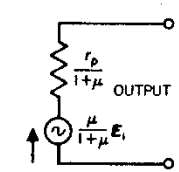
neglecting C_{gp}	neglecting C_{pk}	neglecting C_{gk}

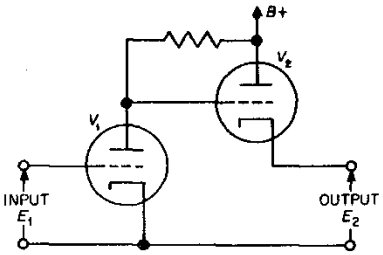

Fig. 3

Fundamental and harmonic current amplitudes and power are found from

$$^{M}I_{p1}=i_b'-{}^{M}I_{p3}+{}^{M}I_{p5}-{}^{M}I_{p7}+{}^{M}I_{p9}-{}^{M}I_{p11}$$

$$^{M}I_{p3}=0.4475(b+f)+(d/3)-0.578d-\tfrac{1}{2}{}^{M}I_{p5}$$

$$^{M}I_{p5}=0.4(a-f)$$

$$^{M}I_{p7}=0.4475(b+f)-{}^{M}I_{p3}+0.5{}^{M}I_{p5}$$

$$^{M}I_{p9}={}^{M}I_{p3}-\tfrac{2}{3}d$$

$$^{M}I_{p11}=0.707c-{}^{M}I_{p3}+{}^{M}I_{p5}.$$

Even harmonics are not present due to dynamic characteristic symmetry. The direct-current and power-input values are found by the 7-point analysis from curve PL and doubled for two tubes.

CLASSIFICATION OF AMPLIFIER CIRCUITS

The classification of amplifiers in classes A, B, and C is based on the operating conditions of the tube. Another classification can be used, based on the type of circuits associated with the tube.

A tube can be considered as a four-terminal network with two input terminals and two output terminals. One of the input terminals and one of the output terminals are usually common; this common junction or point is usually called "ground."

When the common point is connected to the filament or cathode of the tube, we can speak of a grounded-cathode circuit: the most-conventional type of vacuum-tube circuit. When the common point is the grid, we can speak of a grounded-grid circuit, and when the common point is the plate or anode, we can speak of the grounded-anode circuit.

This last type of circuit is most commonly known by the name of *cathode-follower*.

A fourth and most-general class of circuit is obtained when the common point or ground is not directly connected to any of the three electrodes of the tube. This is the condition encountered at uhf where the series impedances of the internal tube leads make it impossible to ground any of them. It is also encountered in such special types of circuits as the *phase-splitter*, in which the impedance from plate to ground and the impedance from cathode to ground are made equal to obtain an output between plate and cathode balanced with respect to ground.

Design information for the first three classifications is given in Table 3, where

Z_2 = load impedance to which output terminals of amplifier are connected

$\mathbf{E}_1$ = phasor input voltage to amplifier

$\mathbf{E}_2$ = phasor output voltage across load impedance Z_2

$\mathbf{A}$ = voltage gain of amplifier = $\mathbf{E}_2/\mathbf{E}_1$

Y_1 = input admittance to input terminals of amplifier

$\omega = 2\pi \times$ (frequency of excitation voltage $\mathbf{E}_1$)

$j=(-1)^{1/2}$.

AMPLIFIER PAIRS

The basic amplifier classes are often used in pairs or combination forms for special characteristics. The availability of dual triodes makes these combined forms especially useful.

Grounded-Cathode—Grounded-Plate

This pairing provides the gain and 180-degree phase reversal of a grounded-cathode stage (Fig. 3) with a low source impedance at the output terminals. It is especially useful in feedback circuits or for amplifiers driving a low or unknown load impedance. In tuned amplifiers, the possibility of oscillation must be considered. Direct coupling is useful for pulse work, permitting large positive input and negative output excursions.

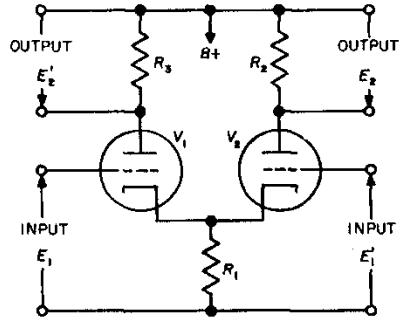

Fig. 4

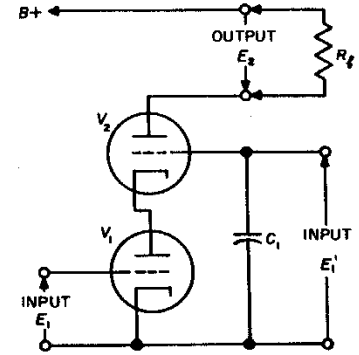

Fig. 5

Grounded-Plate—Grounded-Grid (Cathode-Coupled)

Direct coupling is usual, making a very simple structure. Several modified forms are possible with special characteristics.

Cathode-Coupled Amplifier: As a simple amplifier, R_3 and input E_1' (Fig. 4) are short-circuited. Output E_2 is in phase with input E_1. Gain (with $R_1 \gg 1/g_m$) is given by $\mathbf{A} \approx g_m R_2/2$. Even-harmonic distortion is reduced by symmetry, as in a push-pull stage. Due to the in-phase input and output relations, this circuit forms the basis for various *R–C* oscillators and the class of cathode-coupled multivibrators.

Symmetrical Clipper: With suitable bias adjustment, symmetrical clipping or limiting occurs between V_1 cutoff and V_2 cutoff, without drawing grid current.

Differential Amplifier: With input supplied to E_1 and E_1', the output E_2 responds (approximately) to the difference E_1-E_1'. Balance is improved by constant-current supply to the cathode such as a high value of R_1 (preferably connected from a highly negative supply) or a constant-current pentode. The signal to E_1' should be slightly attenuated for precise adjustment of balance.

Phase Inverter: With R_3 and R_2 both used, approximately balanced (push–pull) outputs (E_2 and E_2') are obtained from either input E_1' or E_1. As a phase inverter (paraphase), one input (E_1) is used, the other being grounded, and R_3 is made slightly less than R_2 to provide exact balance.

Grounded-Cathode—Grounded-Grid (Cascode)

This circuit (Fig. 5) has characteristics somewhat resembling the pentode, with the advantage that no screen current is required. V_2 serves to isolate V_1 from the output load R_l, giving voltage gain equation

$$A=\frac{\mu_1 R_l}{r_{p1}+[(r_{p2}+R_l)/(\mu_2+1)]}.$$

For $R_l \ll \mu r_p$,

$$A \approx g_{m1} R_l.$$

For $R_l \gg \mu r_p$,

$$A \approx \mu_1 \mu_2.$$

As an rf amplifier, the grounded-grid stage V_2 drastically reduces capacitive feedback from output to input, without introducing partition noise (as produced by the screen current of a pentode). Shot noise contributed by V_2 is negligible due to the highly degenerative effect of r_{p1} in series with the cathode. The noise figure thus approaches the theoretical noise of V_1 used as a triode, without the undesirable effects of triode plate-grid capacitance.

Because of the 180° phase relation of input and output, this circuit is also valuable in audio feedback circuits, replacing a single stage with considerable increase in gain (for high values of R_l).

The grid of V_2 provides a second input connection E_1' useful for feedback or for gating. The voltage gain from E_1' to the output is considerably reduced, being given by

$$A=R_l\mu/(R_l+\mu r_p).$$

For $R_l \ll \mu r_p$,

$$A_2 \approx R_l/r_{p1}.$$

For $R_l \gg \mu r_p$,

$$A_2 \approx \mu.$$

CATHODE-FOLLOWER DATA

General Characteristics

(A) High-impedance input, low-impedance output.
(B) Input and output have one side grounded.
(C) Good wide-band frequency and phase response.
(D) Output is in phase with input.
(E) Voltage gain or transfer is always less than one.
(F) A power gain can be obtained.
(G) Input capacitance is reduced.

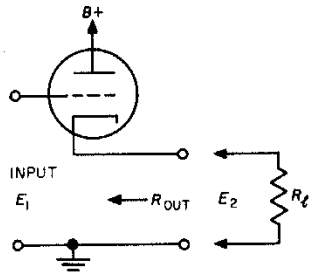

Fig. 6

General Case (Fig. 6)

Transfer $= E_{out}/E_{in} = g_m R_l/[g_m R_l + 1 + (R_l/r_p)]$

R_{out} = output resistance

$= r_p/(\mu+1)$ or approximately $1/g_m$

g_m = transconductance in mhos (1000 micromhos = 0.001 mho)

R_l = total load resistance

Input capacitance $= C_{gp} + [C_{gk}/(1+g_m R_l)]$.

Specific Cases

(**A**) To match the characteristic impedance of the transmission line, R_{out} must equal Z_0 (Fig. 7).

(**B**) If R_{out} is less than Z_0, add resistor R_c' in series (Fig. 8) so that $R_c' = Z_0 - R_{out}$.

(**C**) If R_{out} is greater than Z_0, add resistor R_c in parallel (Fig. 9) so that

$$R_c = Z_0 R_{out}/(R_{out} - Z_0).$$

Note 1: Normal operating bias must be provided. To couple a high impedance into a low-impedance transmission line, for maximum transfer choose a tube with a high g_m.

Note 2: Oscillation may occur in a cathode-follower if the source becomes inductive and load capacitive at high frequencies. The general expression for voltage gain of a cathode-follower (including C_{gk}) is given by

$$\mathbf{A} = \frac{\mu Z_2 + Z_2 r_p/Z_{gk}}{r_p + Z_2(1+\mu) + Z_2 r_p/Z_{gk}}.$$

The input admittance (Table 3)

$$Y_1 = j\omega[C_{gp} + (1-\mathbf{A})C_{gk}]$$

may contain negative-resistance terms causing oscillation at the frequency where an inductive grid circuit resonates the capacitive Y_1 component.

The use of a simple triode (or pentode) grounded-cathode circuit with a load resistor equal to Z_0 provides an equally good match with slightly higher gain ($g_m R_l$), but will overload at a lower maximum voltage. The anode-follower provides output approximating the cathode-follower without the risk of oscillation.

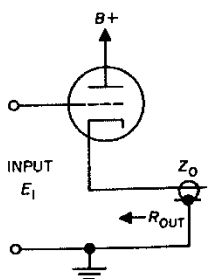

Fig. 7

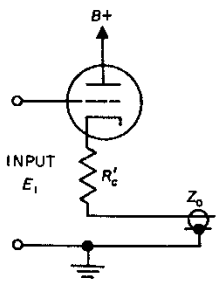

Fig. 8

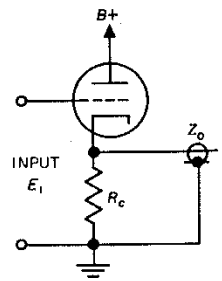

Fig. 9

NEGATIVE FEEDBACK

The following quantities are functions of frequency with respect to magnitude and phase.

E, N, D = signal, noise, and distortion output voltage with feedback

e, n, d = signal, noise, and distortion output voltage without feedback

A = voltage amplification magnitude of amplifier at a given frequency

$\mathbf{A}$ = amplification including phase angle (complex quantity)

β = fraction of output voltage fed back (complex quantity); for usual negative feedback, β is negative

ϕ = phase shift of amplifier and feedback circuit at a given frequency.

Reduction in Gain Caused by Feedback (Fig. 10)

The total output voltage with feedback is

$$E + N + D = e + \frac{n}{1-\mathbf{A}\beta} + \frac{d}{1-\mathbf{A}\beta}.$$

It is assumed that the input signal to the amplifier is increased when negative feedback is applied, keeping $E = e$.

$(1-\mathbf{A}\beta)$ is a measure of the amount of feedback. By definition, the amount of feedback expressed in decibels is

$$20 \log_{10} |1-\mathbf{A}\beta|$$

voltage gain with feedback $= \mathbf{A}/(1-\mathbf{A}\beta)$

change of gain $= 1/(1-\mathbf{A}\beta)$.

If the amount of feedback is large, i.e., $-\mathbf{A}\beta \gg 1$,

voltage gain becomes $-1/\beta$

and so is independent of $\mathbf{A}$.

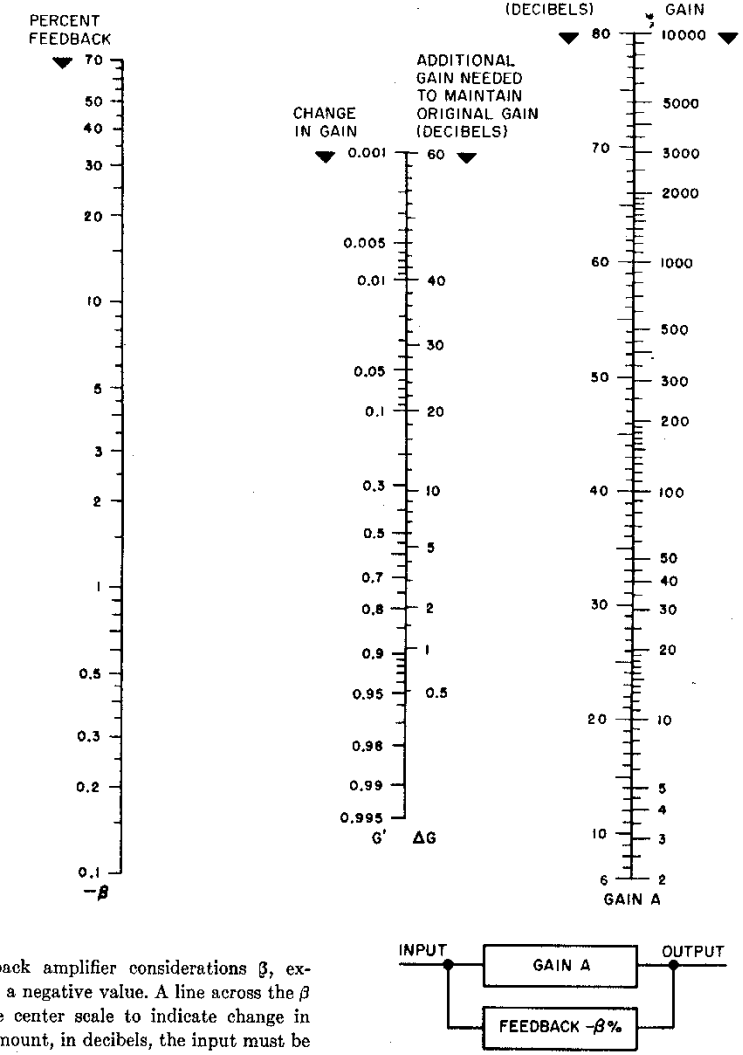

Fig. 10—In negative-feedback amplifier considerations β, expressed as a percentage, has a negative value. A line across the β and A scales intersects the center scale to indicate change in gain. It also indicates the amount, in decibels, the input must be increased to maintain original output.

In the general case when ϕ is not restricted to 0 or π

$$\text{voltage gain} = \mathbf{A}/(1+|\mathbf{A\beta}|^2-2|\mathbf{A\beta}|\cos\phi)^{1/2}$$

$$\text{change of gain} = (1+|\mathbf{A\beta}|^2-2|\mathbf{A\beta}|\cos\phi)^{-1/2}.$$

Hence if $|\mathbf{A\beta}| \gg 1$, the expression is substantially independent of ϕ.

On the polar diagram relating $(\mathbf{A\beta})$ and ϕ (Nyquist diagram), the system is unstable if the point (1, 0) is enclosed by the curve. Examples of Nyquist diagrams for feedback amplifiers will be found in the chapter on Feedback Control Systems.

DISTORTION

A rapid indication of the harmonic content of an alternating source is given by the *distortion factor*, which is expressed as a percentage.

$$\text{(Distortion factor)} = \left[\frac{\text{sum of squares of amplitudes of harmonics}}{\text{square of amplitude of fundamental}}\right]^{1/2} \times 100 \text{ percent.}$$

If this factor is reasonably small, say less than 10 percent, the error involved in measuring it as

$$\left[\frac{\text{sum of squares of amplitudes of harmonics}}{\text{sum of squares of amplitudes of fundamental and harmonics}}\right]^{1/2} \times 100 \text{ percent}$$

is also small. This latter is measured by the *distortion-factor meter*.

RELAXATION OSCILLATORS

Relaxation oscillators are a class of oscillator characterized by a large excess of positive feedback, causing the circuit to operate in abrupt transitions between two blocked or overloaded end-states. These end-states may be stable, the circuit remaining in such condition until externally disturbed; or *quasi-stable*, recovering (after a period determined by coupling-circuit time constants and bias) and switching back to the opposite state. Relaxation oscillators are classified as *bistable*, *monostable*, or *astable* according to the number of stable end-states. Most circuits are adaptable to all three forms. Multistate devices are also possible. A wide variety of circuit arrangements is possible, including multivibrators, blocking oscillators, trigger circuits, counters, and circuits of the phantastron, sanotron, and sanophant class. Relaxation oscillators are often used for counting and frequency division, and to generate nonsinusoidal waveforms for timing, triggering, and similar applications.

Multivibrators

A number of multivibrator circuits are formed from three basic two-stage amplifiers (grounded-cathode–grounded-cathode, grounded-plate-grounded-grid, and grounded-cathode–grounded-grid, or combinations of these types), that readily provide the needed positive feedback with simple resistance or resistance–capacitance coupling. End-states may be any two of the four "blocked" conditions corresponding to cutoff or saturation in either stage. In general, the duration of a quasi-stable state will be determined by the exponential decay of charge stored in a coupling-circuit time constant, (the circuit switching back to the opposite state when the saturated or the cutoff tube recovers gain), while stable states are produced by direct coupling with bias sufficient to hold one tube inoperative. The memory effect of charge storage also operates in the case of stable end-states to ensure completion of transfer across the unstable region. The timing accuracy of an astable or quasi-stable multivibrator is considerably improved by supplying the grid resistors from a high positive voltage ($B+$). The recovery from a cutoff condition thereby becomes an exponential towards a voltage much higher than the operating point, terminating in switchover when the cut off tube conducts. Grid conduction serves to clamp the capacitor voltage during the conducting state, erasing residual charge from the previous state. The starting condition for the next transition is thus more precisely determined and the linearity of the exponential recovery is improved by the more nearly constant-current discharge (since the range from cutoff to zero bias represents a smaller fraction of total charge). The grid-circuit time constant must be appropriately increased to obtain the same dwell time.

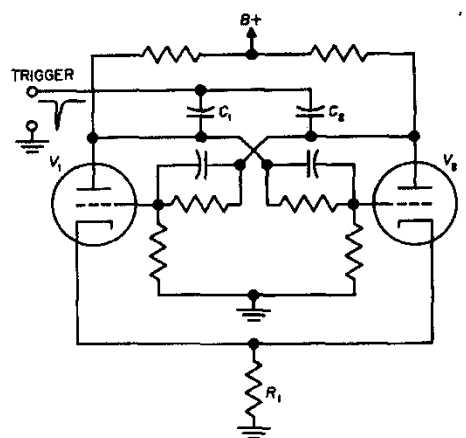

Fig. 11—Symmetrical bistable multivibrator (basic binary counter).

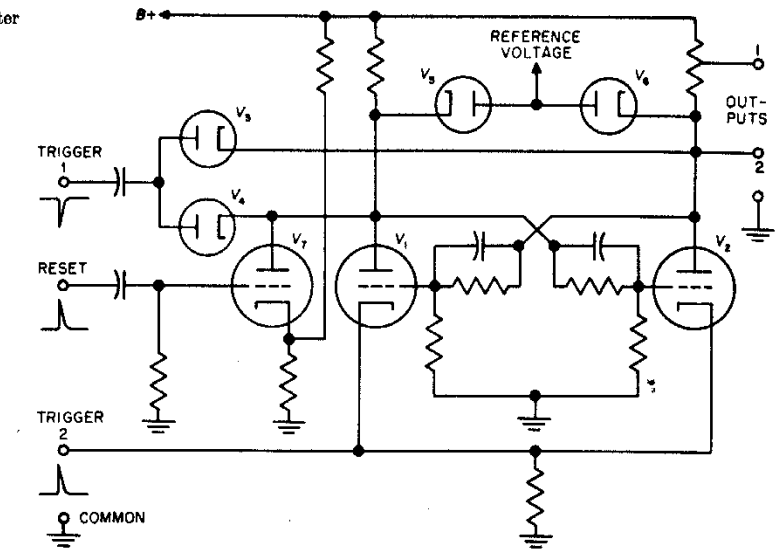

Fig. 12—Binary counter stage.

Bistable Circuits

Bistable circuits are especially suited for binary counters and frequency dividers and as trigger circuits to produce a step or pulse when an input signal passes above or below a selected amplitude.

Symmetrical Bistable Multivibrator: The circuit is shown in Fig. 11. Trigger signal may be applied to both plates, both grids, or if pentodes are used, to both suppressor grids.

Binary Counter Stage: An adaptation of the symmetrical bistable multivibrator is shown in Fig. 12. Alternative trigger inputs are shown with corresponding outputs to drive a following stage. The use of coupling diodes (V_3, V_4) reduces the tendency of C_1, C_2 in the circuit of Fig. 11 to cause misfiring by unbalanced stored charge. Tubes V_5 and V_6 illustrate the application of clamping diodes, especially useful in high-speed circuits, to fix critical operating voltages. Pentodes with plate and grid clamping are suitable for very high speeds.

Schmitt Trigger: The circuit of Fig. 13 has the property that an output of constant peak value (a flat-topped pulse) is obtained for the period that the input waveform exceeds a specific voltage.

Monostable Circuits

Monostable multivibrators are useful for driven-sweep, pulse, and timing-wave generators. The absence of time constants and residual charge "memory" in the stable state reduces jitter when they are driven with irregularly spaced timing signals. Monostable versions may be derived from

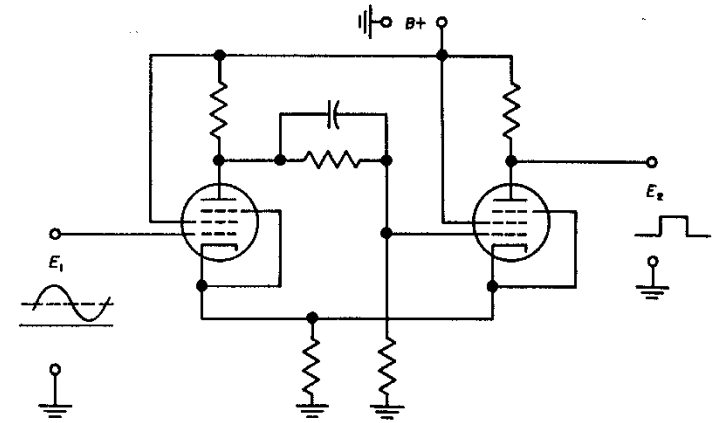

Fig. 13—Basic Schmitt trigger.

Fig. 14—Regenerative clipper (modified Schmitt trigger).

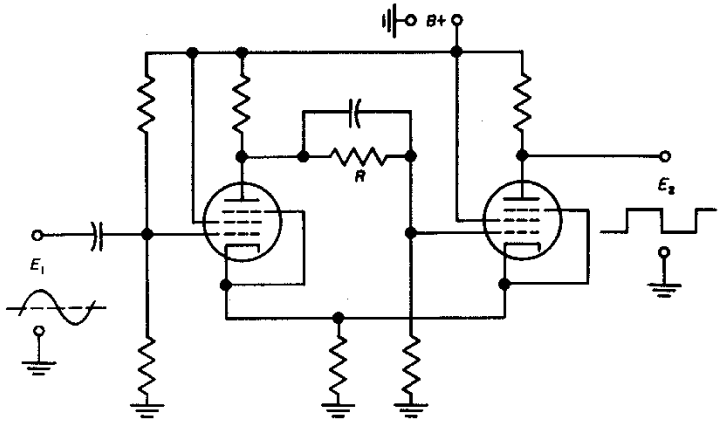

all of the foregoing bistable multivibrators by elimination of the direct (dc) coupling to one or the other grid. The circuit of Fig. 14 with R omitted is commonly used for pulse generation.

Most astable circuits can be made monostable by sufficient inequality of bias. The circuit of Fig. 17 is an example.

Sweep waveforms can be produced by integration of pulse outputs. The phantastron class of Miller sweep generators is also particularly useful for this purpose.

Driven (One-Shot) Multivibrator: The circuit is given in Fig. 15. Equations are

$$f_{mv}=f_s$$

f_{mv} = multivibrator frequency in hertz

f_s = synchronizing frequency in hertz.

Conditions of operation are

$$f_s>f_n \quad \text{or} \quad \tau_s<\tau_n.$$

where

f_n = free-running frequency in hertz

τ_s = synchronizing period in seconds

τ_n = free-running period in seconds.

Fig. 15—Driven (one-shot) multivibrator schematic and waveforms.

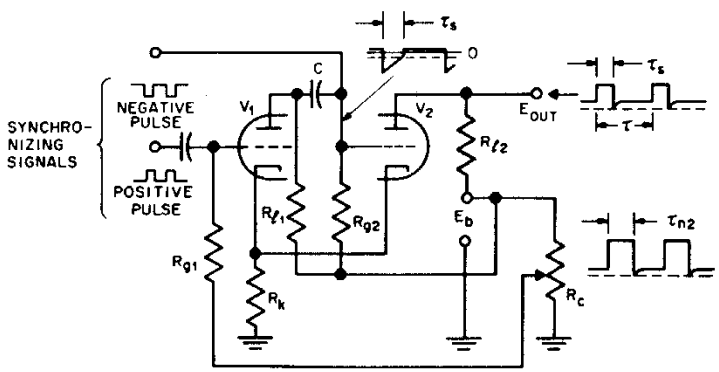

At the control resistor R_c

$$\tau_{n2}=R_{g2}C\log_e[(E_{b1}-E_{m1}+E_{c2})/(E_{c2}+E_{x2})].$$

where

E_{b1} = plate-supply voltage V_1

E_{m1} = minimum ac voltage on plate of V_1

E_{c2} = bias voltage of V_2

E_{x2} = cutoff voltage corresponding to E_{b1}.

Regenerative Clipper: Bias on the first grid places the circuit of Fig. 14 in the center of the unstable region, giving regenerative clipping.

Phantastron: The phantastron circuit is a form of monostable multivibrator with similarities to the Miller sweep circuit. It is useful for generating very short pulses and linear sweeps. It uses a characteristic of pentodes: that while cathode current is determined mainly by control-grid potential, the screen-grid, suppressor-grid, and plate potentials determine the division of current between plate and screen. In certain tubes, such as the 6AS6, the transconductance from suppressor grid to plate is sufficiently high so that the plate current

Fig. 16—Cathode-coupled phantastron.

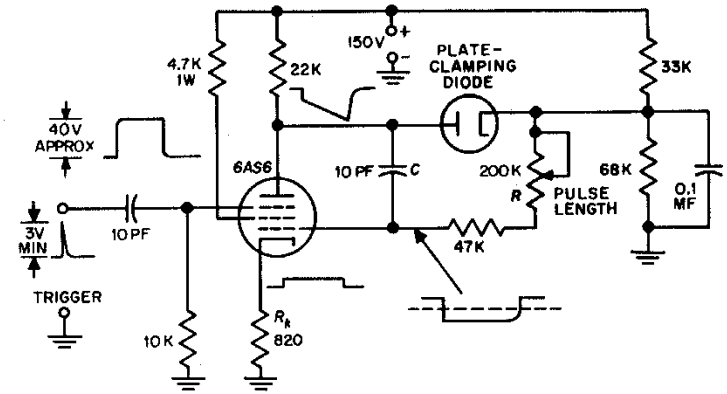

may be cut off completely with a small negative bias on the suppressor.

A typical phantastron circuit is shown in Fig. 16. During operation it switches between two states of interest.

(**A**) *Stable*: The control grid is slightly positive and draws current. Cathode current is maximum and the suppressor is biased negatively to plate-current cutoff by the cathode current in R_k. The plate is at a high potential determined by the clamping diode, and the screen potential is low.

(**B**) *Unstable*: When a positive trigger is applied to the suppressor grid (or a negative trigger to the control grid, cathode, or plate) the plate conducts, driving the control grid negative, reducing the cathode current, and taking most of the screen current. The plate potential then runs down linearly as in the Miller circuit.

The end of this period comes when the control grid goes positive again, resulting in increase of cathode current, suppressor cutoff, and heavy screen current.

In the circuit shown, the pulse width is adjustable from 0.3 to 0.6 microsecond. For longer pulses, it is possible to get a wide range of control both by varying R and C and by varying the plate-clamping potential.

Decreasing R_k results in astable operation.

Astable Circuits

The operating principles of the multivibrator and the exponential recovery from quasi-stable states are illustrated by the analysis of the free-running multivibrator.

Free-Running Zero-Bias Symmetrical Multivibrator: Exact equation for semiperiod (Figs. 17 and 18)

$$\tau_1=\{R_{g1}+[R_{l2}r_p/(R_{l2}+r_p)]\}C_1 \times\log_e[(E_b-E_m)/E_x]$$

where

$\tau=\tau_1+\tau_2=1/f$, $\tau_1=\tau_2$, $R_{g1}=R_{g2}$, $C_1=C_2$.

f = repetition frequency in hertz

τ = period in seconds

τ_1 = semiperiod in seconds

r_p = plate resistance of tube in ohms

E_b = plate-supply voltage

E_m = minimum alternating voltage on plate

E_x = cutoff voltage corresponding to E_b

C = capacitance in farads.

Fig. 17—Schematic diagram of symmetrical multivibrator and voltage waveforms on tube elements.

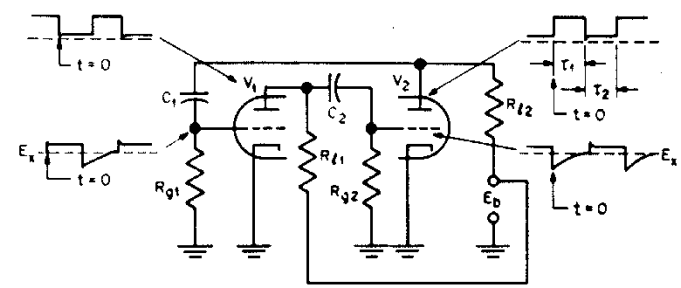

Approximate equation for semiperiod, where $R_{g1} \gg [R_{l2} r_p/(R_{l2}+r_p)]$, is

$$\tau_1 = R_{g1} C_1 \log_e[(E_b - E_m)/E_x].$$

Equation for buildup time is

$$\tau_B = 4(R_l + r_p)C$$

$$= 98 \text{ percent of peak value.}$$

Free-Running Zero-Bias Unsymmetrical Multivibrator: See symmetrical multivibrator (above) for circuit and terminology; the waveforms are given in Fig. 19.

Equations for fractional periods are

$$\tau_1 = \{R_{g1} + [R_{l2} r_p/(R_{l2}+r_p)]\} C_1 \times \log_e[(E_{b2} - E_{m2})/E_{x1}]$$

$$\tau_2 = \{R_{g2} + [R_{l1} r_p/(R_{l1}+r_p)]\} C_2 \times \log_e[(E_{b1} - E_{m1})/E_{x2}]$$

$$\tau = \tau_1 + \tau_2 = 1/f.$$

Free-Running Positive-Bias Multivibrator: Equations for fractional period (Fig. 20) are

$$\tau_1 = \{R_{g1} + [R_{l2} r_p/(R_{l2}+r_p)]\} C_1 \times \log_e[(E_{b2} - E_{m2} + E_{c1})/(E_{c1} + E_{x1})]$$

$$\tau_2 = \{R_{g2} + [R_{l1} r_p/(R_{l1}+r_p)]\} C_2 \times \log_e[(E_{b1} - E_{m1} + E_{c2})/(E_{c2} + E_{x2})]$$

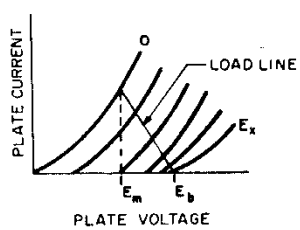

Fig. 18—Multivibrator potentials on plate-characteristic curve.

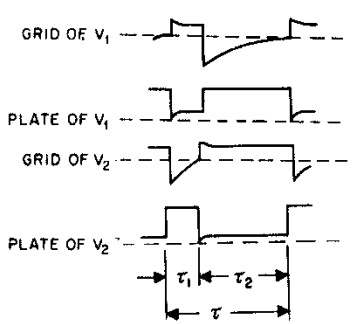

Fig. 19—Unsymmetrical multivibrator waveforms.

where

$\tau = \tau_1 + \tau_2 = 1/f$

E_c = positive bias voltage.

Blocking Oscillators

The blocking oscillator (Figs. 21–23) is a single-tube relaxation oscillator using a close-coupled (current) transformer that imposes a fixed current ratio between grid current and plate current, while also providing the polarity reversal for positive feedback. There are, therefore, two end-states that satisfy the requirement i_p/i_g = turns ratio: one in the positive-grid region, with large grid current, and one at cutoff, with both currents zero. Astable and monostable forms are illustrated in the following discussion.

Astable Blocking Oscillator: Conditions for blocking are

$$E_1/E_0 < 1 - \epsilon^{1/\alpha f - \theta}$$

where

E_0 = peak grid volts

E_1 = positive portion of grid swing in volts

f = frequency in hertz

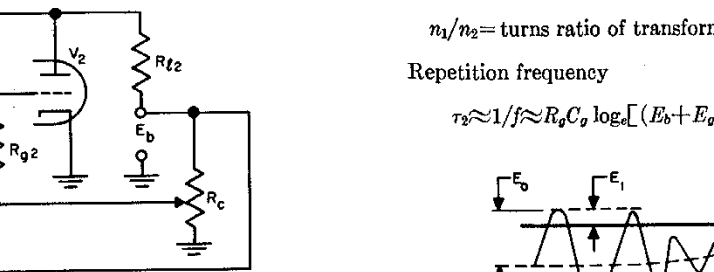

Fig. 20—Free-running positive-bias multivibrator.

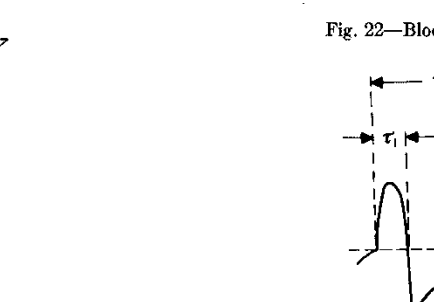

Fig. 21—Free-running blocking oscillator—schematic and waveforms.

α = grid time constant in seconds

$\epsilon = 2.718$ = base of natural logs

θ = decrement of wave.

(A) Use strong feedback

$= E_0$ is high.

(B) Use large grid time constant

$= \alpha$ is large.

(C) Use high decrement (high losses)

$= \theta$ is high.

Pulse width is

$$\tau_1 \approx 2(LC)^{1/2}$$

where

τ_1 = pulse width in seconds

L = magnetizing inductance of transformer in henries

C = interwinding capacitance of transformer in farads.

$$L = M(n_1/n_2)$$

where

M = mutual inductance between windings

n_1/n_2 = turns ratio of transformer.

Repetition frequency

$$\tau_2 \approx 1/f \approx R_g C_g \log_e[(E_b + E_g)/(E_b + E_x)]$$

Fig. 22—Blocking-oscillator grid voltage.

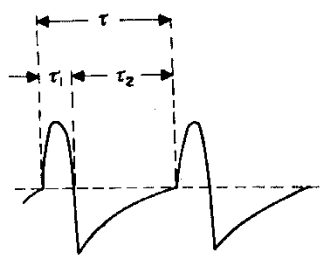

Fig. 23—Blocking-oscillator pulse waveform.

where

$\tau_2 \gg \tau_1$

f = repetition frequency in hertz

E_b = plate-supply voltage

E_g = maximum negative grid voltage

E_x = grid cutoff in volts

$\tau = \tau_1 + \tau_2 = 1/f.$

Astable Positive-Bias Wide-Frequency-Range Blocking Oscillator: Typical circuit values (Fig. 24) are

R = 0.5 to 5 megohms

C = 50 picofarads to 0.1 microfarad

R_k = 10 to 200 ohms

R_b = 50 000 to 250 000 ohms

Δf = 100 hertz to 100 kilohertz.

Monostable Blocking Oscillator: Operating conditions (Fig. 25) are:

(A) Tube off unless positive voltage is applied to grid.

(B) Signal input controls repetition frequency.

(C) E_c is a high negative bias.

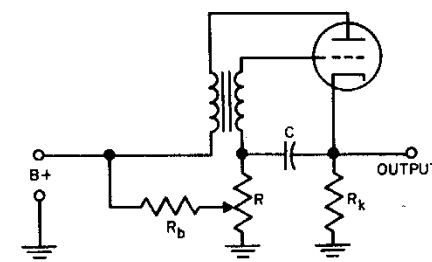

Fig. 24—Free-running positive-bias blocking oscillator.

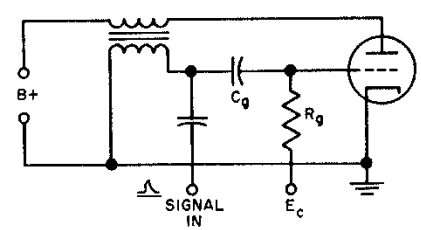

Fig. 25—Driven blocking oscillator.

Synchronized Astable Blocking Oscillator: Operating conditions (Fig. 26) are

$$f_n < f_s \quad \text{or} \quad \tau_n > \tau_s$$

where

f_n = free-running frequency in hertz

f_s = synchronizing frequency in hertz

τ_n = free-running period in seconds

τ_s = synchronizing period in seconds.

Gas-Tube Oscillators

A simple relaxation oscillator is based on the negative-resistance characteristic of a glow discharge, the two end-states corresponding to ignition and extinction potential of the discharge. Two astable forms are discussed. The circuit of Fig. 27 may also be used with a simple diode (neon lamp), omitting the grid resistor and bias. The circuit of Fig. 28 may be made monostable if the supply voltage is less than the ignition voltage at the selected bias.

Astable Gas-Tube Oscillator: This circuit is often used as a simple generator of the sawtooth waveform necessary for the horizontal deflection of a cathode-ray-oscilloscope beam. Equation for period (Fig. 27)

$$\tau = \alpha RC(1+\alpha/2)$$

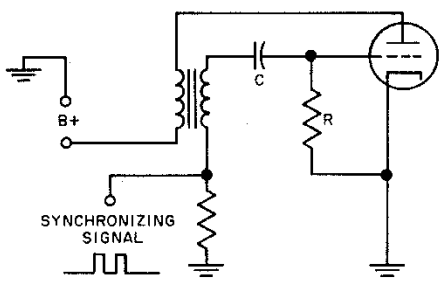

Fig. 26—Synchronized blocking oscillator.

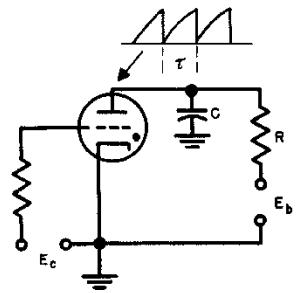

Fig. 27—Free-running gas-tube oscillator.

where

τ = period in hertz

$\alpha = (E_i - E_x)/(E - E_x)$

E_i = ignition voltage

E_x = extinction voltage

E = plate-supply voltage.

Velocity error

= change in velocity of cathode-ray-tube spot/trace period

Maximum percentage error $= \alpha \times 100$ if $\alpha \ll 1$.

Position error

= deviation of cathode-ray-tube trace from linearity.

Maximum percentage error $= (\alpha/8) \times 100$ if $\alpha \ll 1$.

Synchronized Astable Gas-Tube Oscillator: Conditions for synchronization (Fig. 28) are

$$f_s = Nf_n$$

where

f_n = free-running frequency in hertz

f_s = synchronizing frequency in hertz

N = an integer.

For $f_s \neq Nf_n$, the maximum δf_n before slipping is given by

$$(E_0/E_s)(\delta f_n/f_s) = 1$$

where

$\delta f_n = f_n - f_s$

E_0 = free-running ignition voltage

E_s = synchronizing voltage referred to plate circuit.

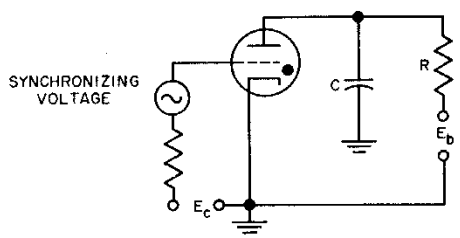

Fig. 28—Synchronized gas-tube oscillator.